Impact Assessment of Wind Farm Blockage in Complex Terrain

P.P.K.Kashyap

Impact Assessment of Wind Farm Blockage in Complex Terrain

by

P.P.K.Kashyap

to obtain the degrees of

Master of Science
in Aerospace Engineering at
Delft University of Technology

Master of Science
in Engineering (European Wind Energy)
at Technical University of Denmark

To be defended on 20th October, 2022

Supervisors:	Dr. ir. D.J.N. Allaerts	TU Delft
	Dr. H. Sarlak	DTU
	Prof.dr. S.J. Watson	TU Delft
	Mr. Jim Bleeg	DNV
Thesis committee:	Dr.ir. A.H. van Zuijlen	TU Delft
Thesis work duration:	November 2021	October 2022
Student number:	TU Delft - 5258979	DTU - s203217

Cover photo by Tui Hu Tan Kailong, China

Report template adapted from https://github.com/Inventitech/phd-thesis-template

An electronic version of this thesis is available at
https://repository.tudelft.nl and https://findit.dtu.dk

TU Delft

DTU

Acknowledgements

First and foremost, I would like to thank Dr.ir. Dries Allaerts for taking me in as a thesis student under his supervision. I am grateful for all the brainstorming sessions, continued support, and guidance throughout the project phase. I also extend my gratitude to Professor Simon Watson for his valuable insights. I would also like to thank Prof.dr. Hamid Sarlak for his continued valuable suggestions throughout this thesis. Additionally, I am also grateful for the administrative support during some tough situations I was going through in terms of my health in the middle of the thesis. This thesis would have been incomplete without the help and guidance at every stage by Ir. Mehtab Khan. I am grateful for all the impromptu and long meetings almost every day in the last three months of my project. Also, I am thankful to Mr. Jim Bleeg from DNV for promoting this idea to be chosen by master's students as a thesis project. Additionally, I would like to thank Hrishikesh Sivanandan for helping me with the SOWFA-based RANS packages used in this thesis and other OpenFOAM-related queries.

Secondly, I am profoundly grateful to my beloved parents for their trust and belief in my abilities. Their support in all aspects of my life and especially during the thesis project made me stay strong. Also thankful for continuously motivating me to keep my chin up and work towards making this thesis a success. There are not enough words in the vocabulary that could possibly provide justice to express the extent of love and blessings you have showered upon me.

Thirdly, I would like to thank my project supervisor during my undergraduate thesis Prof. Dr. Supreeth for inspiring me to take up wind energy. Without him, I would probably not have found sought wind energy as a career option. I would also like to thank Dr.ir. Shreyas Srivatsa for guiding me over the past two years and instilling in me, the necessary discipline for a master's student. A token of gratitude to all my mates in the European Wind Energy Masters (EWEM) programme without whom there would have been a huge void intellectually and socially.

I also extend my gratitude to Prajwal H.P. and Arjun Adiga for their help and guidance during my master's programme. I specifically appreciate the help given to me with respect to OpenFOAM software and my technical writing skills. Additionally, I would like to thank my friend Adithya Thonse for providing unconditional support and basic guidance with Python coding skills. Furthermore, I thank Shrikrishna Hebbar for being a huge source of inspiration all these years and more specifically during the hard times I was facing in the past few months. You both have had a huge impact on my personality which has obviously been reflected in my work.

Lastly, but most importantly I humbly bow down before Prabhu Anjaneya and Sadguru Datta for blessing me throughout my professional learning. It is their omnipresence and divine grace, that got me to this position to defend my thesis.

P.P.K.Kashyap
Copenhagen, September 2022

Abstract

Measurement campaigns and CFD simulations have recently identified a large-scale flow phenomenon called wind-farm flow blockage. This is found to bear a significant and far-reaching reduction in wind speed upstream of a wind farm. The wind farm blockage is attributed to the cumulative induction effects of multiple wind turbines placed in series. Wind-farm flow blockage has important consequences on energy production because it reduces the available kinetic energy in the incoming wind flow. In turn, this causes leading wind turbines in a wind farm to produce less energy than they each would in isolation. To date, the physics of this global blockage effect is not entirely understood, and they are therefore an active research topic. Due to the increasing demand for wind energy, reducing annual energy production (AEP) uncertainties and power production bias seems to be a challenge for wind energy researchers. Understanding wind farm blockage in complex terrain becomes crucial to account for uncertainties and power production bias.

This thesis set out to perform Reynolds-Averaged Navier-Stokes (RANS) simulations to assess the impact of wind-farm flow blockage in complex terrain using the open-source software OpenFOAM. A laterally infinite row of turbines is simulated on top of a 2-D hill defined by the mathematical curve 'Witch of Agnesi'. The set of simulations is performed for varying atmospheric conditions: truly neutral and stable free atmospheric conditions. Thermal stratification imposed under stable conditions is of particular interest due to the excitation of atmospheric gravity waves (AGWs) by the turbine array and the topology. The velocity fields due to the presence of the turbine array on top of the hill are compared to the ones without. The resulting flow reduction is then compared to the cases without the hill in order to assess the impact of complex terrain on wind farm blockage. A series of sensitivity analyses are performed for varying inter-array spacing and hill size variations in order to further the understanding of wind farm blockage.

The results obtained in this study show that the magnitude of wind farm blockage is amplified due to the presence of the hill. Additionally, the excitation of AGWs is seen to have a major impact on the wind farm blockage due to alterations caused to the pressure field. The impact of blockage is seen to be dominant up to at least 10-15 turbine diameters upstream of the turbine array under truly neutral conditions. While the effects are more pronounced and much more dominant under stable free atmosphere conditions. All the stable free atmosphere cases simulated show a reduction ranging from 1-4% at different upstream locations while neutral cases show slightly lower yet non-negligible reduction due to blockage.

This study ultimately concludes that the existing 'wakes-only' approach for estimating energy losses still has a significant power production bias. Therefore accounting for the blockage effects in the farm upstream is also equally important and must be analysed before commissioning a wind farm.

Contents

List of Figures

List of Tables

1

Introduction

Energy has become one of the most essential aspects of daily activities in the world. Non-renewable energy sources have been known to produce a good amount of energy required for all day-to-day activities but with a substantial negative impact on the environment especially with increased CO_2 emissions. This has led to a plethora of issues with respect to climate change due to an imbalance in the naturally permitted oxygen and carbon levels in the atmosphere. Recent studies have shown that the global temperature levels are increasing steadily and there has been a net increase by almost 1.2° C in the past century since the start of the industrial revolution in different parts of the world shown in the article "Global Temperatures", 2022. There have been predictions that if the same trend continues, then the temperature changes can increase further as shown in Figure 1.1. The 2015 Paris agreement makes efforts in the direction of keeping the global temperature rise under control. In accordance with this, countries around the world have borne the responsibility to invest in and improve renewable energy production specifically in the wind and solar farm installations Davies, 2020.

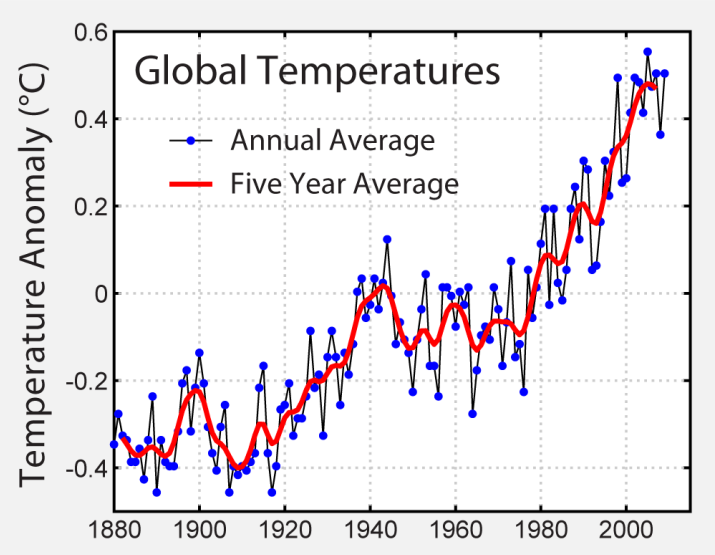

Figure 1.1: Annual Temperature Changes [Davies, 2020]

International Renewable Energy Agency, 2019 report suggests that there has been nearly a 21% compound annual growth rate (CAGR). Figure 1.2 shows that there has been nearly 542 GW of installed onshore wind energy capacity by the end of 2018 as opposed to 17 GW capacity in the year 2000. International Renewable Energy Agency, 2019 report also has drafted a plan for the next 30 years and predicted the potential increase in wind energy production and limiting to global emissions by the year 2050. According to this, it has been found that wind energy is expected to see a net increase of about 4500 GW over the next few years leading to a reduction in nearly 6.3 gigatonnes of CO_2 emissions.

The report by Global Wind Energy Council Lee and Zhao, 2021 also provided data prediction and an estimate of the necessary 12% CAGR of wind power installations in order to have a net zero emission by 2050. Despite the expected hiccups and issues with exports of raw materials, construction and installation caused due to the COVID-19 pandemic, the year 2020 saw a record installation of 93 GW globally as seen in Figure 1.3. The following year 2021, also saw an annual growth of 88 GW of additional installation of onshore wind farms. However, in order to achieve the goal set by the Paris Agreement, the installations of wind energy both onshore or offshore needs tremendously enhanced efforts from across the globe.

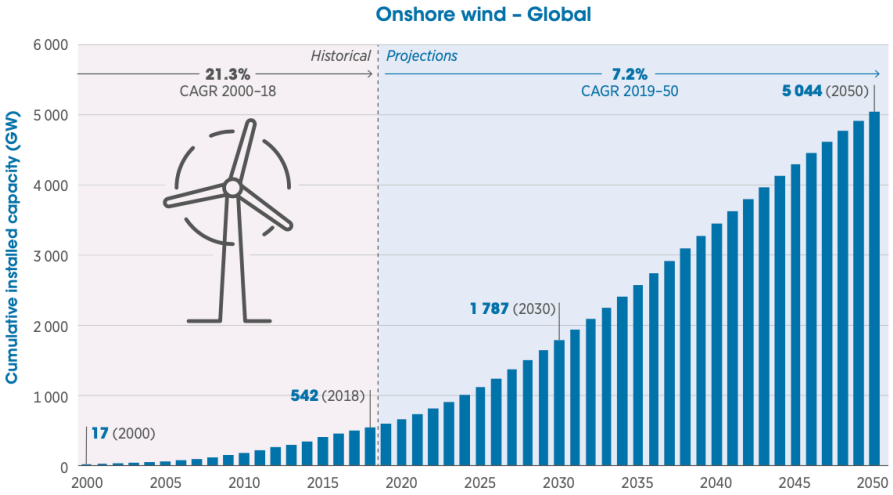

Figure 1.2: Global historical data and future prediction on the installation of onshore wind energy based on International Renewable Energy Agency, 2019

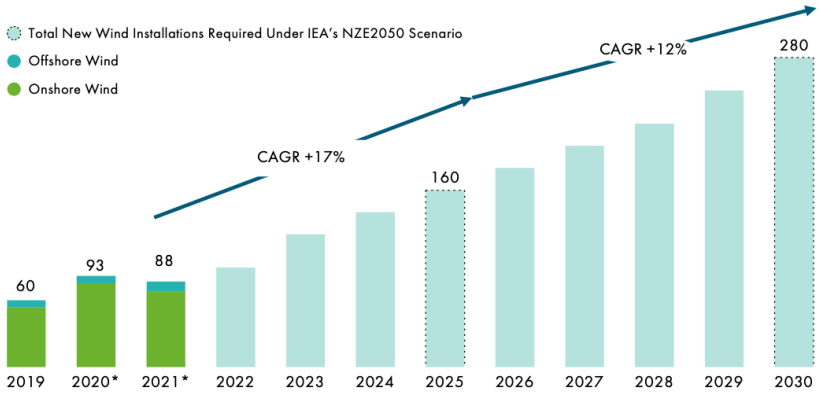

Figure 1.3: Data from GWEC market intelligence providing a prediction of wind energy installation for the next three decades. Lee and Zhao, 2021

As of 2020, it has also been recorded by Lee and Zhao, 2021 that the contribution of renewable energy has been around 60% of the global power mix which is in line with the goal set by the United Nations. Wind Europe report by O'Sullivan, 2022, estimated that nearly 15% (447 TWh) of the energy consumption (2921 TWh) by the European Union and the United Kingdom as of 2021 was found to be from wind energy. Based on all the current trends and future predictions, there is a necessity to have higher power production capability and profitability for wind farms.

While these are the improvements brought in on a wind turbine scale [Clausen and Wood, 1999 and Thresher et al., 2008], there have been several efforts to bring improvements in the Annual Energy Production (AEP) and have fewer uncertainties in estimating the energy production on a wind farm scale. Porté-Agel et al., 2020 elucidates a detailed analysis of the current challenges in efficient AEP

estimations such as the inclusion of wake effects, the effectiveness of wake prediction, deep array effects, and wind farm-induced wake effects to name a few. While there have been efforts to reduce the uncertainties in the AEP of wind farms there have also been more recent challenges encountered. In order to better understand the new challenges, the mesoscale phenomena due to the atmospheric boundary layer (ABL) on a wind turbine or a wind farm needs to be analysed.

1.1. Atmospheric Boundary Layer

In classical fluid mechanics, the boundary layer is defined as the layer of a fluid flow that is directly influenced by the surface features and the drag imposed on the flow which leads to the formation of the boundary layer. Extending the same knowledge onto the surface of the earth gives the definition of ABL as explained by Stull, 2017. ABL is the most essential part of the troposphere where most of the daily human activities happen. It is the region of the atmosphere where buoyancy forces are dominant and results in the creation or destruction of turbulent motions specifically under unstable and stable conditions respectively. Therefore, a better understanding of ABL is necessary to model flows that primarily influence wind farm characteristics.

1.1.1. Governing parameters of ABL

Surface Roughness (z_o)

Roughness is essentially a surface parameter influencing the aerodynamics of flows over rough surfaces that is important to define the wind velocity profile within the ABL. As Stull, 2017 and Gryning et al., 2007 explain, roughness induces drag to the wind speed in the surface layer and is also one of the driving factors for the cause of turbulence as well as defining turbulent intensity within the surface layer. Also, it is a surface property dependent on surface topology. In practice, trees, forests, hills, and other elevations are considered as surfaces of higher roughness lengths. On the other hand, smooth surfaces such as seas, oceans, or other waterbodies are considered as surfaces with lower surface roughness lengths. For the sake of numerical analysis, these surfaces are assigned empirically derived roughness lengths as shown in Emeis, 2014.

Velocity Profile (u)

According to Gryning et al., 2007, the velocity profile of the boundary layer flow and specifically over a rough surface through the turbulent boundary layer aloft is driven by three main parameters: surface roughness (z_0), friction velocity (u_*), and atmospheric stability. However, u_* defines the logarithmic profile of the velocity within this layer [Stull, 2017]. Log-law profile of the wind velocity in the surface layer is mathematically defined as -

$$u(z) = \frac{u_*}{\kappa} \ln\left(\frac{z}{z_o}\right) \tag{1.1}$$

Here, κ is the von Karman constant, which is assumed to be $\kappa = 0.4$. Based on several studies and observed data such as by Emeis, 2014, the wind shear profile, wind velocity profile, lapse rate, and potential temperature together define air turbulence in the surface layer of the atmosphere. It is important to note that the velocity at the ground surface in the ABL is zero due to the no-slip assumption in most fluid problems. Eventually, the velocity increases gradually until it reaches the geostrophic wind speed at the top of the ABL.

Potential Temperature (θ)

The transport of air parcels in the boundary layer is governed by a parameter that defines the temperature change due to adiabatic transport into regions of higher or lower pressure. This temperature change occurs due to the work done by/on the parcel and is proportional to the latent heat contained within the parcel. This is known as the 'potential temperature' (θ) and is mathematically defined as -

$$\theta = T \cdot \left(\frac{P_o}{P}\right)^{R/c_p} \tag{1.2}$$

Here, T is the known absolute temperature at an ambient pressure level P, P_o is the standard reference pressure and according to Stull, 2017, this value is 100 kPa. R is the universal gas constant and

c_p is the specific heat capacity at constant pressure. Potential temperature becomes a major driving factor for the turbulent mixing, atmospheric stability, wind flows and many other physical phenomena occurring within the ABL. Potential temperature (θ) and its impact on the ABL is explained in Stull, 2017. The potential temperature gradient $\frac{\partial \theta}{\partial z}$ defines the stability of the atmosphere.

Capping Inversion

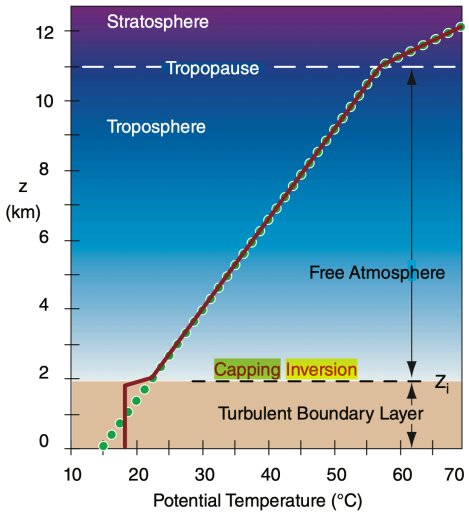

Figure 1.4: Structure of the atmosphere [Stull, 2017]

The boundary layer closest to the ground is known to be highly turbulent which leads to enhanced mixing and therefore the ABL is often termed the 'mixed layer'. There is a region above the ABL that is usually not affected by the turbulent motion of the air parcel which is termed as 'free atmosphere' and has a strong thermal stratification. This division of layers of the atmosphere is shown in Figure 1.4 taken from Stull, 2017.

A region of the atmosphere that is in the interface of the so-called mixed layer and the free atmosphere is the one where there is a sudden step change in the potential temperature θ before subjecting to strong stable stratification. This layer is known as the capping inversion as per Stull, 2017. Allaerts, 2016 observed that the so-called capping inversion has an impact on the atmospheric flows and prevents the turbulent gust and transport of momentum from the ABL to the free atmosphere. The characteristic parameters of the capping inversion are the inversion base height and capping inversion strength. LES studies about the influence of the inversion strength on limiting the growth and development of ABL have been conducted by Wu and Porté-Agel, 2017, Abkar and Porté-Agel, 2013 and Allaerts and Meyers, 2014. These studies have concluded that growth and the depth of the boundary layer is an important parameter that governs the turbulence intensity (TI) of the layer which is essential for estimating loads on wind turbines.

1.1.2. Atmospheric Stability

The capability of movement of an air parcel from an initial position to a new position and the tendency of the parcel to attain a new position or regain its initial position is defined as the stability of that particular air parcel from Stull, 2017. Based on this definition, in nature stability is divided mainly into three types: neutral, stable, and unstable conditions. Neutral condition is when an air parcel displaced from its initial position, attains a new position and does not regain or go on to attain a new position unless displaced again. Unstable condition is when an air parcel is displaced it attains a new position and continues to do so. Lastly, stable condition is when an air parcel is displaced, it regains its initial position.

Obukhov, 1971 hypothesized that the characteristic turbulence of the atmosphere is defined by the relative buoyancy in relation to the wind shear. This is one of the main parameters used to determine the stability of the atmosphere and has been used in several ABL-related studies.

$$L = -\frac{u_*^3 \overline{\theta}}{\kappa g \left(\overline{w'\theta'}\right)} = -\frac{u_*^3}{\kappa (g/\overline{\theta}) \left(\overline{w'\theta'}\right)} \tag{1.3}$$

Here, u_* is the friction velocity, κ is the von Karman constant, $\overline{\theta}$ is the mean absolute temperature, g is the acceleration due to gravity, $\left(\overline{w'\theta'}\right)$ is the kinematic heat flux at the surface. The underlying assumption behind the Obukhov length as hypothesised by Obukhov, 1971 is that the characteristic length L is the height from the ground within the surface layer above which buoyancy forces dominate the turbulent kinetic energy and the effects of shear and friction velocity are considered negligible as explained by Emeis, 2014.

There are multiple ways in which the stability of the atmosphere is parameterised. Based on Stull, 2017, stability is also characterised by the Richardson Number (Ri) which indicates the heat transfer within the parcel and it essentially measures the relative creation of TKE by buoyancy and destruction by shear. Numerically, Ri is represented as -

$$Ri = \frac{g}{\theta_o} \frac{(\partial\theta/\partial z)}{(\partial u/\partial z)^2} \tag{1.4}$$

Here, θ_o is the mean absolute temperature of the air parcel, g is the acceleration due to gravity, and the numerator and denominator terms are the potential temperature gradient and velocity gradient respectively. However, in the case of a uniform velocity profile at the inlet, the Richardson number Ri does not hold well to define the stability condition of the atmosphere. Based on the frequency at which the air parcel oscillates within the atmosphere, the Brunt-Väisälä frequency (N) determines the atmospheric stability. Stull, 2017, Allaerts, 2016 and Wu and Porté-Agel, 2017 hold the Brunt-Väisälä frequency as an important parameter to determine stability especially for wind farm flows. It is mathematically defined as -

$$N = \sqrt{\frac{g}{\theta} \frac{\partial\theta}{\partial z}} \tag{1.5}$$

Here, g is the acceleration due to gravity in ms^{-2}, θ is the reference potential temperature in K and $\frac{\partial\theta}{\partial z}$ is the potential temperature gradient within the domain under study in K/km.

In general, under lack of radiation or latent heat release, the heating or cooling of the surface determines the thermal stability of the atmosphere. Therefore, as mentioned earlier, ABLs are divided mainly into three types. The three classifications of boundary layers are Neutral Boundary Layer (NBL), Stable Boundary Layer (SBL), and Convective/Unstable Boundary Layer (CBL).

In the case of no surface heat flux, the potential temperature θ remains constant with vertical distance from the surface. This is known as a statically neutral boundary layer (NBL). This is presumably the simplest form of the boundary layer and there have been extensive research studies done by Shingai and Kawamura, 2004, Deusebio et al., 2014 and Hess and Garratt, 2002. Due to the fact that surface heating is considerably small at sea, NBLs are more commonly found in offshore conditions. On the contrary, Stull, 2017 and Garratt, 1989 observed that over land the NBLs are experienced only during a very small part after sunset or cloudy conditions.

In the case of a positive surface heat flux from the ground or due to radiative cooling from the top due to the presence of clouds, more dense parcels of air overlie less dense air parcels. This type of ABL is therefore known as the convective boundary layer (CBL) and is found to be statically unstable. CBL is a standard type of boundary layer found during daytime and is influential for wind farms as they give rise to high turbulent intensities and convective radiations. LES studies by Kim et al., 2003 and Wu and Porté-Agel, 2017 focus on CBL influences on wind farms.

Lastly, in the case of negative heat flux from the ground, air parcels of low temperatures are formed and the temperature of the air parcels gradually increases with vertical distance from the ground. This is the reason less-dense air parcels overlie more-dense air parcels. The particular type of boundary layer is known as a stable boundary layer (SBL). In onshore cases, SBLs are typically formed after sunset and are typically very thin with high shear and wind veer. This leads to lesser mixing of winds and therefore suppresses turbulence. Therefore, this becomes an essential part of wind farm simulations.

Once the mechanics of ABL and the different classifications are understood, the focus needs to be shifted to wind farm flows. The mechanism of wind farm flows is explained in detail in the following section.

1.2. Wind Farm Flows

Flows around wind turbines are quite different from the flows that occur in reality where the wind turbines are placed within a cluster of other wind turbines. There is a cumulative effect of wind turbine flow characteristics which influence each other and the influence of the surrounding environment which also has an impact on the behaviour of the wind turbine. The influence of ABL on the wind farms and in turn the influence of the wind farms on the ABL are important aspects of understanding wind farm flows.

1.2.1. Wind Farm Flow Anatomy

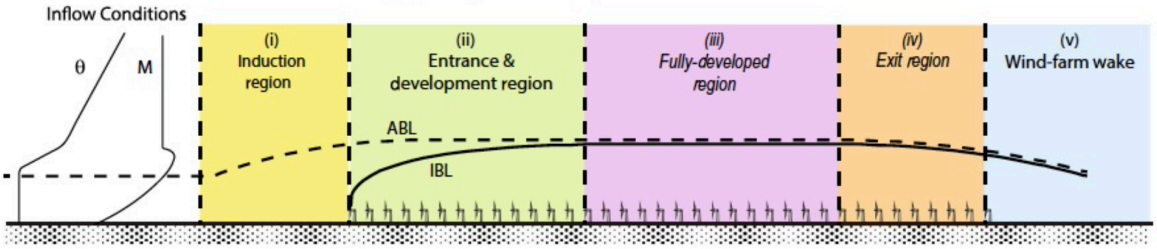

Figure 1.5: Anatomy of Wind Farm Flows Porté-Agel et al., 2020

Wu and Porté-Agel, 2017 and Porté-Agel et al., 2020 established that the entire wind farm can be divided into four or five different regions based on the stratification strength of the free atmosphere. Figure 1.5 is the representation of a wind farm flow anatomy by virtue of a strong free atmosphere stratification. The flow regions in the wind farm are 1) Induction region 2) Entrance & Development region 3) Fully-developed region 4) Exit region and 5) Wind-farm wake.

1. **Induction region** - Porté-Agel et al., 2020 and Branlard and Forsting, 2020 found that this region of the wind farm is formed by the virtue of the cumulative effect of the individual induction zones of each turbine in the foremost row of the wind farm. The inflow conditions far upstream of a wind farm are essentially under ambient free atmosphere conditions and as the flow approaches the induction region there is a reduction in wind speed known as 'wind farm blockage' which has been validated using RANS modelling as per Bleeg et al., 2018, Bleeg and Montavon, 2022 Allaerts and Meyers, 2017, analytical modelling as per Segalini, 2021, cylindrical vortex models as per Branlard and Forsting, 2020 and wind tunnel experiments Nishino and Draper, 2015. This particular region of wind farm flows has been a part of recent studies in the industry and has been discovered as a potential cause for the underestimation of the annual energy production of a wind farm. The magnitude and reason for the reduction are attributed to different wind farm scales by authors of Branlard and Forsting, 2020, Nishino and Draper, 2015 and Strickland and Stevens, 2020 such as turbine induction zones, thrust coefficient, turbine spacing, and farm layout. Allaerts and Meyers, 2014 and Wu and Porté-Agel, 2017 also attributed the reasons to mesoscale phenomena such as atmospheric gravity waves, ABL stability, and free atmosphere stratification. More details about this are provided in other sections of this report.

2. **Entrance & development region** - This region is in the immediate downstream of a wind turbine where the wind flow velocity within the ABL is reduced due to the loss of kinetic energy as a result of the momentum extraction of the wind turbine. The entire domain has to be maintained in a mass equilibrium state i.e. conservation of mass. Therefore, there is an upward displacement of the ABL which gives rise to the formation of the internal boundary layer (IBL) as explained by Porté-Agel et al., 2020 and Wu and Porté-Agel, 2017.

3. **Fully-developed region** - Wu and Porté-Agel, 2017 classify the region where the streamwise changes in the properties of the flow are negligible is regarded as the fully-developed region. In

this region the IBL grows in such a way that the height is asymptotically equal to the height of ABL. Porté-Agel et al., 2020, Abkar and Porté-Agel, 2013 and Wu and Porté-Agel, 2017 discovered that the ABL and IBL heights are constant and approximately equal to each other in this region.

4. **Exit region** - This region in lay terms is the opposite of the entrance and development region because of the increase in flow velocity and the mass flux is in the downward direction. This results in the reduction of the ABL and IBL heights of the wind farm especially when the wind farms are very large. LES studies by Porté-Agel et al., 2020, Wu and Porté-Agel, 2017, Allaerts, 2016, Allaerts and Meyers, 2017 Allaerts and Meyers, 2018 and Abkar and Porté-Agel, 2013 have shown that this region triggers vertically propagating gravity waves which have an impact all the way in upstream of the wind farm.

5. **Wind-farm wake** - This is downstream of the wind farm trailing edge where the flow recovers to its initial upstream velocity profiles. However, recent studies from CFD modelling and satellite measurements have shown a wind speed deficit of up to at least $2-10\%$ in comparison with the upstream velocity magnitudes. The review by Porté-Agel et al., 2020 observed that this velocity deficit can exist at any distance ranging from 5-20 km downwind of wind farms (especially in large wind farms).

1.2.2. Two-Way Interaction of Wind Farm and ABL

The different regions of the wind farm were explained in the previous section and these regions were formed as a result of the influence of the ABL on the wind farm. The review by Porté-Agel et al., 2020 most recent numerical studies and field measurements have shown that the existence of wind farms also majorly influences the ABL. Few of such phenomenon which is relevant for this research are listed here with relevant theoretical background -

1. **IBL Formation** - As explained earlier, IBL becomes a very important part of the entrance region and fully developed region of the wind farm flow regime. Jegede and Foken, 1999 explained that the IBL is defined as the region of the ABL developed due to a change in the surface roughness parameters. Garratt, 1989 on the other hand observed that IBL formation primarily occurs in coastal regions, complex terrain regions, or regions encompassing large forest canopies due to a sudden change in the surface features. However, Wu and Porté-Agel, 2017 examined that in the case of wind farms, the long rows of turbines act as a surface of changed roughness which leads to the formation of IBL and therefore leads to the vertical transport of momentum in the ABL. The review by Porté-Agel et al., 2020 showed that the development of IBL is known, studies have also shown that there is a rate of growth of the IBL which occurs in presence of large wind farms and therefore higher magnitude of flow deceleration is observed. On the other hand, Allaerts and Meyers, 2018, Allaerts, 2016 and Sivanandan, 2021 observed that the vertical transport of momentum due to the development of IBL coupled with conservation of mass and momentum leads to the formation of atmospheric gravity waves which affect the far upstream region of the wind farm.

2. **Wind Farm induced Gravity Waves** - One of the recent discoveries in the field of wind energy research is that of the self-induced gravity waves. Atmospheric gravity waves occur in nature when there is a topographical feature that causes a vertical transport of momentum in a stably stratified layer of flow. As explained earlier, the studies done by Smith, 2010, Allaerts, 2016 and Allaerts and Meyers, 2018 have shown that wind farms can be a potential source of vertical transport. Due to this, the streamlines above the IBL potentially trigger gravity waves in the inversion layer and the stable free atmosphere. LES studies done by Allaerts and Meyers, 2017 and Wu and Porté-Agel, 2017 displayed that the gravity waves triggered by the wind farm are one of the reasons for the far upstream wind speed reduction which was recently discovered as the so-called 'wind farm blockage'.

3. **Wind Farm Blockage** - This phenomenon is a consequence of the two-way interaction between atmosphere and wind farm Bleeg et al., 2018. Large wind farms and wind farms on top of hills have shown that gravity waves cause blockage far upstream and conversely LES study done by Allaerts and Meyers, 2018 has also shown that wind farm blockage also causes the vertical displacement of the streamlines and momentum transport thereby triggering gravity waves. More

detailed analysis and literature survey on the causes, implications and consequences of wind farm blockage is elaborated in **Chapter 2**.

Wind farm blockage effects studied by Bleeg et al., 2018 and Bleeg and Montavon, 2022 and wind farm induced atmospheric gravity wave effects studied by Allaerts, 2016, Allaerts and Meyers, 2018 and Wu and Porté-Agel, 2017 have been the most recent inclusions in the reasons for wind energy research to face hindrance and the effects which have been quite ignored by the wind industry in the past years. Wind farm blockage is a mesoscale phenomenon caused in a wind farm specifically in the first row of the wind farm. There have been several observations regarding the understanding of the underlying physics behind this phenomenon. But, in the recent past, most of the research efforts by Bleeg et al., 2018, Segalini and Dahlberg, 2019 and Segalini, 2021 have been towards quantifying the blockage effects and studying the sensitivity of blockage to changing physical conditions in the atmosphere. The most recent studies in this area have been with respect to wind farms in an onshore environment on a simple flat terrain, offshore environment, and different turbine layouts but there is lacking evidence and study of these effects on complex terrains. As found by Lee and Zhao, 2021, Forsting et al., 2016 and Hylleberg, 2014 the demand for wind energy is increasing, and there is an increasing need for wind farms to be operated in more complex terrain features primarily due to the availability of larger wind speeds and less turbulence intensity. As an implication of the recently discovered wind farm blockage effects and the need for wind farms to be located in more and more complex terrains, there is a necessity to investigate the effects of blockage upstream of a wind farm in such a terrain. In this direction, this study focuses on assessing the impact of wind farm blockage on a set of tightly spaced infinite lateral wind farms on top of a hill with a certain height and half-width. At this point, having known the research gap and need of the hour for wind farm research paves the way to elucidate the research objectives of this particular study and the questions that are going to be answered.

1.3. Research Objective

> "To gain a better understanding of the newly discovered mesoscale phenomenon known as the wind farm blockage by conducting a numerical simulation of a row of tightly spaced turbines on a hill whose shape is defined by the mathematical curve 'Witch of Agnesi' and determining the affecting parameters of the blockage such as the Venturi effect, atmospheric gravity waves triggered by the hill under stable free atmosphere conditions and truly neutral conditions.".

The primary research objective of this thesis is further divided into sub-objectives in order to achieve it and answer all the research questions. The sub-objectives of this thesis project are listed below -

- The first sub-objective (**SO1**) is to assess the effect of the two-way interaction between the wind farm and the atmosphere by conducting a CFD simulation of infinite laterally spaced turbines on a domain in neutral stability conditions with a uniform velocity profile.
- Second sub-objective (**SO2**) is to assess the same conditions as in **SO1** for stable free atmosphere conditions. This is expected to give rise to wind farm-induced gravity waves influencing the farm scale blockage.
- Third sub-objective (**SO3**) is to assess the impact of having a two-dimensional hill defined by the mathematical curve 'Witch of Agnesi'. The hill is expected to trigger gravity waves specifically in stable free atmosphere conditions. This is expected to further influence the blockage in the wind farm upstream.
- Fourth sub-objective (**SO4**) is to cumulatively assess the impact of the hill on the blockage magnitude upstream under truly neutral atmospheric conditions as well as stable free atmosphere stratification. A comparison of **SO1** and **SO2** with **SO3** isolates the effect of blockage caused due to the hill.

1.4. Research Questions

The research questions that will be answered throughout the course of this thesis are mentioned below along with the sub-questions (SQ) -

- **Question 1** How does a 2-D hill impact the magnitude of blockage upstream of the wind farm?
    1. How does the height and half-width of the hill impact the physical phenomena affecting the wind farm?
    2. Can the placement of the wind turbines on the hill affect blockage?
- **Question 2** How to quantify the blockage effect caused due to presence of the row of turbines?
    1. Can the blockage magnitude be quantified directly in terms of velocity reduction at several upstream locations?
    2. Do pressure variations also represent blockage magnitude at the wind farm upstream?
- **Question 3** How is the blockage magnitude sensitive to changing atmospheric conditions?
    1. What is the impact of changing stability conditions on the flow field over a terrain complexity?
    2. How does the blockage magnitude vary under a stable free atmosphere in comparison with truly neutral atmospheric conditions?
- **Question 4** How sensitive is the blockage magnitude to varying turbine spacing distances?

1.5. Report Structure

In order to answer the research questions and achieve the research objective of this study, the work done during the course of the research culminates into this report. The report is structured into the following chapters.

- **Chapter 2** is the Literature Review that provides extensive exposure to the current research outcomes and the gap in research particularly pertaining to this study.
- **Chapter 3** is the Simulation Methodology that explains the rationale behind the choice of flow modelling and the governing equations that are solved to obtain the flow fields.
- **Chapter 4** is the Simulation Setup where the domain specifications and the specific boundary, as well as initial conditions for the simulation, are elaborated.
- **Chapter 5** is the Simulation Results in which the results obtained from the study are explained in detail. Along with this, relevant explanations for the physical understanding of the flow and blockage effects are provided.
- **Chapter 6** lastly is the Conclusion and Recommendations for the current study and future wind farm research enthusiasts are elaborated respectively.

1.6. Summary

In the current chapter, initially, the need and rise in wind energy production in recent years were discussed. This is followed by a brief overview of the challenges wind energy is facing currently. Identified challenges are heavily influenced by the atmospheric boundary layer and several parameters that govern them. So a detailed description of the ABL and its salient features relevant to the current study were discussed. Lastly, the challenges of two-way interaction between wind farms and ABL was introduced. This forms the preamble for the study on the impact of terrain complexities on wind farm blockage. In order to carry out the research, a set of research objectives and research questions were also mentioned.

The following chapter sheds light on the currently available research relevant to the present study. A literature review on terrain complexity's impact on ABL and the resulting influence on wind farms is carried out. This is followed by a review of current literature on topology-induced and wind farm-induced AGWs. Lastly, a section on the currently available research pertaining to wind farm blockage is discussed.

2

Literature Review

The current chapter sheds light on the important factors that affect the flow scenario expected to be observed in the present study. The chapter is divided into two sections mainly. The first section presents current literature findings and research hypotheses surrounding the effects of terrain features on a wind farm. Later, in the second chapter, research pertaining to the wind farm blockage is discussed in detail. Detailed discussion on the most recent research findings and research gaps relevant to the present study is presented.

2.1. Effect of Terrain Features on a Wind Farm

Terrain features become an important part of wind energy research as more and more wind farms are getting commissioned over the years. Thus, there is a constant need for more space especially when wind farms are being planned for onshore conditions. In an offshore environment, there are constraints with respect to the wind farm area, number of turbines, and turbine spacing specifically due to high infrastructure & operational costs. In an onshore environment, there are constraints with respect to the wind farm area, number of turbines, and turbine spacing but construction and operation is much more affordable. The constraints that occur are because of the surrounding urban areas potentially cause acoustic issues, agricultural lands, monuments, and natural reserves causing potential damage to the environment clearly elucidated in International Renewable Energy Agency, 2019 and Hylleberg, 2014.

In order to have more efficient wind farms in the onshore environment, wind farms are required to be planned in more complex terrain features. Placing wind turbines on top of hills/mountains or other complexities assists in higher wind speeds. This has its own downside with respect to on-field measurements because of the drawbacks from the measuring instruments, uncertainties caused due to modeling constraints, and lack of capability for experimental calculations Castellani et al., 2015. So a better understanding of the terrain features and their impact on boundary layer flows and the subsequent impact on wind farm performance is discussed here.

2.1.1. Terrain Complexity

To conduct an extensive analysis of the different terrain features affecting the ABL and the wind farm, there needs to be a way in which terrain complexity is quantified. A site ruggedness index is defined in order to get the complexity of a given terrain. The site ruggedness index (RIX) is defined as the fraction or part percentage of the terrain which is considered to be steep with a certain defined slope bounded within a certain boundary of observation defined by O'sullivan et al., 2010. A comprehensive literature review by Porté-Agel et al., 2020 showed that a certain terrain is considered steep or complex if the ruggedness index is a positive integer ($RIX >> 0$) in which case there will be a requirement for more careful and better modeling of the terrain features.

The terrain features such as hills, mountains, grasslands, and forests have an impact on the flow above because of the varying surface roughness these terrain features offer to the altering velocity profile Stull, 2017. Higher surface roughness potentially imposes higher shear-generated turbulence resulting in changes in TI. Changing TI implies that the resulting loading on the wind turbine blades is also changing. Teneler, 2011 defined obstacles such as buildings as a porous surface when repre-

sented on a map and that needs to be considered when modeling terrain complexities. As suggested by Porté-Agel et al., 2020, terrain-induced turbulence has an impact on the wake velocity profiles, atmospheric gravity waves, impact on power production of the turbines.

2.1.2. Effect on ABL

Stangroom, 2004 demonstrated that steepness of the topography cause unexpected and high magnitude speed ups causing an unnecessary impact on the resulting flows. It was also observed that the terrain features result in compression of the different layers of the flow above especially in stably stratified flows. In highly complex cases, some studies especially by Porté-Agel et al., 2020 observed that these dramatic speed-ups lead to the flow being pushed towards the side of the terrain features potentially reducing the wind resource available at the top of the terrain which is of importance, especially for wind turbine siting.

According to Teneler, 2011, the terrain can be classified into three types based on the orographical features: flat, hilly, and mountainous. A terrain in which surface roughness is the only parameter that alters the ABL flow is considered as flat terrain. Hilly terrain is the one where the slope is not too steep and the ABL flows are slightly accelerated causing an increase in the available kinetic energy at the top of the hill. Mountainous terrains are the ones where the slope is too steep causing flow separation at the lee side of the mountains. Alfredsson and Segalini, 2017, defined a layer as the so-called 'roughness sublayer' within the bottommost part of the ABL which is direct influence by the terrain features. According to the study, terrain features cause severe distortion of the streamlines in the ABL resulting in turbulent motion and a source of momentum exchange.

Hills and mountains can also trigger a specific mesoscale phenomenon known as the atmospheric gravity waves (AGWs). AGWs have an impact on the wind speeds because of the periodic increase and decrease in the velocity leading to periodic changes in the power production of the wind farm as well. LES studies by Wu and Porté-Agel, 2017 and Allaerts and Meyers, 2018 have shown that this is a consequence of the strong stable stratification of the ABL and also of the stratification strength of the free atmosphere.

2.1.3. Flow over 2D Hill

Two-dimensional hills with gentle slopes are considered a potential terrain complexity. This is because the hill causes a distortion of the streamlines of the flow layers surrounding the hill. Due to this effect, the classical approaches of logarithmic velocity profiles break down. There have been recent field measurement studies that complement this physical phenomenon established by Hyvärinen and Segalini, 2017. The steepness of the hills also determines the behaviour on the leeward side which results in flow separation. Jackson and Hunt (1975) approached flow over hills more comprehensively when they found a linearised approach to solving flow around hills. In their theory, they hypothesized that the vertical component of velocity is proportional to the slope of the hill.

O'sullivan et al., 2010 conducted a numerical analysis of the flow over a hill defined by the mathematical curve 'Witch of Agnesi' named after the great Italian mathematician Maria Agnesi. They complimented the reasonable assumption made by Jackson and Hunt where they observed that the flow around a hill can be distinguished into the inner region and outer region is driven by viscosity and pressure respectively. Linearised models proposed by Segalini, 2017 found that the primary challenge was mainly in determining the Reynolds stresses at the wall regions closest to the hill. The generation of turbulent kinetic energy (TKE) is also majorly impacted due to the presence of the hill and it was observed that there was about a 5% discrepancy in the TKE with the flat terrain case.

2.1.4. Effects on Wind Farm

The effects of the terrain features on the ABL and flow modifications due to the structure of the hill leads to understanding the effects of terrain features on the wind farm. There have been several studies both experimentally and numerically performed to understand these effects. Segalini, 2017 performed a linearised numerical simulation of wind farms over a hill and compared it with the case of a no hill. This showed that a set of turbines downstream of a wind turbine strongly deflected the direction of the wake. This gives rise to skewed inflow conditions causing increased later loading on the turbines downstream. Another similar study performed by Hyvärinen and Segalini, 2017 shows that the hub height wind speed caused a 13% increase on top of the hill causing more available kinetic energy at the top of the hill.

Terrain features also play a role in the wake effects of upstream wind turbines which have an impact on the turbines downstream. Higher elevation and roughness cause more ambient turbulence leading to faster recovery of the wake was observed based on the work done by Castellani et al., 2015. On the contrary, Alfredsson and Segalini, 2017 showed that the wind speed increase on top of the hill did not necessarily increase the available energy on the top of the hill. The authors attributed this effect to the fact that momentum transfer is a two-dimensional phenomenon. There is a vertical and horizontal transfer of momentum which results in the constant energy available. Hyvärinen and Segalini, 2017 also observed a faster wake recovery in the presence of a hill at the site which resulted in yielding better power performance on the downstream turbines.

A major drawback in the modelling of wind farms over complex terrain was observed by Porté-Agel et al., 2020 who showed from different literature that the wake behaviour is not modelled in a more accurate fashion. The wake models which are used in the industry are mainly empirical and therefore the resulting superposition methods do not accommodate for the effects of the complex terrain features. Segalini, 2017 also observed the impact of the terrain features to have an impact on the wind farm blockage. The wind farm on top of the hill observed a higher impact of wind farm blockage. Especially under stable atmospheric conditions, the hill leads to the formation of atmospheric gravity waves. The gravity waves cause oscillatory wind speeds on the leeward side of the hill and to a certain degree on the windward side as well. This effect is seen to have a higher impact on the blockage.

Segalini, 2017 observed another additional characteristic of wind farm flows over a hill, is that the downward deflection of the wakes was seen especially in the center of the wind farm row. They also observed that placing the wind turbines all along the curve of the hill has an impact on the performance of the turbines. The turbines located on the crest of the hill experienced a speed up and thus had higher power performance while the turbines placed along the curve of the hill faced a deficit of kinetic energy thus leading to reduced power performance.

2.2. Wind Farm Blockage

The main scope of the present study is to analyse the impact of blockage on a row of tightly spaced turbines placed on top of a two-dimensional hill which is in the shape of the popular mathematical curve 'Witch of Agnesi'. In this direction, a section of the literature survey is dedicated to understanding the phenomenon of wind farm blockage based on existing research. The physical understanding of blockage, techniques implemented to measure blockage as well as the implications and consequences of wind farm blockage are discussed in detail in this particular section.

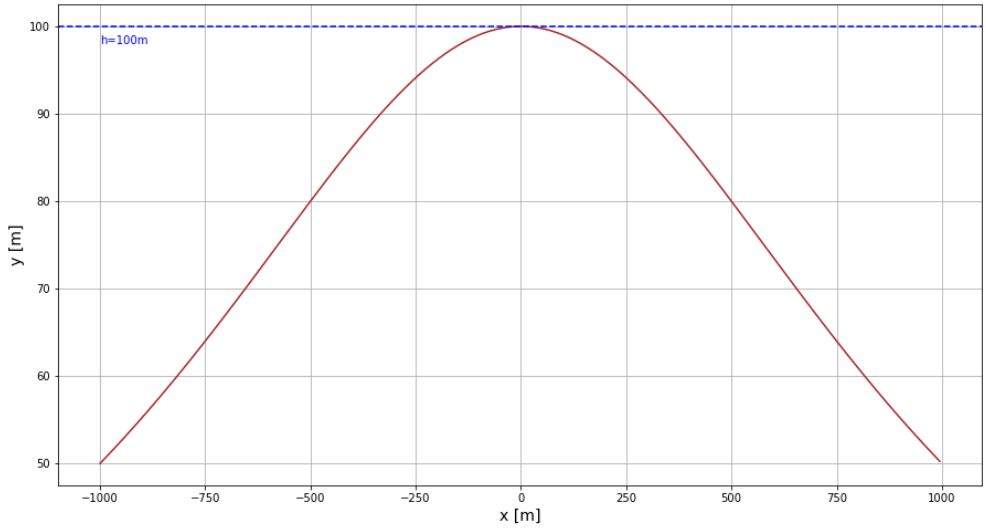

Figure 2.1: 'Witch of Agnesi' curve

The effect of blockage occurs upstream of a wind turbine and wind farms. Until recent times, the only consideration made by the industry and the researchers was the wakes from the turbines which is the so-called 'wakes-only' approach, and the blockage effects were attributed to the turbine scale and farm scale which was just about a few turbine diameters upstream. This was posing critical challenges in the wind resource assessment mainly of a bias in the AEP estimates and power production. This issue was first brought to light by DNV when the work by Bleeg et al., 2018 was published. Ever since this discovery, there have been extensive efforts from several researchers in academia as well as the industry to dwell deep into this particular mesoscale phenomenon and have a better understanding of the physics behind it.

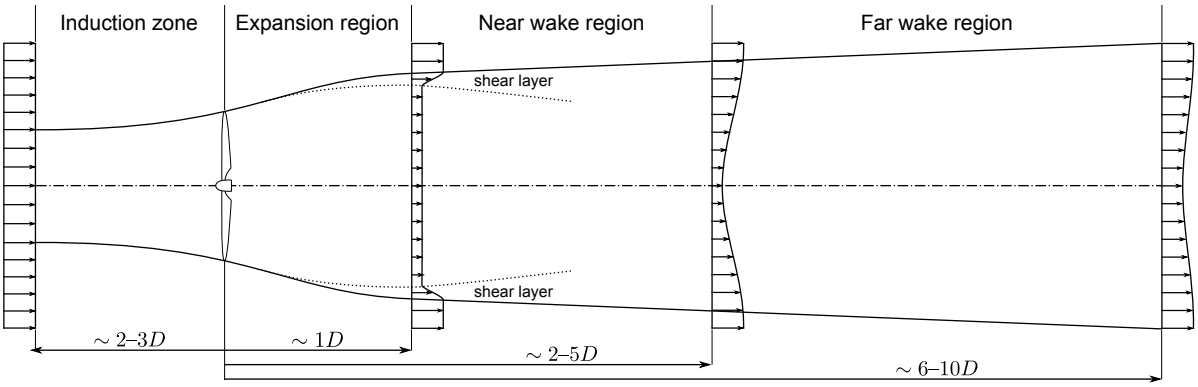

Figure 2.2: Anatomy of flow around a turbine [Figure by D.Allaerts]

The blockage is seen upstream of a wind turbine primarily due to the induction effects arising from the thrust generated by the turbine. As explained in previous sections, there is a drop in velocity and a resulting increase in pressure in the induction zone following the detailed theoretical background explained by Hansen, 2015 and Manwell et al., 2010 shown in Figure 2.2. Based on this the blockage effects can be classified into two types: 1. Turbine Scale Blockage and 2. Farm Scale Blockage. The critical details of physics and the behaviour of these blockage effects are presented in the following sections.

2.2.1. Turbine Scale Blockage

As mentioned on occasions within this report, turbine scale blockage is a phenomenon observed in the upstream. The thrust force exerted by the wind turbine on the flow causes the incoming wind to gradually decelerate resulting in a reduced velocity and increased pressure profile. This deceleration is also referred to as the induction from the turbine. This particular definition of induction zone effects on wind turbines/wind farms is given by Popescu and Flåtten, 2021 as well as Sommer, 2021. As noticed by Segalini and Dahlberg, 2019 and Medici et al., 2011 The understanding and quantification of this phenomenon becomes important especially during power curve measurements. The current techniques involves taking into account the free stream wind speeds considered for defining the power curve of a turbine based on field measurements is done based on the assumption that U_∞ measured by the met mast is the velocity experienced by the turbine as well. Nishino and Draper, 2015 numerical analysis showed that the blockage effects in a wind farm can be separated into two parts that is 'array-scale' and 'device-scale' which also compliments the fact that the blockage effects due to each individual turbine is equally very important.

Medici et al., 2011 conducted an experimental and numerical analysis of the wind turbine induction effects and found that the upstream effects of a wind turbine are more pronounced at about $95 - 98\%$ of the freestream wind speed at $2D$ distance away from the rotor and thus implying the importance of the local blockage effects. An analytical model developed by Segalini Segalini, 2021 also indicates a similar effect where a flow deceleration is observed in the turbine induction zone atleast 4 diameters in front of the turbine. However, the reduction is more pronounced at $0.955U_\infty$ and the effects start diluting farther upstream. As an extension of understanding these effects, the study by Forsting et al., 2016 compliments the observations and this analysis is done on the a complex terrain. Here it is observed that the induction zone is less affected by the surface conditions and more affected by the thrust of

the wind turbine. The induction zone was seen to be affected only at the region which is close to the surface. The induction zone also assumed the shape of the inflow rather than the shape of the terrain.

LES studies done by Sanchez Gomez et al., 2021 included the effects of different atmospheric stability on the blockage. There is also an extensive observations on the impact of the strength of the inversion layer on the effects of blockage and resulting velocity reduction. A strong free atmosphere stratification yielded a reduction of 1.18% and a weak stratification yielded a reduction of about 0.79% highlighting the importance of stability conditions for the blockage effects. This study ultimately concluded that blockage is aggravated by increasing stability conditions of the atmosphere. On the same lines to the research done here, very similar conclusions were drawn based on the studies done by Bleeg et al., 2018 and van Til, 2021.

The techniques and observations done in these studies are expected to be found in this study. More specifically the effects of stablity conditions on the magnitude of turbine scale blockage and also the extent to which the it is affected due to the presence of a hill.

2.2.2. Farm Scale Blockage

Now that the induction zone effects on an individual turbine scale is understood, it is important to shift focus towards the blockage effects on a wind farm scale. The wind farm scale blockage effect is attributed to different physical phenomena acting on the wind farm from each individual turbine to the mesoscale effects of the wind farm. More understanding of this effect is required to better estimate the energy production of a wind farm and reduce the uncertainties as much as possible.

Bleeg et al., 2018 as mentioned several times earlier in this report was the pioneering research on this concept. In this study, real wind farm data using two different at met masts at different distances upstream from the first row of turbines was conducted and compared to numerical simulations. Simulation results indicated that the front row of turbines experienced a velocity reduction by almost 3.2% and when the same front row simulated in isolation yielded a reduction of about only 1.2%. This clearly indicated that there exists a farm scale blockage and that the traditional 'wakes-only' approach is no longer valid due to the two-way interaction between the turbines within a given wind farm. Similarly, Segalini and Dahlberg, 2019 conducted an experimental and numerical analysis of these effects. They observed a similar behaviour and also gave rise to a new hypothesis about the impact of thrust coefficient. The simulations observed a higher impact due to blockage at thrust coefficients below rated wind speeds i.e. in the plateau of the thrust curve where there is highest induction. Branlard and Forsting, 2020 conducted a numerical analysis and a vortex model analysis of the blockage effects. They observed a wind speed reduction of about 2% in the upstream of about $2D$ from the front row of turbines. They also observed a relative error of about 0.2% between the numerical simulations and the vortex model. Nygaard et al., 2020, also observed a similar deficit in the wind speed in the upstream of the turbine and implemented a simple combined blockage and wake model to assess the two-way interaction of the wind turbines and finally correct the long standing 'wakes-only' approach for energy production estimation. All these authors observed that the induction effects were dominant at the centre of the row and least at the corner of the rows. A possible explanation for this was that the centre turbine has the highest effect of the cumulative induction from all turbines in the wind farm.

Some studies done recently have contradicted this proposition of the centre of the row having the least power production due to blockage and the corner turbines having the highest power production. This is specifically for single isolated row of turbines which are aligned closely. Nishino et.al. Nishino and Draper, 2015 observed this phenomenon by analysing the power coefficient of a single turbine and then increasing the number of turbines on either side of the isolated turbine. The power coefficient was seen to increase of the turbine in focus. The authors of Strickland and Stevens, 2020 also observed this effect and attributed it to the so-called Venturi effect. An infinite wind farm case (single row of turbines) yielded a $2-10\%$ increase in the power production in the middle of the row of turbines. McTavish et.al. conducted a wind tunnel experiment and also observed a similar increase of about $3-9\%$ in the middle of the row of turbines and saw reduction towards the corner edges of the row of turbines McTavish et al., 2015. Popescu et.al. Popescu and Flåtten, 2021 also observed an increase in the power production in the centre of the row compared to the corners. However, they attributed this effect to the increase in potential energy (pressure) for the central turbine while reducing kinetic energy (velocity). They also distinguished the effects for the wind farm blockage as line effect and row effect based on the influence of the induction zones from the turbines. This particular effect is of importance to this study because of the single row of tightly spaced turbines being considered.

All these studies have shown the effect of turbine spacing and wind farm layout to be an important factor for the magnitude of blockage and extent of velocity reduction. van Til, 2021 in his thesis found that the staggered layout had blockage losses of about 10% while aligned layout gave a loss of only about 3%. Similarly Bleeg et al., 2018, Segalini and Dahlberg, 2019, Strickland and Stevens, 2020 also showed similar effects where the staggered layouts had larger blockage effects implying that turbine scale induction zones have a stronger impact than farm scale induction zones.

Another most important aspect of wind farm blockage that needs proper understanding and more research is the effect of stability on blockage. Segalini and Dahlberg, 2019, the analytical model by Segalini, 2021 regard atmospheric stability as an important factor that influences blockage. Similar to wake effects resulting from stability conditions it only seems intuitive to consider that stable conditions aggravate blockage effects. Recent study by Gomez et.al. Sanchez Gomez et al., 2021 through their LES simulations showed that ABL height and the strength of the free atmosphere stratification had an impact on the blockage. This is complimentary to the findings from Wu and Porté-Agel, 2017 where a strong a stratification resulted in gravity waves being triggered from the top of the wind farm that convects all the way to the leading edge of the wind farm and created a high pressure region. Allaerts et.al. Allaerts and Meyers, 2018 also attributed the formation of atmospheric gravity waves to be a major cause for the upstream flow deceleration which is an implication of atmospheric stability. Thesis study by van Til, 2021 also attributes blockage to be a phenomenon affected by stability where the results showed the impact of very unstable and very stable conditions to have a strong impact on the magnitude of velocity reduction.

2.3. Summary

This chapter highlighted the outcomes of various studies in the recent past in order to provide a pretext to the formulated research objectives and questions. It included the influence of terrain complexities on ABL and consequently on wind farms. A specific detail was provided on the available literature regarding 2D hill simulations. An extension of this was the excitation of AGWs by topology and also due to wind farms. Lastly, a focus on effects of blockage was provided based on current literature. A clear distinction of the novelty of the current study over previous research is thus established.

3

Simulation Methodology

In order to obtain a prediction of the atmospheric flows in a wind farm, there are various methods implemented in the industry. There are typically four main methods used in the industry at the moment: 1. Analytical modelling 2. CFD modelling 3. Experimental analysis 4. Field measurements. Each of these techniques has certain advantages and disadvantages.

While CFD models provide the best possible accuracy, the downside is with the computational time and expenses. On the other hand analytical models are not the ideal case with the anticipated accuracy but give a good computational benefit. Field measurements are mainly performed for maintenance purposes and are not the ideal way to predict the entire flow field [Castellani et al., 2015]. In this thesis, CFD modelling approach is implemented considering the accuracy of the approach and affordable computational stress. This chapter elucidates the rationale behind using a URANS model to investigate the research question and the underlying governing equations required for numerically solving the flow cases. Details are also provided on the external forces such as Actuator Disk forces (implemented to represent wind turbine) and Damping Forces (implemented to tackle the spurious AGWs reflections) along with the way in which the blockage magnitude is computed.

3.1. Rationale behind RANS/URANS

Reynolds-Averaged Navier-Stokes (RANS) models are one of the most common turbulence closure models used to model ABL flows. The RANS models are known for relatively good accuracy and faster computation even at larger Re. Especially in comparison with LES and DNS, RANS closure models are known to provide better computational advantage [Pope, 2000]. However, RANS models are steady state models which do not consider the temporal changes in the flow which could potentially serve as a problem in certain flow cases. There are different approaches used to tackle the closure problem such as $k-\epsilon$, $RNGk-\epsilon$, $k-\omega$, $k-\omega SST$ among other variants formed in recent years. As an extension of this approach, the temporal changes can be modelled using the unsteady RANS ($uRANS$) models.

Bleeg et al., 2018 in their study implemented the $k-\epsilon$ RANS model and initially compared the results with on-field met-mast measurements. They concluded that RANS models provide results with good accuracy barring the skew in the observed measurements which the RANS models could not capture. However, it is also worth noting that, wind farm blockage is a phenomenon arising from two-way interaction between wind farms and the ABL. However, the study by Sessarego et al., 2018 used both RANS modelling and LES along with a comparison to field measurements. It was found that LES yielded better agreement with measurements than RANS. The mean power difference percentage was found to be around 20% for the RANS simulations while it was only around 7% for the LES simulations. The authors attributed this anomaly to the fact that RANS models are incapable of capturing the continuously changing wind speeds and wind directions within the wind farm. Avila et al., 2013, in their study found that the $k-\epsilon$ model in its standard form has a discrepancy in accurately defining a fixed mixing length for the ABL flows which resulted in deeper boundary layers having enhanced mixing and turbulence. An $RNGk-\epsilon$ was found to provide a faster convergence when compared to $k-\omega$ and standard $k-\epsilon$ in a study conducted by Castellani et al., 2015. However, this model does have its incapability in optimal modelling of the near wake flow field. Prospathopoulos et al., 2011 conducted

a study on the wake predictions of wind turbines using $k-\omega$ model. Neutral and stable atmospheric conditions were used to predict the wake velocity deficits in the regions near a wind turbine. The major issue they found was although the $k-\omega$ model performs very well for wall-bounded flows, there were significant under estimations in the near wake region. This was attributed to the fact that the blade and tip vortices create non-equilibrium flow conditions leading to an enhanced turbulence dissipation. In order to counter this problem, the authors also suggested several modifications to the standard model. Meyer Forsting et al., 2017 conducted a study of the upstream effects by applying CFD modelling and vortex modelling. The results showed that CFD models gave a better overall prediction and consistency when compared to the vortex model. This is a sensible deduction because vortex models are traditionally analytical models and lack physical accuracy.

Studies done by Castellani et al., 2015, Segalini, 2017 and Montavon et al., 2009 indicated that complex terrain also has an impact on the accuracy of the CFD models. This is because turbulence is a highly stochastic phenomenon and especially in complex terrains and the severe wind veer also gives a lower response time to the flows leading to higher uncertainties and inaccuracies in the flow prediction. However, Montavon et al., 2009 also showed that using $k-\epsilon$ model in complex terrains considered in their case which is the Black Law onshore wind farm to have shown good fidelity and modelling capabilities. The minor disagreement in certain regions of the flow was attributed to the simplified assumptions in modelling the wind turbine and the varying surface roughness changes.

Sivanandan, 2021 conducted a study of the AGWs resulting in a CNBL due to wind farm using uRANS as a precursor simulation. This was done to get a time-averaged solution as the inlet conditions to the domain using a steady solver. A similar study was conducted at DTU by Sommer, 2021 using RANS modelling on PyWake Ellipsys to assess the global blockage effects in wind farms. It was concluded that there was a very good agreement between the RANS simulation results with the LES results. The blockage phenomenon was examined using two conditions one is a flexible capping inversion and the other with a fixed one. In the case of the fixed capping inversion, the simulations showed very good agreement with LES results indicating time averaging is not an absolute necessity and the simulations with flexible capping showed minor discrepancies.

However, the studies mentioned earlier [barring the one by Sivanandan, 2021] did not specifically deal with the stability conditions and the resulting excitation of gravity waves. The behaviour of AGWs is an unsteady phenomenon and consistently alters the velocity and pressure fields in the domain. In this study, the hill and the turbine array are expected to excite gravity waves in the domain. Allaerts, 2016, Wu and Porté-Agel, 2017, Abkar and Porté-Agel, 2013 all conducted wind farm simulations involving stability conditions with an LES solver. This explains that the behaviour of AGWs keeps changing with time and attaining a stable solution for such cases requires simulations to run over a long period of time. However, LES simulations are computationally more expensive and time-staking. Owing to the limited time schedule, a solver with slightly lower fidelity than LES seems reasonable. The use of an unsteady solver might eventually leads to a quasi-steady state solution even with larger time iterations. However, owing to the computational constraints and reasonably good fidelity requirement an unsteady RANS solver is used in the present study.

3.2. Governing Equations

Fluid motion is governed by the Navier-Stokes equation which is based on Newton's II law of motion. Atmospheric flows specifically are governed by the compressible Navier-Stokes equation that describes a range of scales of motion. The length and time scales present in the atmosphere are large planetary scales [$\approx 10^5 km$], mesoscales [$\approx 5km$ to several 1000s of km] and the lowest dissipative scales of turbulence [$\approx 10^{-3} m$]. The compressible Navier-Stokes equation for governing the flow is given by -

$$\underbrace{\rho\left(\frac{\partial U}{\partial t} + U \cdot \nabla U\right)}_{\text{Inertia Forces}} = \underbrace{-\nabla p}_{\text{Pressure Forces}} + \underbrace{\nabla \cdot \left(\mu(\nabla U + (\nabla U)^T) - \frac{2}{3}\mu(\nabla \cdot U)I\right)}_{\text{Viscous Forces}} + F_{ext} \tag{3.1}$$

In Equation 3.1, U is the velocity field, p is the pressure field, ρ is the density of the fluid and μ is the dynamic viscosity of the flow. Inertia forces of the fluid are encompassed within the mass represented by the fluid density along with the temporal and spatial acceleration of the flow. On the RHS, pressure forces and viscous forces are expressed. External forces acting on the flow are depicted by buoyancy forces, turbine forces, and damping forces.

Apart from the momentum equation, the conservation of mass is governed by the continuity equation given by -

$$\frac{\partial \rho}{\partial t} + \nabla \cdot (\rho U) = 0 \tag{3.2}$$

The non-isothermal flow problems resulting from natural convection of the flow are given by the Boussinesq approximation. According to this approximation, the flow density ρ is responsible only to give rise to buoyancy forces (ρg) and is essentially negligible in the rest of the equation. This also implies that the density variations have no impact on the flow field.

By multiplying the inertia forces by a constant density term (ρ_0) and buoyancy treats density as a function of pressure and temperature, Equation 3.1 becomes -

$$\rho_0 \left(\frac{\partial U}{\partial t} + U \cdot \nabla U \right) = -\nabla p + \nabla \cdot (\mu(\nabla U + (\nabla U)^T)) - \frac{2}{3}\mu(\nabla \cdot U)I) + \rho g + F_{turb} + F_{damp} \tag{3.3}$$

The density term in the above equation is expressed as the sum of a reference fluid density (ρ_0) and a fluctuating component (ρ'). So the resultant momentum and continuity equations are as follows -

$$\underbrace{\frac{\partial(\rho_0 + \rho')U}{\partial t}}_{1} + \underbrace{\nabla \cdot ((\rho_0 + \rho')UU)}_{2} = -\nabla p + \nabla \cdot (\mu(\nabla U + (\nabla U)^T)) - \frac{2}{3}\mu(\nabla \cdot U)I) + (\rho_0 + \rho')g + F_{turb} + F_{damp} \tag{3.4}$$

$$\underbrace{\frac{\partial(\rho_0 + \rho')}{\partial t}}_{1} + \underbrace{\nabla \cdot ((\rho_0 + \rho')U)}_{2} = 0 \tag{3.5}$$

1 represents the temporal component and 2 represents the convective component of the inertia forces. Additionally, Boussinesq approximation treats density in the temporal term as a constant ($\rho = \rho_0$). Thus, the continuity equation further reduces to -

$$\nabla \cdot U = 0 \tag{3.6}$$

By substituting the reduced continuity equation into the momentum equation given by Equation 3.4 and assuming constant dynamic viscosity yields -

$$\rho_0 \left(\frac{\partial U}{\partial t} + U \cdot \nabla U \right) = -\nabla p + \mu \nabla^2 U + \rho g + F_{turb} + F_{damp} \tag{3.7}$$

Dividing Equation 3.7 by the reference density ρ_0 gives -

$$\left(\frac{\partial U}{\partial t} + U \cdot \nabla U \right) = -\frac{1}{\rho_0}\nabla p + \nu \nabla^2 U + \frac{\rho}{\rho_0} g + F_{turb} + F_{damp} \tag{3.8}$$

Now treating density as a function of changing temperature, the coefficient of thermal expansion needs to be introduced. A linearised version of this is given by -

$$\beta = -\frac{1}{\rho_0}\left(\frac{\partial \rho}{\partial T}\right) \approx \frac{1}{\rho_0}\frac{\rho - \rho_0}{T - T_0} \Rightarrow \rho - \rho_0 \approx -\rho_0 \beta (T - T_0) \Rightarrow \frac{\rho}{\rho_0} \approx [1 - \beta(T - T_0)] \tag{3.9}$$

Now the buoyancy term in Equation 3.8 is rewritten as -

$$\frac{\rho g}{\rho_0} = [1 - \beta(T - T_0)]g \tag{3.10}$$

Substituting Equation 3.10 into the momentum equation Equation 3.8 yields -

$$\left(\frac{\partial U}{\partial t} + U \cdot \nabla U \right) = -\frac{1}{\rho_0}\nabla p + \nu \nabla^2 U + [1 - \beta(T - T_0)]g + F_{turb} + F_{damp} \tag{3.11}$$

In the present study, since the buoyancy effects are significant. Therefore a governing equation for the potential temperature (θ) of the flow field needs to be solved. This is given by -

$$\frac{\partial \theta}{\partial t} = -\nabla \cdot u\theta + \nabla \cdot \kappa_{eff} \nabla \theta \tag{3.12}$$

κ_{eff} is the sum of the viscous and turbulent contributions of the thermal diffusion coefficient. Additionally, radiative and phase change heat transfer effects are assumed to be negligible.

3.2.1. Turbine Force

In this section, the most essential part of wind farm flow modelling is discussed which is modelling the forces induced by the turbine on the flow. The forces emerging from the turbine blades are input into the governing equations in terms of the body force terms in the Navier-Stokes equation. However, there are three ways in which a turbine can be modelled in a wind farm. The three models are: 1. Full blade resolved 2. Actuator Disk method (ADM) 3. Actuator Line method (ALM). Full-blade resolved rotor modelling is more complex and computationally expensive. Since the focus of this study is a mesoscale phenomenon on a wind farm scale, full blade resolution is redundant and out of the scope of this project. Therefore, a brief comparison of the other two methods is provided in this section.

In the actuator disk method (ADM), the averaged axial forces on the turbine is represented on the surface of the disk. Studies by Martínez et al., 2012 and Lavaroni et al., 2014 elaborate on the method in which the forces acting on a wind turbine are represented using an actuator disk. A standard actuator disk model uses the equivalent representative forces on a wind turbine is used on a circular disk with a given swept area. The AD has evenly distributed forces on the representative circular surface similar to that of a wind turbine. The disk behaves as a permeable membrane through and around which the flow passes modelled using RANS/uRANS techniques. Lavaroni et al., 2014 noted that this technique does not take into account the viscosity effects at the turbine/airfoil scale and is thus not modelled. Martínez et al., 2012 and Revaz and Porté-Agel, 2021 found standard ADM technique to show good agreement with LES/fully resolved simulations. An advanced version of this is the rotating ADM where the turbine is simulated as a porous disk that occupies a certain swept area. This swept area is discretised into a finite number of elements. Lift and drag forces on each of these elements are computed as shown by Martínez et al., 2012 and an average of these forces on the entire disk is used. The forces exerted by the turbine and the representation by actuator disk and actuator line methods are shown in Figure 3.1. The performance of this method was analysed by Revaz and Porté-Agel, 2021 using LES where it was shown that the ADM has a uniform force distribution over the surface of the disk. Martínez et al., 2012 in their research found that using this approach, the tip and root vortex structures are not created which leads to some discrepancies in the obtained results.

In the actuator line method, instead of taking the actuator disk approach, each blade is discretised into elements. The lift and drag forces are computed based on the local flow parameters based on the description by Martínez et al., 2012. This model however is shown to give good predictions of the root and tip vortices. Therefore, the performance is seen to be very good in the near-wake region as well. There is another observation made that the velocity is higher in the center of the wake because of the exclusion of hub and nacelle made by Martínez et al., 2012 and Revaz and Porté-Agel, 2021.

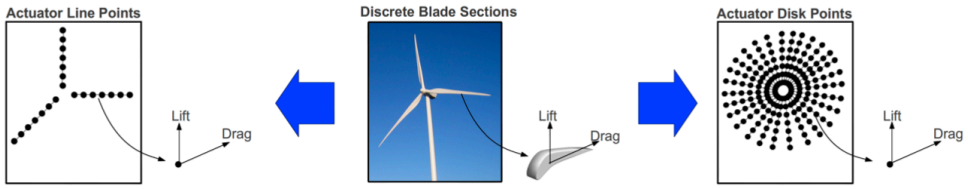

Figure 3.1: Representation of the rotating ADM and ALM approach Martínez et al., 2012

Martínez et al., 2012 also provided a comparison of the computational expense of each of these models. If the focus of the study is the far wake then the ADM approach gives the computational advantage whereas the tip and root vortices modelling in the ALM approach is a tedious process. If the field of interest is in the near wake region then the ALM approach is more suitable. However, in the

present study, the focus is on the upstream of the turbines and therefore the ADM model seems like a good option.

In order to estimate the magnitude of blockage in a wind farm, the wake effects of the turbine or the root and tip vortex effects are not of paramount importance. Therefore, using an actuator disk model representative of the external turbine forces F_{turb} seems to be a reasonable simplification. Besides, all the previous work done on wind farm blockage by Bleeg et al., 2018, Bleeg and Montavon, 2022, Segalini and Dahlberg, 2019 seems to yield a reasonably good representation of the wind farm upstream effects.

In this study, the classical actuator disk approach is used from the available ADM modules in OpenFOAM6. In this case, the Actuator Disk is defined as a non-rotating fixed cylinder with a given rotor radius, thickness and followed by the rotor swept area. A schematic representation of an actual wind turbine as an Actuator Disk is shown in Figure 3.2. The AD model also requires a user-defined power coefficient (C_P) and thrust coefficient (C_T) which in turn mimics the thrust force induced by the wind turbine on the freestream wind.

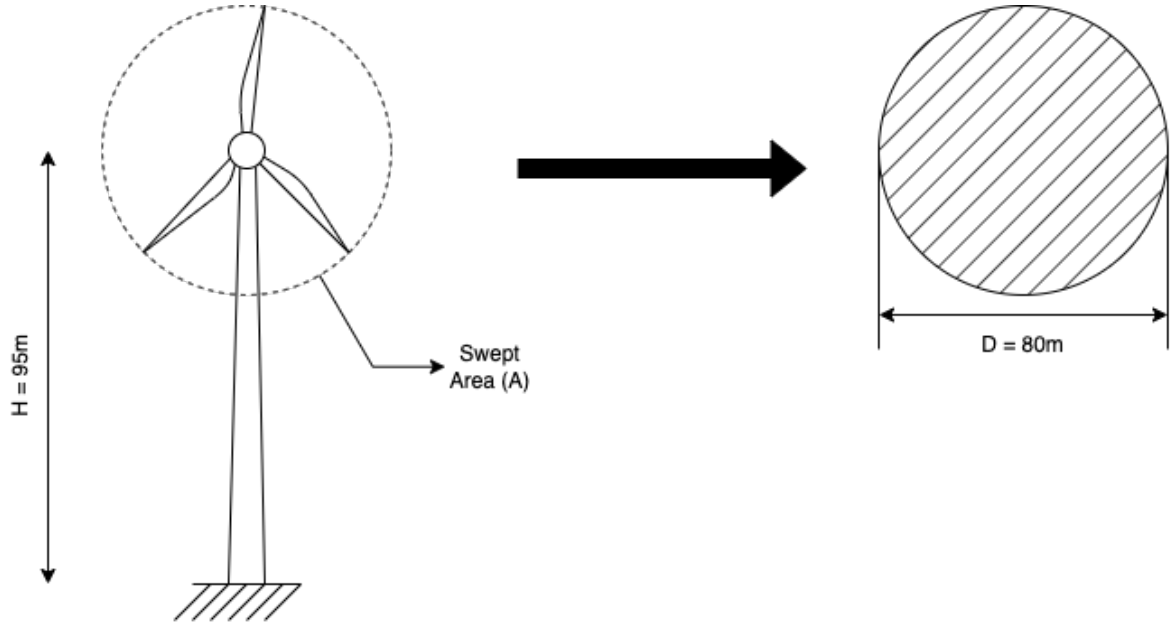

Figure 3.2: Representation of a Wind Turbine as an Actuator Disk

The force contribution F_{turb} in the momentum equation given by Equation 3.11, is estimated based on the thrust exerted by the actuator disk at a given velocity and at a given position in the wind farm. The simplification of a turbine force into an actuator disk force is explained by Bastankhah et al., 2021 and is mathematically given by -

$$F_i = \frac{T_i}{\rho \pi R^2} \Delta(x - x_i) H(R^2 - [(y - y_i)^2 + (z - z_i)^2]) \tag{3.13}$$

Here, T_i is the thrust force at a given turbine location and x_i, y_i and z_i are the coordinates of that specific turbine. R is the disk radius and H is a Heaviside step function. Further details of Equation 3.13 are beyond the scope of this work.

However, in OF6, the implementation of the thrust force exerted by the Actuator Disk is based on the freestream velocity at a certain point given in the far upstream location. It is highly important that the reference velocity is free of disturbances due to the terrain or due to the turbine itself. The method implemented in this study is expected to have minor discrepancies as the Blade Element Momentum Theory is not used to obtain the overall thrust forces exerted by the actuator disk on the flow as explained in detail in Supreeth, Arokkiaswamy, Raikar, Prajwal, et al., 2019, Supreeth, Arokkiaswamy, Raikar, and H. P., 2019 and Supreeth et al., 2021.

The disk-based approach has been extensively used by a lot of wind energy researchers all these years by Allaerts, 2016; Branlard et al., 2020; Wu and Porté-Agel, 2017. In the present study, a Ves-

tas V80-2MW turbine is used bearing a rotor diameter of $80m$ and a hub height of $95m$ as shown in Figure 3.2. The detailed specification of the turbine being used is taken from the work done by Mokhi and Addaim, 2020 and summarised in Table 3.1.

Parameter	Value
Diameter (D)	$80m$
Hub Height (H)	$95m$
Rated Power (P)	$2MW$
Cut-in Wind Speed (V_{in})	$3ms^{-1}$
Cut-out Wind Speed (V_{out})	$25ms^{-1}$
Power Coefficient (C_P)	0.4
Thrust Coefficient (C_T)	0.8

Table 3.1: Wind Turbine Specifications

This study is conducted at a free stream wind speed of $U_0 = 10ms^{-1}$. Therefore, the turbine is supposed to be operating below the rated wind speed where the thrust coefficient remains constant. From Figure 3.3, it can be seen that at the given free stream wind speed, the design thrust coefficient is 0.8. . Additionally, the effects of tower shadow are not considered in this thesis.

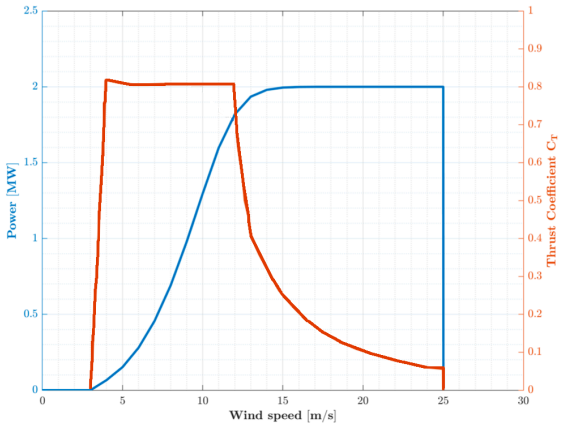

Figure 3.3: Power Curve and Thrust Coefficient Curve of Vestas V80-2MW Turbine. Figure reproduced from Mokhi and Addaim, 2020

3.2.2. Damping Force

As explained in Chapter 2, AGWs are triggered by virtue of a wind farm. However, in the present study, a two-dimensional hill of a certain height and half width triggers AGWs of higher wavelength and intensity. Since the case study is on a row of turbines on top of a hill, the AGWs are triggered by virtue of both the hill and the wind farm. However, the hill plays a vital role in assisting the conditions necessary for triggering the vertically growing waves. Once the flow enters the domain and encounters the hill, waves are generated in the free atmosphere due to strong stability conditions. Modelling of AGWs have remained a challenge in wind farm simulations mainly due to the spurious reflections from the domain walls. Studies by Allaerts, 2016, Wu and Porté-Agel, 2017 and Sivanandan, 2021 have explicitly examined and worked around ways to tackle the numerical problem caused by the reflection of gravity waves. The AGWs triggered propagate upwards as well as downwards and as they approach the domain walls, get reflected and compromise the fidelity of the model.

In order to solve this issue numerically, damping layers are to be introduced on the different boundaries. These damping layers are designed in such a way that the gravity waves are absorbed due to the synthetically induced diffusion in both vertical and horizontal directions. The damping layers (also known as Sponge Layers) are added to the actual domain size. Klemp and Lilly, 1977 was a pioneering study on predicting the vertical wavelength of gravity waves triggered by a hill. In order to mitigate the reflection issues arising from the downward convecting waves, the authors found the depth of the damping layer to be of the same order of magnitude as the vertical wavelength of the waves.

The Rayleigh damping is imposed in the form of an external force F_{damp} in the momentum equation as in Equation 3.11. The expression for the damping force is as follows -

$$F_{damp} = d(U_{ref} - U) \tag{3.14}$$

d in Equation 3.14 is the local damping coefficient within the layer based on the local velocity and follows a cosine function.

$$d = \frac{d_{max}}{2}\left(1 - f \cdot \left(\Pi \frac{z - z_{start}}{w}\right)\right) \tag{3.15}$$

In Equation 3.15, z_{start} is the point at which the Rayleigh damping layer starts. d_{max} is the maximum amplitude of the damping coefficient which is $0.025s^{-1}$ and w is the thickness of the damping layer.

The vertical wavelength of the gravity waves based on Allaerts, 2016 and Klemp and Lilly, 1977 is mathematically defined as -

$$\lambda_z = \frac{2\pi U}{N} \tag{3.16}$$

Here, N is the Brunt-Väisälä frequency. For the current case, the free atmosphere lapse rate 0f $1K/km$ theoretically yields a vertical wavelength of around $6.3km$. On the other hand, Lu and Porté-Agel, 2011 and Abkar and Porté-Agel, 2013 used a $300m$ damping layer without a specific mention of the damping coefficients. For the present case study, this does not seem to be a feasible solution as it is more suitable for a small wind farm case and not with complex terrain. Sivanandan, 2021 used a $5km$ thick damping layer with a damping coefficient of $0.1s^{-1}$ for a RANS simulation. Gadde and Stevens, 2019 also used a damping layer of $1km$ with a damping coefficient of $0.016s^{-1}$ again for an LES study of a wind farm and not with complex terrain.

On the other hand, Hills and Durran, 2012 imposed a $16km$ thick damping layer with a damping coefficient of $0.005s^{-1}$ for a flow over the three-dimensional hill. The case of Haupt et al., 2019 of flow simulations over a $100m$ tall hill is the closest case to the present study wherein a damping layer of $5km$ with a damping coefficient of $0.005s^{-1}$ is used. The authors also noticed that having a damping layer in all of the domain boundaries better models the spurious behavior of the AGW reflections instead of just at the top boundary. This method considerably shortens the physical domain. However, LES cases are always different from the setup of a RANS case. Therefore, a careful comparison of the various cases is made by using a $10km$ damping layer on all the boundaries with a damping coefficient of $0.025s^{-1}$.

3.3. Unsteady Reynolds-Averaged Navier Stokes Equations

The momentum equation is shown earlier in this Chapter, in Equation 3.11. It was established by Irish mathematician, Osborne Reynolds, that an instantaneous fluid property can be decomposed into a time-averaged component and fluctuating components. In this case particularly, the instantaneous flow velocity U is decomposed into a time-dependent mean velocity component $\overline{U}$ and fluctuating component u'. More specifically given by -

$$U(x, y, z, t) = \overline{U}(x, y, z, t) + u'(x, y, z, t) \tag{3.17}$$

Every term in the momentum equation is therefore decomposed into the mean and fluctuating terms. This is done following the decomposition properties of mean and fluctuating components of velocity and the derivation of the RANS equations is explained in detail by Pope, 2000. Applying the properties of Reynolds averaging to the momentum and continuity equation of fluid flow, the X, Y, and Z momentum equations in RANS form are derived as follows -

$$\frac{\partial \overline{U}}{\partial t} + \overline{U}\frac{\partial \overline{U}}{\partial x} + \overline{V}\frac{\partial \overline{U}}{\partial y} + \overline{W}\frac{\partial \overline{U}}{\partial z} + \frac{\partial \overline{u'u'}}{\partial x} + \frac{\partial \overline{v'u'}}{\partial y} + \frac{\partial \overline{w'u'}}{\partial z} = -\frac{1}{\rho_0}\frac{\partial p}{\partial x} + v\nabla^2\overline{U} + F_{\text{ext}} \tag{3.18}$$

$$\frac{\partial \overline{V}}{\partial t} + \overline{U}\frac{\partial \overline{V}}{\partial x} + \overline{V}\frac{\partial \overline{V}}{\partial y} + \overline{W}\frac{\partial \overline{V}}{\partial z} + \frac{\partial \overline{u'v'}}{\partial x} + \frac{\partial \overline{v'v'}}{\partial y} + \frac{\partial \overline{w'v'}}{\partial z} = -\frac{1}{\rho_0}\frac{\partial p}{\partial y} + v\nabla^2\overline{V} + F_{\text{ext}} \tag{3.19}$$

$$\frac{\partial \overline{W}}{\partial t} + \overline{U}\frac{\partial \overline{W}}{\partial x} + \overline{V}\frac{\partial \overline{W}}{\partial y} + \overline{W}\frac{\partial \overline{W}}{\partial z} + \frac{\partial \overline{u'w'}}{\partial x} + \frac{\partial \overline{v'w'}}{\partial y} + \frac{\partial \overline{w'w'}}{\partial z} = -\frac{1}{\rho_0}\frac{\partial p}{\partial z} + v\nabla^2\overline{W} + F_{\text{ext}} \tag{3.20}$$

Now from Equation 3.18, Equation 3.19 and Equation 3.20 it can be observed that the left-hand side of the equations with the fluctuating velocity components give rise to the closure problem. The closure problem occurs due to the fact that there are more unknowns than the number of equations. Therefore, a direct solution can not be obtained. There are several techniques such as algebraic one-equation models or two-equation models used. In this thesis, turbulence closure is achieved by using a $k-\epsilon$ model containing two transport models for turbulent kinetic energy (k) and turbulent dissipation rate (ϵ). The rationale behind choosing this particular model is explained earlier in this section. On the other hand, $k-\epsilon$ models are widely used for research related to ABL flows and wind farm simulations. The turbulence transport equations for k and ϵ are shown below.

$$\frac{\partial k}{\partial t} = B + P - \epsilon + \frac{\partial}{\partial z}\left(\frac{\nu_t}{\sigma_k}\frac{\partial k}{\partial z}\right) \tag{3.21}$$

$$\frac{\partial \epsilon}{\partial t} = \frac{\epsilon}{k}(C^*_{\epsilon 1}P - C_{\epsilon 2}\epsilon + C_{\epsilon 3}B) + \frac{\partial}{\partial z}\left(\frac{\nu_t}{\sigma_\epsilon}\frac{\partial \epsilon}{\partial z}\right) \tag{3.22}$$

In Equation 3.21 and Equation 3.22, $C_{\epsilon 1}$, $C_{\epsilon 2}$ are model specific coefficients and σ_k and σ_ϵ are Schmidt numbers for k and ϵ respectively. The values of these model coefficients used for this particular study are given in Table 3.2. Also, B and P are rates of buoyancy and rate of shear production for TKE.

Coefficient	Value
$C_{\epsilon 1}$	1.52
$C_{\epsilon 2}$	1.833
$\sigma_{\epsilon 2}$	2.95
σ_k	2.95
C_μ	0.03

Table 3.2: $k-\epsilon$ Model Coefficients based on Sanz Rodrigo et al., 2017

Apart from the model coefficients mentioned in Table 3.2, there is a Eddy viscosity term (ν_t) which is very important to define the turbulence in the fluid flow domain. This term is defined as follows -

$$\nu_t = C_\mu \frac{k^2}{\epsilon} \tag{3.23}$$

3.4. Blockage Magnitude

Unlike most engineering wake models, the blockage magnitude in the induction region of a wind turbine/wind farm can not be estimated directly. Therefore, the results from the numerical simulations are required to be represented as a function of a physical parameter - Velocity (U), Static pressure (P) or power production. Since the underlying physics behind blockage effects is not completely understood, there are no prescribed standard ways to estimate these effects. A meticulous analysis of available research is carried out to implement an optimal way of quantifying the blockage magnitude.

Bleeg et al., 2018, used met mast measurements as well as simulation results of velocity field before and after commissioning of the wind farm. Studies done by Medici et al., 2011, Segalini and Dahlberg, 2019 and Nygaard et al., 2020 estimated blockage directly by the difference in velocity fields with and without the presence of the turbines. However, by doing this, the apparent impact of turbine scale blockage as opposed to farm scale blockage cannot be differentiated. In order to differentiate between the turbine scale and farm scale blockage effects comparison of power production by a wind farm is compared with that of an isolated turbine. Studies done by Forsting and Troldborg, 2015, Popescu and Flåtten, 2021 and Strickland and Stevens, 2020 implemented this methodology.

However, for the present case, it is deemed appropriate to implement part of the methodology as described in Bleeg et al., 2018 and Medici et al., 2011. The velocity fields are first obtained for cases without a turbine array (U_{before}) and then for cases with the turbine array (U_{after}). The difference in velocity fields as shown in Equation 3.24 yields percentage reduction due to the induction effects.

$$\Delta U = \frac{U_{after} - U_{before}}{U_{ref}} \times 100 \tag{3.24}$$

Now in order to isolate the effects of the hill and quantify the impact on blockage due to the hill, the difference in velocity fields is estimated. First, velocity reduction for a turbine array on a hill (ΔU_{hill}) is obtained followed by the velocity reduction for a turbine array on a flat terrain (ΔU_{flat}). The difference in the velocity reduction for these two cases isolates the effects caused by the hill.

$$\Delta U_{eff} = \frac{\Delta U_{hill} - \Delta U_{flat}}{U_{ref}} \times 100 \tag{3.25}$$

It is important to note that, $\Delta U_{eff} < 0$ implies that the blockage caused on a flat terrain is higher than the blockage caused in a hilly terrain. On the other hand, $\Delta U_{eff} > 0$ implies that the blockage caused on a hilly terrain is higher than that caused on a flat terrain.

3.5. Summary

In this chapter, methodology implemented in the current study was introduced. Firstly, a brief overview of RANS/URANS techniques used for wind farm simulations was provided. Secondly, the governing equations involved in the current study with the Navier-Stokes equation along with external body forces such as turbine and damping forces were highlighted. Thirdly, the modification to the Navier-Stokes equation by Reynolds averaging and the $k-\epsilon$ modelling techniques were explained. Lastly, an account on the ways in which blockage magnitude is computed in the present study in comparison to existing literature is presented.

4

Simulation Setup

Once the methodology of the simulation is explained and understood, it is now important to shift the focus to the specification of the domain for the numerical simulation. In this chapter, the dimensions of the fluid flow domain, and initial and boundary conditions necessary to model the fluid flow are discussed. The present research is done using the open source software `OpenFOAM`. The details of the solver used along with the different utilities are also elaborated.

Specific details are also provided on the different sensitivity studies that are conducted in this research. Primarily, the blockage magnitude is computed for cases with different hill heights and half widths that account for different hill sizes (S_h). On the other hand, in order to answer the research questions mentioned earlier, studies are also done for different inter-array spacing. The domain setup for all of the baseline cases along with all the modified cases is discussed in detail in the following section.

4.1. Domain Specifications

In this section, the case setup is discussed in detail. The domain characteristics need to be in such a way that the flow physics is accurately captured. Domain constraints are set in such a way that the different physical phenomena arising firstly due to the hill and also due to the presence of the turbine are satisfied. Based on the findings from previous studies done by Allaerts, 2016, Bleeg et al., 2018, Ollier et al., 2018, Bastankhah et al., 2021 and Hills and Durran, 2012 the different phenomena that are expected to be observed in the present study are as follows -

1. Temperature stratification in the domain leading to a stable free atmosphere has an effect on the flow field.
2. Presence of the hill in a stable atmosphere triggers AGWs
3. Vertical propagation of the AGWs towards the top of the domain triggered by the hill as well as the wind farm.
4. Vertically propagated waves are also found to be advected downstream on the leeward side of the hill and in the wake of a wind farm.
5. Studies also show that perturbations caused by the AGWs are also observed a few kilometers upstream of the hill/wind farm.
6. Wind turbine wakes that propagate several diameters downstream.
7. Upstream effects of the turbine induction zone that causes blockage.

In order to account for the physics of the flow, it is necessary for the domain to be long enough both in the upstream as well as downstream directions. Additionally, the domain also has to be tall enough to account for the vertically propagating waves. In the present study, the domain is defined in a similar manner to the studies by Allaerts, 2016 and Allaerts and Meyers, 2018.

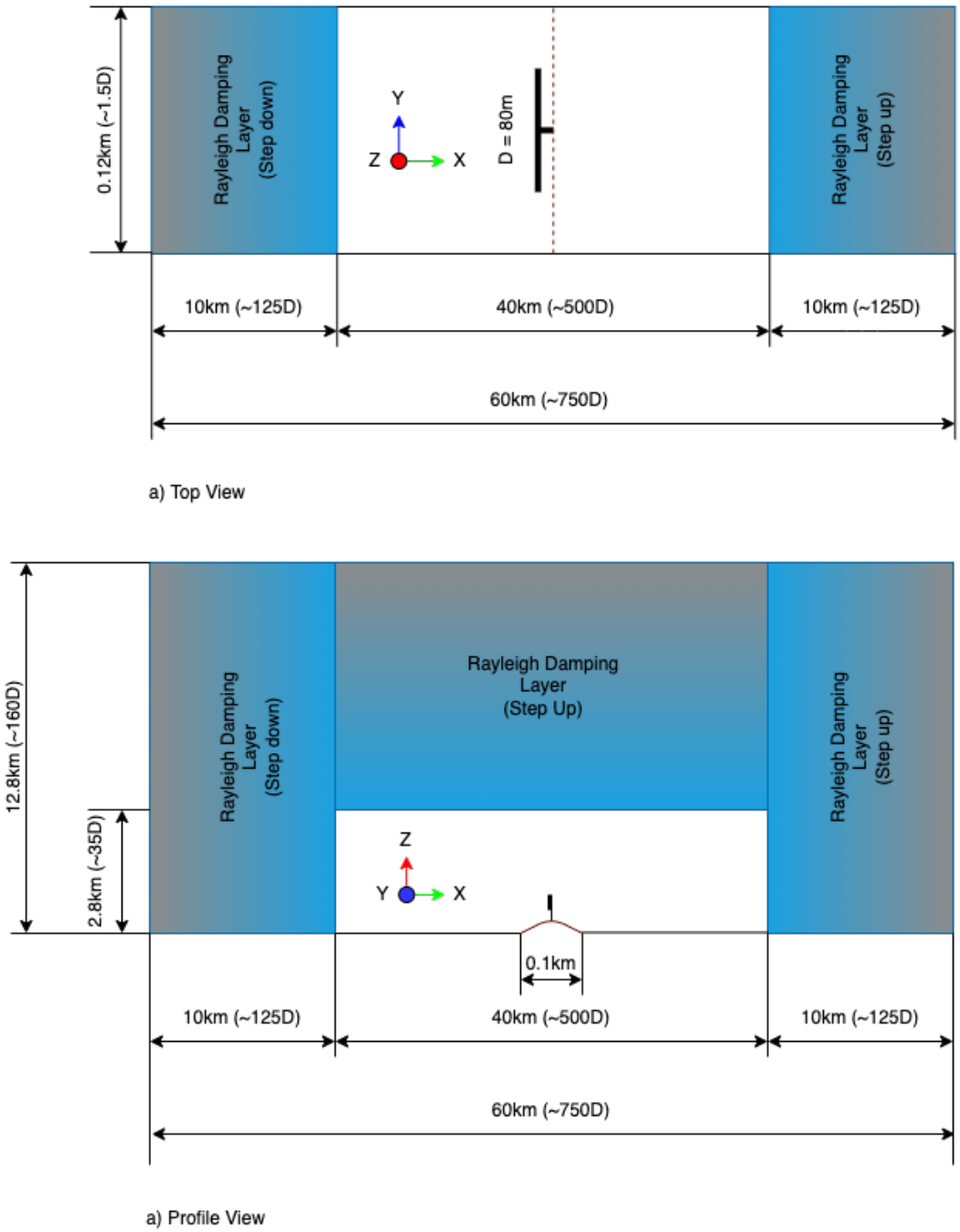

Figure 4.1: Planar view of the flow domain with a slice at the hub height on the XY plane to obtain the top view and a slice at centre of the actuator disk along the XZ plane to obtain the profile view.

As shown in Figure 4.1, the domain dimensions are $60km$ in the streamwise direction (X axis), $12.8km$ in the vertical direction (Z-axis), and $0.12km$ in the spanwise direction (Y-axis). The short spanwise length is representative of the spacing between the turbines and essentially makes the simulation computationally less expensive. Additionally, since the current study is to analyse and understand the behaviour of blockage for a case with a single row of turbines, this seems to be a reasonable choice. The domain also contains the hill at the center of the domain upon which a turbine is located. In accordance with the turbine specifications mentioned in Chapter 3, the diameter of the actuator disk is chosen to be $80m$.

Figure 4.1, also shows the Rayleigh damping layer implemented to model the damping forces as

explained in Chapter 3. As mentioned earlier, there is very little literature available on the damping characteristics that need to be implemented for the present problem. However, based on the guidance provided by Allaerts, 2016, Gadde and Stevens, 2019 and Sivanandan, 2021 a damping layer thickness of $10km$ is implemented at the inlet, outlet, and the top boundaries. The more challenging aspect of modelling a complex terrain with stable stratification is avoiding the spurious reflections from the domain walls is the damping coefficient. After a series of trials and errors, a suitable damping coefficient of $0.025s^{-1}$ is chosen for the present study.

The studies mentioned in Chapter 3, such as Allaerts and Meyers, 2017 and Klemp and Lilly, 1977 damp out the spurious reflections from domain walls by implementing a uniform damping throughout. However, in the present case, a configuration similar to the one implemented by Sivanandan, 2021 is used. Depending on the wall at which the damping layer is placed, a step-up or a step-down configuration is implemented. A step-down configuration is used at the inlet while the other two boundaries, use a step-up configuration. The location of the damping layer drives the configuration of the damping region.

In `OpenFOAM`, the domain of interest is developed using the `blockMeshDict` utility. The first block is up to a vertical distance of $300m$, there on the second block extends up to $2800m$ and the last block extends for the last $10000m$. An empty domain with hexahedral cells is created using the `blockMeshDict` utility with a suitable resolution to appropriately capture the flow physics. However, in order to have the features of the hilly terrain in the domain, another `OpenFOAM` utility `moveDynamicMesh` is used. First, the terrain is created in stl format with a certain hill height and hill width and then, the stl mesh is moved into the empty block using the `moveDynamicMesh` utility. This particular step in the domain formation helps in avoiding the high skewness of the cells surrounding the hill and also reduces the non-orthogonality of the mesh. A high cell skewness and non-orthogonality lead to divergence of the solution. The use of open source software with a wide range of functionalities is a powerful tool in carrying out CFD simulations on the simplest of cases to the most complex cases.

At the vertical extremes where the damping layer is placed, the mesh is made coarser. This is in line with the studies by Wu and Porté-Agel, 2017, Allaerts and Meyers, 2017, Sivanandan, 2021. It is shown that the damping layer performs well with coarse mesh resolution thereby giving an advantage with computational time. The bottom-most block consists of both the hill and the actuator disk which therefore requires a higher mesh resolution in all directions. The main driving parameters of a certain mesh resolution choice are as follows -

1. Presence of the hill on the lower wall resulting in a flow speed up.
2. Actuator disk on the lower wall which results in additional modelling of wake as well as the induction zone.
3. Combined induction effects and AGW effects caused by the hill and the turbine.

Prospathopoulos et al., 2011 performed RANS simulations to assess wind turbine wake properties. The authors employed a mesh resolution of $\Delta x = 12m$, $\Delta y = 9m$, and $\Delta z = 10m$ and found that modelling actuator disks in RANS simulations yielded reasonably good results. Ollier et al., 2018, with a study of a ridge and a wind farm very similar to the present case implemented a $2m$ mesh resolution at the bottom wall. The authors had 32 levels of increasing mesh resolution with a geometric progression. A comparative study between actuator disks and a fully resolved rotor case, Stergiannis et al., 2016 conducted a mesh convergence study involving a range of cells from very fine to very coarse. The authors chose a domain size of $1150mmX2700mmX1654mm$ with a range of mesh of 0.67 million, 2.91 million, 11.9 million and 92.6 million cells. It was concluded that for the area of interest in the far wake or in the upstream, very fine mesh resolution would be computationally redundant. A moderately fine mesh with 14 million cells throughout the domain with a refinement in the AD region yielded good confirmation with the fully resolved rotor case. In the case of LES studies for a three-dimensional hill and with the case of a turbine Liu and Stevens, 2021 implemented a mesh with $5.6m$ resolution in all directions. However, as one may be aware, RANS simulations are far less computationally expensive, and therefore slightly decreasing the resolution would still yield reasonable results. In support. of this argument, Sivanandan, 2021 used a mesh resolution of $12mX12mX12m$ resolution at the location of the AD and a much lower resolution further upwards where the damping layer is placed.

Based on the literature, the bottom-most block of the domain with a resolution of $\Delta x = 10m$, $\Delta y = 8m$, and $\Delta z = 10m$ in the streamwise, spanwise, and vertical directions respectively is created. The

second block has a mesh resolution of $\Delta x = 20m$, $\Delta y = 8m$ and $\Delta z = 40m$. The third block being only the damping layer in the domain the mesh is made much coarser with a resolution of $\Delta x = 40m$, $\Delta y = 8m$, and $\Delta z = 160m$. The variation in the streamwise and vertical resolution of the top blocks is to further optimise the computational time of the simulations. The domain specification are further explicitly explain in Table 4.1.

Domain Specifications	
Domain Size	L_x x L_y x L_z = 60 x 0.12 x 12.8km
Vertical Grid Resolution	N_{z_1} = 30, z_1 = 10m
	N_{z_2} = 63, z_2 = 40m
	N_{z_3} = 63, z_3 = 160m
Horizontal Grid Resolution	N_{x_1} = 6000, x_1 = 10m
	N_{x_2} = 3000, x_2 = 20m
	N_{x_3} = 1500, x_3 = 40m
Lateral Grid Resolution	N_y = 15, y = 8m

Table 4.1: Setup of the computational domain

4.1.1. Sensitivity to Inter-array Spacing

The first set of simulations of the hill in a stable free atmosphere and a truly neutral atmosphere are performed on the domain dimensions as mentioned in the previous section. The turbine spacing is replicated based on the studies done by Bleeg and Montavon, 2022. Initially, the spacing is set at 1.5 times the diameter of the disk which yields a numerical value of $120m$. Strickland and Stevens, 2020 also analysed the blockage effects on a single row of turbines with different spacing and initially starting with a spacing of $1.5D$.

Numerical simulation studies done by Forsting and Troldborg, 2015, Meyer Forsting et al., 2017, Segalini and Dahlberg, 2019, Bleeg and Montavon, 2022 found that the blockage magnitude is sensitive to the spacing between turbines, especially for a single row of laterally spaced turbines. Therefore, as a part of one of the Research questions mentioned earlier, it would be interesting to know the change in blockage magnitude along with the effects of the hill. A sensitivity study is done for a range of turbine spacing distances based on the studies done by Segalini and Dahlberg, 2019, Strickland and Stevens, 2020 and Bleeg and Montavon, 2022.

Cases	**Spacing (Δ_y)**	**Distance [in km]**	**Dimensions (X x Y x Z) [in km]**	**Resolution (Δx x Δy x Δz) [in m]**
Baseline Case (Case I)	1.5D	0.12	60 x 0.12 x 12.8	10 x 8 x 10
Case II	2D	0.16	60 x 0.16 x 12.8	10 x 8 x 10
Case III	2.5D	0.2	60 x 0.2 x 12.8	10 x 8 x 10
Case IV	3D	0.24	60 x 0.24 x 12.8	8.5 x 8 x 10

Table 4.2: Sensitivity study cases with different inter-array spacing and the corresponding mesh resolution

Table 4.2 shows the different Cases of the inter-array spacing considered in this study. For each of the cases, the dimensions of the domain need to be altered to accommodate for the lateral spacing between the turbines. As shown in the table, the streamwise and vertical dimensions of the domain remain unaltered. Along with the alterations in the lateral spacing of the domain, there is an increase in the number of cells in the lateral direction in order to maintain the same mesh resolution.

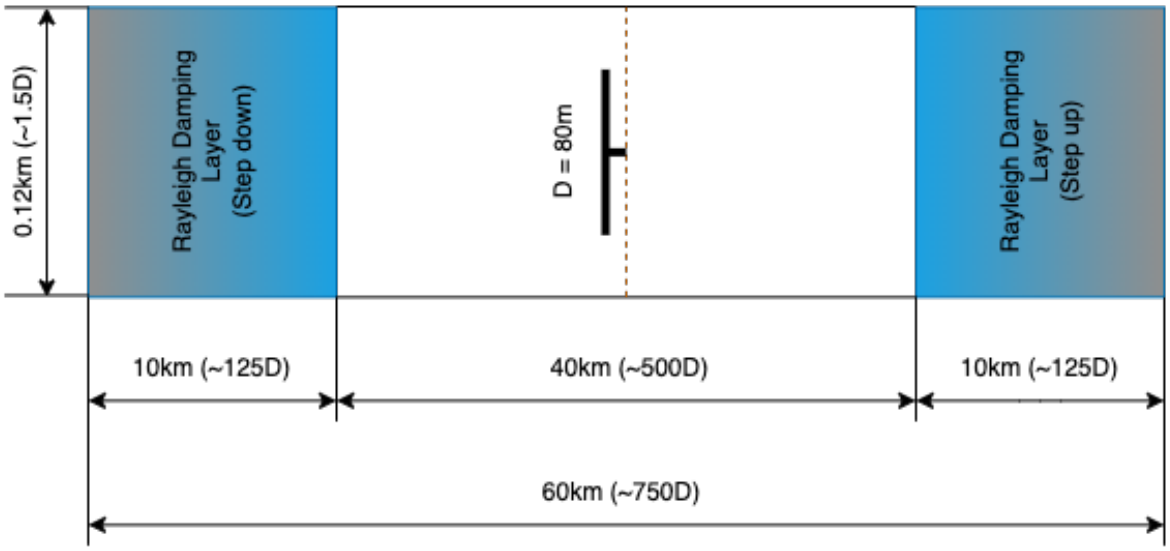

Figure 4.2: Case I: Top view of the flow domain along the XY plane at hub height with an inter-array spacing of 1.5D

Figure 4.2 shows the placement of the actuator disk and the spacing in the lateral direction. The lateral spacing of the wind farm in this particular case is $1.5D$ and forms the baseline case for all comparisons in this study. As part of the main research question of this study, this particular case also answers the question of the effect of blockage due to the tightly spaced infinite array of turbines on top of a hill.

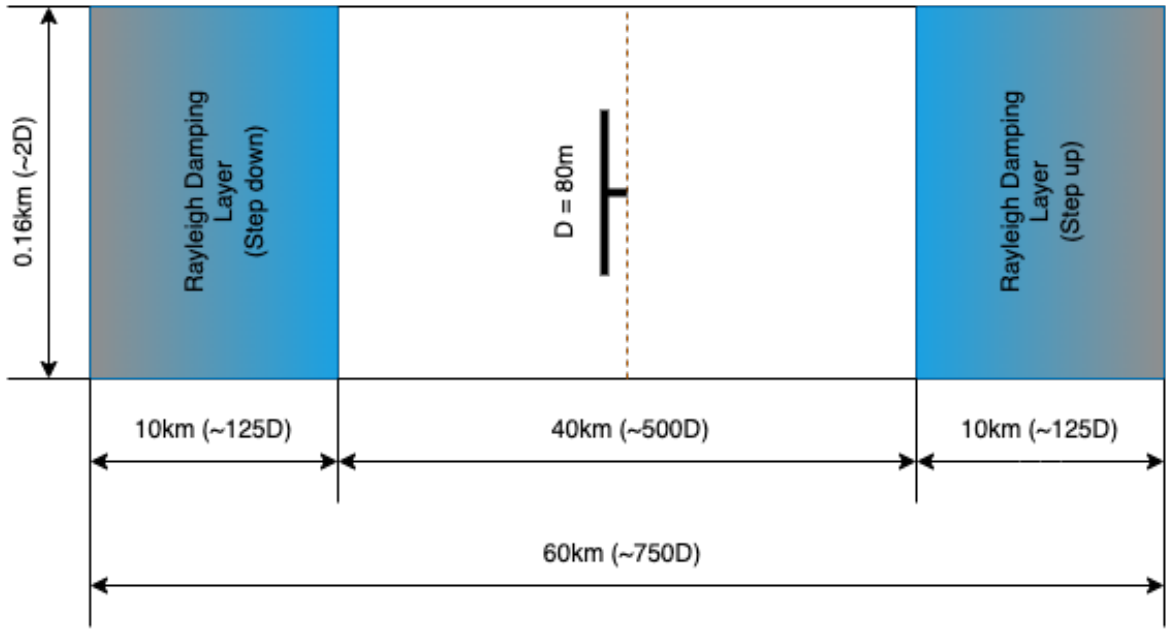

Figure 4.3: Case II: Top view of the flow domain along the XY plane at hub height with an inter-array spacing of 2D

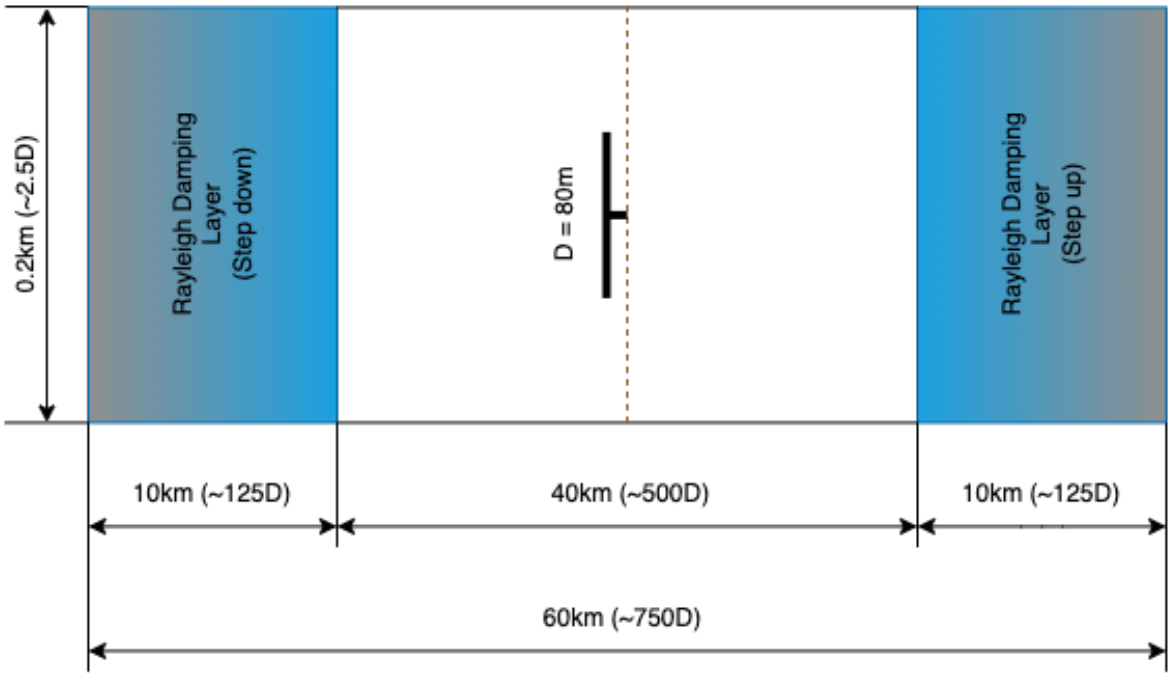

Figure 4.4: Case III: Top view of the flow domain along the XY plane at hub height with an inter-array spacing of 2.5D

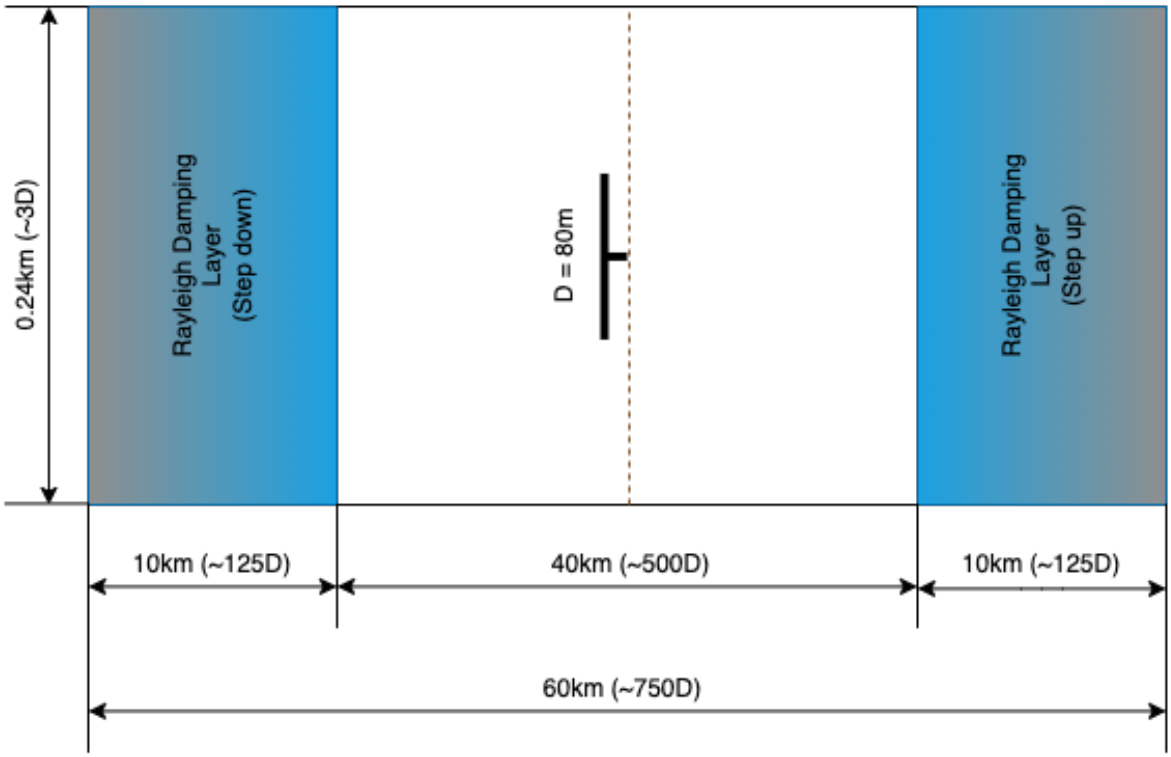

Figure 4.5: Case IV: Top view of the flow domain along the XY plane at hub height with an inter-array spacing of 3D

Subsequently, an analysis of blockage magnitude is done for different spacing. In the present study, an assumption of an infinite lateral array is made. The spacing of the lateral domain walls

accurately represents the spacing between the turbines within the single row. For this purpose, the same streamwise and vertical lengths as that of the baseline case are retained. Experimental analysis by McTavish et al., 2015 showed that a closely spaced turbine array enhances power production by $6-9\%$ due to the Venturi effect. Similar effects were also observed by Strickland and Stevens, 2020 with nearly a 10% increase in the power production for a tightly spaced array of turbines when compared to a less dense array spacing. Thus showing that blockage effects in certain cases enhance the overall power production within an array of turbines.

Figure 4.3 and Figure 4.4 each show the increased spacing to $2D$ and $2.5D$ respectively. The mesh resolution is also adjusted accordingly in order to capture the effects of the induced blockage effects and the downstream wake effects. On the other hand, Figure 4.5 represents the lateral spacing of $3D$. The lateral mesh resolution is adjusted to the same as the other cases. Additionally, `moveDynamicMesh` utility requires the adjustment of the mesh resolution in the streamwise direction as well and with the same resolution of the previous cases, leads to a divergence in the solution. A better analysis is required in order to understand the utility and a grid convergence study is recommended as a further extension of this particular research.

4.1.2. Sensitivity to Hill Size Variations

The hill used in the present case is two-dimensional and defined by the mathematical curve 'Witch of Agnesi'. The name is derived from the renowned Italian mathematician Maria Agnesi. The curve is a function of the hill height (h), streamwise distance (x) and the half width of the hill (L). This is mathematically defined as -

$$y = \frac{h}{1 + \left(\frac{x}{L}\right)^2} \tag{4.1}$$

Studies done by Shutts and Gadian, 1999 and Gisinger, 2018 show that the dimensions of the topology affect excitation of AGWs. It was observed that the increasing base width of the hill: steepness or shallowness of the hill results in changing velocity fluctuations. The amplitude of variation of the vertical wavefronts seemed to have a major influence due to the profile of the hill. Gisinger, 2018 studied several cases of the hill dimensions by maintaining the flow parameters constant. For the steepest case of the hill, it was observed that the wavefronts had higher wave amplitudes than the other cases. Additionally, the induction effects caused by the hill were also observed to be stronger. The AGWs and induction effects of the hill are expected to influence the blockage effects in the upstream of the farm. Therefore, a sensitivity study of the hill variations is necessary to further better understand the blockage phenomenon. A non dimensional parameter, size of the hill (S_h) is defined in the present case as a ratio of the height to the base width of the hill. This is mathematically defined as -

$$S_h = \frac{h}{L} \tag{4.2}$$

In order to avoid complexities and streamline the analysis, the hill height (h) is kept constant while the base width of the hill (L) alone is varied. The four hill cases are classified into: shallowest, moderately shallow, moderately steep and steepest. In addition to this, other driving parameters of the AGWs such as the Brunt-Väisälä frequency (N), freestream reference velocity (U_{ref}) and the potential temperature gradient ($\partial\theta/\partial z$) are kept constant. Thus, the variation in AGWs and the resulting blockage effects are isolated solely to the change in base width of the hill. The four hill size cases considered in the current study are as shown in the Figure 4.6. Note that the figure only shows the streamwise location where the hill begins on the windward side and tapers on the leeward side. Studies have shown that the change in the dimension of the hill results in flow variations due to the changes in Froude number. It is a non-dimensional number that is yielded due to the ratio of inertia forces to gravitational forces. It is mathematically defined as -

$$Fr = \frac{U}{NL} \tag{4.3}$$

In Equation 4.3, U is the velocity of the flow and N is the Brunt-Väisälä frequency and L is the width of the hill. The variation in the Fr results in changes in the properties of the flow and thus influencing the

excitation of gravity waves. However, the comparison of gravity wave variation due to Froude number is not considered in this study. This would form a good research as an extention of the present study.

As shown in Table 4.3, the base width of the hill is varied from $600m$ to $1200m$. The case of the shortest base width of $600m$ is considered to be the steepest case as the difference between the hill and the base width is small. The profile is considered shallowest when the hill height is much smaller than the base width. Therefore, the case $1200m$ base width is considered as the shallowest case. The baseline case in the present study is considered to be the moderately shallow hill with a base width of $1000m$.

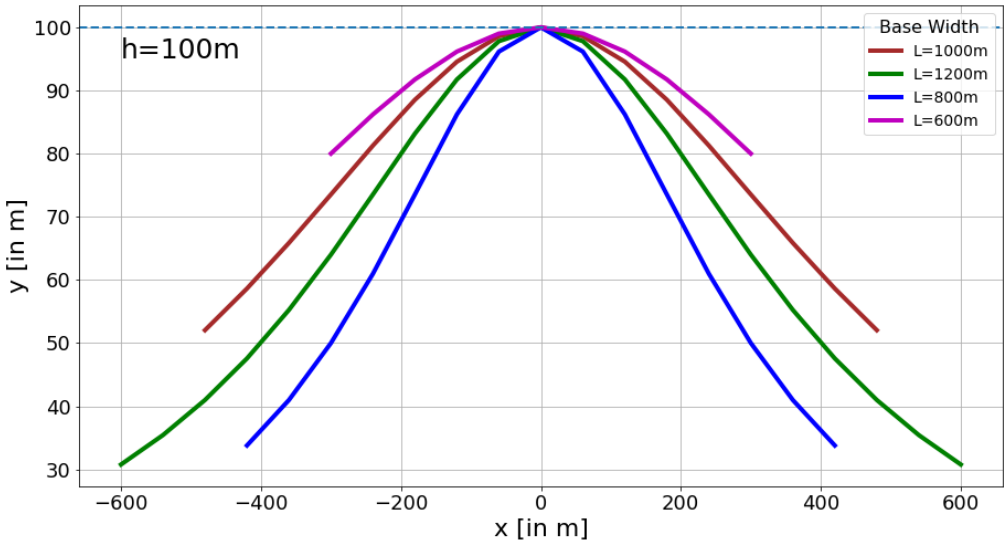

Figure 4.6: Hill curve defined by 'Witch of Agnesi'

Hill Height, h (in m)	Base Width, L (in m)	Hill Size, S_h	Remarks
100	600	0.17	Steepest
	800	0.125	Moderately steep
	1000	0.1	Moderately shallow
	1200	0.08	Shallowest

Table 4.3: Hill size variations along with the hill profile

4.2. Initial & Boundary Conditions

The basic boundary conditions of the domain used at the inlet and outlet boundaries of the flow domain are shown in Table 4.4. Neumann boundary condition is when a derivative of a specific variable is defined at the wall and on the contrary, Drichlet boundary condition specifies a particular value at that boundary. In the case of the Neumann BC, a `zeroGradient` type of BC is used at the walls specified in Table 4.4. The velocity BC at the inlet is specified as a `fixedValue` type with a certain initial value. In the present case, a uniform velocity profile with a geostrophic wind speed of $10ms^{-1}$ for the stable free atmosphere case as well as the truly neutral atmosphere case.

As mentioned in previous sections within this report, stable boundary occurs when there is a negative heat flux from the lower boundary and an increase in temperature along the domain vertical distance. A reference potential temperature of $300K$ is used as the initial value and a linearly increasing profile of temperature is used to get a stable stratification as shown in Figure 4.7. On the contrary, for a truly neutral atmosphere, a fixed temperature is initialised at the inlet with a Dirichlet boundary condition.

The boundary conditions of the remaining boundaries are followed similar to the case of Segalini and Dahlberg, 2019 which realistically holds good for a truly neutral atmosphere. However, the same

scenario with the initial and boundary conditions are extended for the stable free atmosphere case. The domain is a 6 faced cube with inlet and outlet of the domain in the streamwise direction, lower and upper walls in the vertical direction. Lastly, the side walls are in the spanwise direction which also determines the inter-array spacing of the row of turbines.

Boundary Condition	**Inlet**	**Outlet**
Dirichlet Condition	U,k,ϵ,T	-
Neumann Condition	-	k,ϵ,ν_t,T

Table 4.4: Boundary Condition types set at the domain inlet and outlet for the flow parameters

Parameter	**Value**
Velocity, U	[10.0 0.0 0.0] ms^{-1}
Pressure, P_{rgh}	0.0 Pa
Turbulent Kinetic Energy, k	$0.2 \cdot 10^{-5}$ m^2s^{-2}
Turbulent Dissipation Rate, ϵ	0.0012 m^2s^{-3}
Turbulent Viscosity, ν_t	0.0 m^2s^{-1}
Reference Potential Temperature, θ	300 K
Potential Temperature Gradient, $\frac{\Delta\theta}{\Delta z}$	0.003

Table 4.5: Initial conditions of the flow parameters

Since an assumption is made for a spanwise-infinite array of turbines, an appropriate choice of boundary conditions needs to be made to ensure that the domain is treated as an infinite array.

- Lower and upper walls of the domain are treated with a `slip` BC for velocity (U), TKE (k), and turbulence dissipation rate (ϵ). In this type of BC, the tangential component of velocity (U) at the wall is a non-zero value.
- Side walls in the lateral spanwise directions are imposed `cyclic` BC. This type of BC essentially makes the domain periodic and thus a spanwise-infinite array.
- The pressure is treated with a `fixedFluxPressure` BC on all the walls but the lateral ones. In `OpenFOAM`, `fixedFluxPressure` treats the flux at that particular boundary based on the value specified by the velocity boundary condition.

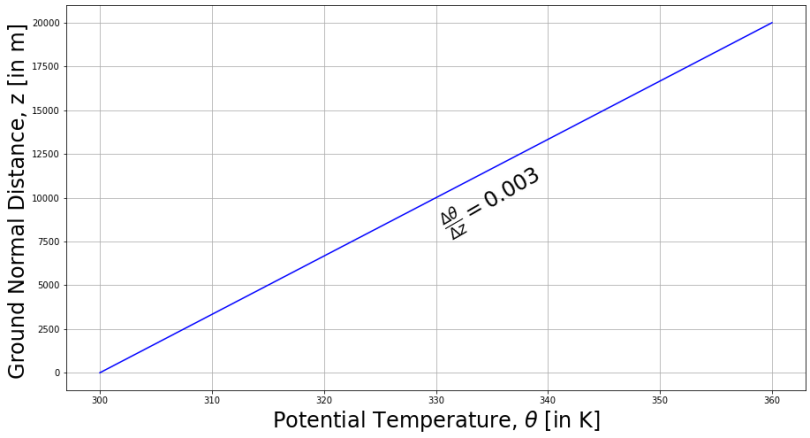

Figure 4.7: Temperature distribution in the free atmosphere normal to the ground

The conditions mentioned in Table 4.5, are initialised into the domain using the `setFieldsABL` utility available on `OpenFOAM` coupled with `SOWFA`. This particular utility allows setting the temperature

fields according to the linear profile of temperature for a stably stratified case. One could possibly extend this work for initialising the velocity, TKE, or turbulent dissipation rate as per the methodology used by Sivanandan, 2021.

It is important to note that with the imposition of `slip` boundary condition on the lower wall, surface roughness parameters are ignored. Therefore, the source of turbulence due to the wall is not taken into consideration. However, in the case of the spanwise infinite wind farm array, the wake propagated by the turbine becomes the major source of turbulence in the flow domain. Along with this, the assumptions of inviscid, incompressible, and uniform inflow are made. The flow conditions in the present case become very similar to a potential flow problem that is eventually governed by a Laplacian of the velocity potential. Given the fact that the initial and boundary conditions of the domain do not essentially generate turbulence, the turbulence properties such as TKE and ϵ become less important to model the flow.

4.3. Solver Setup

As mentioned earlier, in the present study `OpenFOAM` software is used to model the flow cases. However, the software is not easily suitable for solving atmospheric flows for wind farm applications such as imposing a logarithmic inflow profile, temperature stratification, modelling of damping forces, etc. Therefore, `SOWFA` (Simulator fOr Wind Farm Applications) packages, additionally developed by National Renewable Energy Laboratory (NREL) are used which account for the aforementioned characteristics. An extension of these packages was developed particularly for RANS/URANS simulations by Julia Steiner of TU Delft. The solver for URANS simulations `solverWithoutTurbine` is used in the present study.

The URANS solver - `solverWithoutTurbine` built upon the modification to the currently existing `buoyantBoussinesqPimpleFoam` with an additional governing equation for potential temperature as given in Equation 3.12. The pressure-velocity coupling necessary to account for the closure problem is achieved by using the PISO (Pressure-Implicit with Splitting of Operators) algorithm [as explained by Sivanandan, 2021] and is used exclusively for buoyancy effects, turbulence modelling, and flows with dominant transient effects.

4.4. Simulation Suite

In this section, a brief overview of the set of simulations that are carried out in the present study is provided. In order to answer the different research questions and research objectives formulated in the beginning of the study, a well thought out procedure is laid forward. The main objective is to compute the magnitude of blockage for a turbine array on top of a hill under different flow conditions.

As mentioned in Chapter 3, velocity field is required for a case without the turbine array and with the turbine array. Initially, simulations of a flat terrain with and without the turbine array is carried out for truly neutral and stable free atmosphere cases. The resulting blockage from these is computed. This is followed by a set of simulations of a hilly terrain with and without the turbine. Yet again these are carried out under truly neutral atmosphere conditions as shown in Figure 4.8. Along with this, a similar set of simulations are carried out under stable free atmosphere conditions as shown in Figure 4.9. The resulting blockage magnitude from each of these cases is computed along with the hill effective blockage.

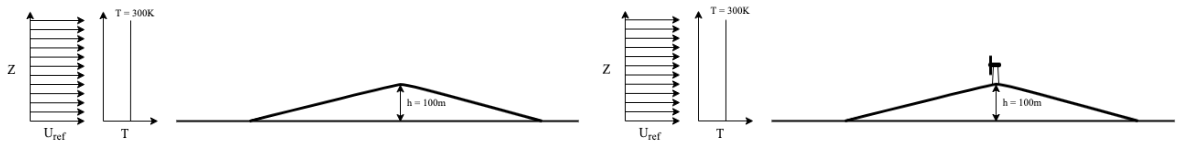

(a) Hill without turbine array (b) Hill with turbine array

Figure 4.8: Hilly terrain setup for truly neutral atmosphere conditions

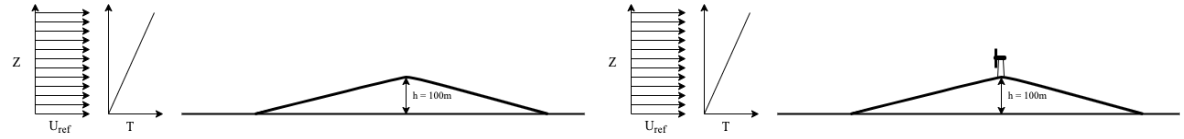

(a) Hill without turbine array (b) Hill with turbine array

Figure 4.9: Hilly terrain setup for stable free atmosphere conditions

Once the baseline simulation cases are carried out and analysed, the same procedure is extended to the sensitivity studies. A set of simulations for a hilly terrain with turbine array for different spacing is carried out. This is done only under stable free atmosphere conditions. Blockage magnitude is computed by comparing with the earlier case of a hilly terrain without turbine array [as in Figure 4.9a]. Similar to the cases as shown in Figure 4.9, a set of simulations is carried out for different hill sizes with and without the turbine array. This is again performed only under stable free atmosphere conditions. This results in blockage magnitude for each of these due to the turbine and eventually the hill effective blockage.

4.5. Summary

In the present chapter, a detailed explanation of the specifications of the domain required for this study was provided. This also included the various sensitivity studies as part of the formulated research questions. Modifications to the domain to account for changing array spacing and hill sizes were discussed. This was followed by a section on the initial & boundary conditions that dictate the characteristics of the flow. This also briefly included the rationale on considering the current case to be something very similar to a potential flow problem. Additionally, details were provided on the solver and the tackling of pressure-velocity coupling for the current case. Ultimately, a section was dedicated to the different simulation cases that are studied in the present research in order to compute the magnitude of blockage.

5

Simulation Results

In this chapter, the various simulation cases deemed necessary are explained and subsequently the research questions are answered. An infinite lateral spacing and a finite streamwise domain are analysed in the present research. This chapter encompasses several sections involving simulation results and discussions for a flat terrain, hilly terrain without turbine array & with turbine array. Also, a sensitivity study of the variations described in the research objectives are discussed. Thereafter, a discussion on blockage effects caused by the flat and hilly terrain in stable and neutral atmospheric conditions is provided.

5.1. Flat Terrain Simulations

In this section, the effects of a laterally infinite array of turbines on a flat terrain are analysed under different atmospheric stability conditions. Subsequently, the excitation of gravity waves resulting from strong stable free atmosphere stratification is presented and elaborated. The resulting velocity and pressure variations from each of these cases are discussed.

As explained in previous sections, in order to compute the effects of blockage, different sets of simulations are required. In coherence with the methodology implemented by Bleeg et al., 2018 and Medici et al., 2011, a set of velocity measurements are needed with the cases before and after commissioning a wind farm. The blockage effects resulting from the turbine are simply a function of the difference in the velocity measurements for the said two scenarios. Based on the initial and boundary conditions assumptions made previously in Chapter 4, the flow domain has no source of turbulence, especially for a flat terrain without the array of turbines. Therefore, a constant inflow velocity of $U_{ref} = 10ms^{-1}$ is observed throughout the domain. This forms the baseline case for the current study in order to compute the effects of blockage and to carry out parametric studies. This is followed by a study of the flat terrain cases in the presence of a laterally spaced infinite turbine array.

From the classical definition of actuator disk theory, kinetic energy is extracted from the flow. Considering an infinite array of turbines, the energy from the approaching flow is extracted leading to a region of momentum deficit in the farm. This phenomenon is clearly visualised by the velocity magnitude contours in tthe ruly neutral condition in Figure 5.1 and in stable free atmosphere conditions in Figure 5.2. The hub height of the turbine is relatively low ($H = 95m$), compensating for the conservation of mass (Continuity equation) a flow acceleration is observed above the turbine. The acceleration of the flow over the turbine array is found to have an effect on the upstream induction region and the flow expands radially outward. Similar effects are observed by Strickland and Stevens, 2020 and Forsting and Troldborg, 2015

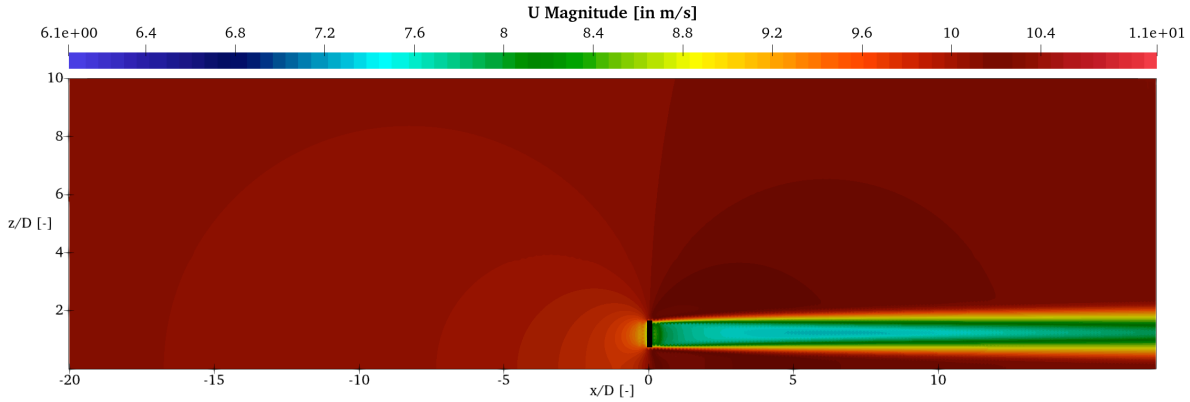

Figure 5.1: Velocity contour in the X-Z plane along the AD in a truly neutral atmosphere

As commonly assumed that the velocity deficit occurs only in the wakes of the turbine, a reduction in velocity is observed upstream of the turbine array as well due to the so-called 'induction zone'. This can be visualised by the contour of velocity upstream in both neutral and stable conditions. The induction zone effects at a turbine scale and wind farm scale are studied by Medici et al., 2011, Forsting et al., 2016 and Segalini, 2021 driven mainly by the thrust coefficient of the turbine (C_T). Similar to these studies, in the near upstream region, the deficit is observed to be much higher compared to the far upstream. Under truly neutral atmospheric conditions, it is observed that the induction effects are uniformly distributed in the radial direction [see Figure 5.1]. At near upstream positions ahead of the turbine at $x = 1D$ velocity is reduced to $U = 9.46ms^{-1}$, at $x = 1.5D$ velocity of $U = 9.65ms^{-1}$ and at $x = 2D$, a velocity of $U = 9.76ms^{-1}$ is observed where the turbine scale induction effects are dominant. Subsequently, the magnitude of velocity deficit is also uniformly decreasing farther away from the turbine.

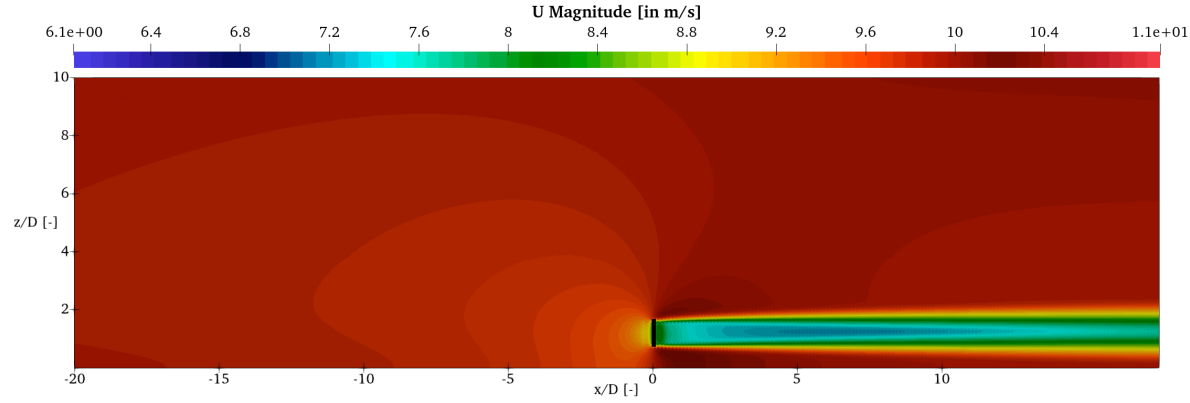

Figure 5.2: Velocity contour in the X-Z plane along the AD in a stable free atmosphere

On the other hand, the induction zone effects are stronger and convecting far more upstream. This is explained due to the fact that a strong temperature stratification hinders turbulence and thereby vertical movement of air parcels. Lack of turbulence in turn leads to restriction in momentum transfer leading to amplified induction effects. Similar effects are also observed by Sanchez Gomez et al., 2021, Allaerts and Meyers, 2018 and Wu and Porté-Agel, 2017. As can be seen from Figure 5.2 at near upstream positions ahead of the turbine at $x = 1D$ velocity is reduced to $U = 9.27ms^{-1}$, at $x = 1.5D$ to a velocity of $U = 9.47ms^{-1}$ and at $x = 2D$ it is found to be $U = 9.55ms^{-1}$. Contrary to the reduction observed in the truly neutral case, the velocity reduction is more pronounced here for a stable free atmosphere. Additionally, the induction region is not uniformly distributed as observed in the neutral case but eventually gets more distorted farther upstream. Although expansion in the flow is observed above the turbine array, the resulting degree of flow acceleration is much less compared to the truly neutral atmospheric conditions. A possible explanation for this is the excitation of AGWs leading to the extraction of momentum above the turbine array. Furthermore, due to the `slip` boundary condition

used in the bottom wall, wall-generated turbulence is also lacking. Therefore, it is important to note that the induction effects observed in the present study could be of a higher magnitude in comparison with more realistic scenarios.

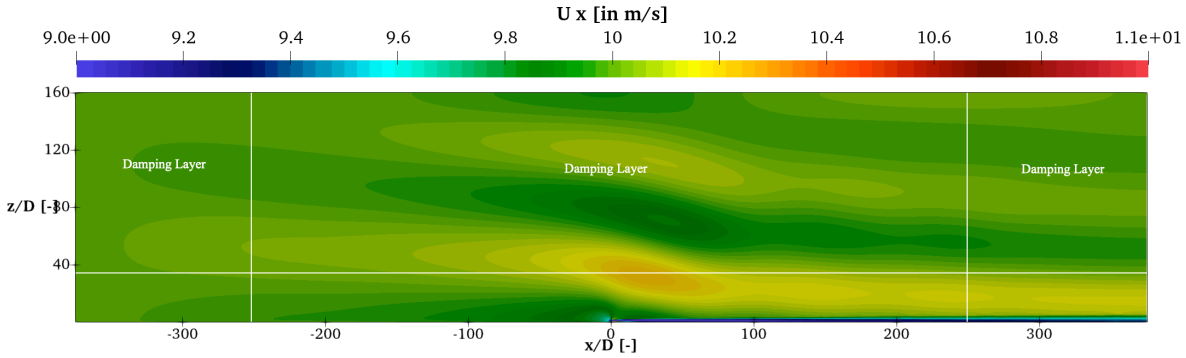

Figure 5.3: Velocity contour displaying excitation of AGWs in a stable free atmosphere due to the presence of a laterally infinite turbine array in a flat terrain

In line with the observations made by Smith, 2010, Allaerts, 2016, Wu and Porté-Agel, 2017 and Sivanandan, 2021, wind farms are seen as a porous semi-permeable topological feature. Therefore, specifically in stable free atmosphere cases with a gradually increasing temperature profile, cold air (higher density) from a lower region is deflected to a region of hot air (lower density). As the air parcel undergoes oscillations due to the temperature stratification AGWs are triggered. The laterally infinite array of wind turbines eventually leads to the merging of the wake deficit far downstream and loss in momentum. Allaerts and Meyers, 2017 observed the boundary layer displacement due to large wind farms leads to excitation of AGWs. On the contrary, in the present study, the excitation of AGWs is explained by the pressure field perturbations resulting from a contorted temperature field. As familiarised by Smith, 2010. AGWs play a pivotal role in determining the flow perturbations and deceleration in upstream of the turbine array. Excitation of AGWs in the vertical direction as seen in Figure 5.3, results in wavefronts with high and low-velocity fluctuations that have a vertical wavelength of $\lambda_z = 6.3km$ from Equation 3.16. These fluctuations are dominant mostly in the vertical direction and as the flow continues downstream of the wind farm array, the velocity fluctuations albeit of a lower magnitude are still observed. Studies have shown that the displacment of the boundary layer also results in the excitation of AGWs. However, this is not of major interest in the present study due to the assumptions of `slip` BC on the bottom wall and a uniform inflow velocity. A boundary layer is not formed in the simulations cases presented here.

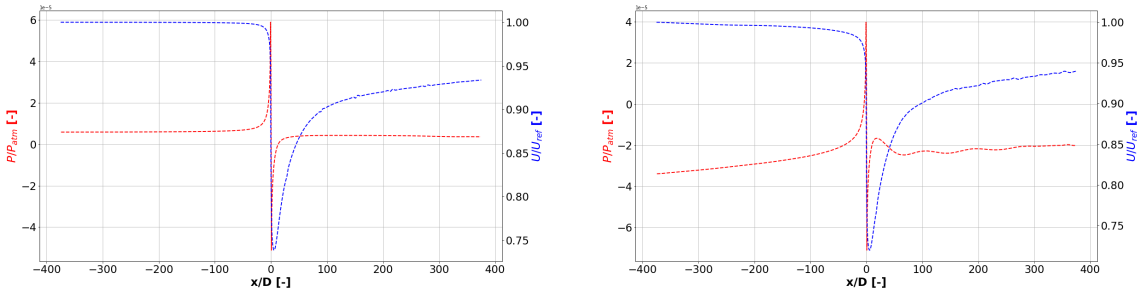

(a) Truly neutral atmospheric conditions

(b) Stable free atmosphere conditions

Figure 5.4: Pressure & velocity profiles at hub height $h = 95m$ in a flat terrain

Furthermore, the pressure and velocity profiles of the flow across the turbine array at hub height ($h = 95m$) explain the upstream effects. Considering the flow across the actuator disk to be through a stream tube, Bernoulli's equation describes the behavioural changes in the flow properties. As can be observed in Figure 5.4a, the pressure of the flow increases at the disk where the stagnation occurs. An increase

in pressure leads to a deficit in velocity which explains the energy extraction by the disk. Although the pressure eventually recovers to its inlet value in the wake the velocity is not fully recovered. While in a truly neutral case there is a drastic change in pressure and velocity, a stable free atmosphere case shows an adverse pressure gradient (see Figure 5.4b). The gradually increasing pressure ahead of the turbine array leads to AGW-induced velocity reduction. Due to the excitation of AGWs in the stable free atmosphere, an oscillatory behaviour is observed in both pressure and velocity. The fluctuations of velocity in the vertical direction are observed in the contour plot Figure 5.3 and along the same lines, minor fluctuations are also observed in the downstream direction.

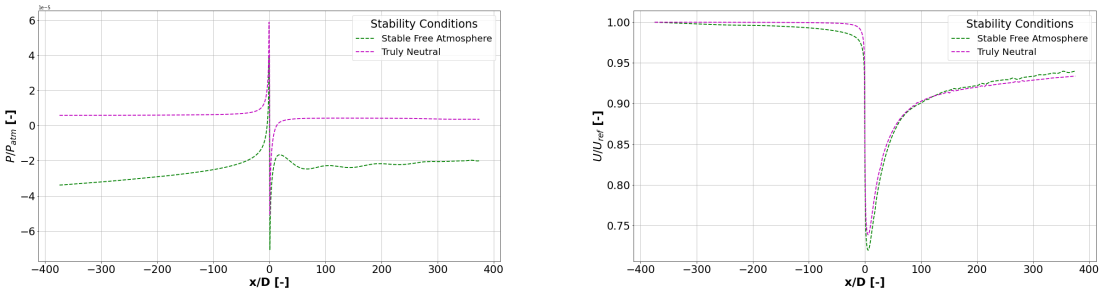

(a) Pressure profile at hub height ($h = 95m$)

(b) Velocity profile at hub height ($h = 95m$)

Figure 5.5: Pressure & velocity profile comparison in a flat terrain for a truly neutral & stable free atmosphere conditions

A comparison of the pressure profiles at hub height across the turbine array for stable free atmosphere and truly neutral conditions is shown in Figure 5.5a. For a truly neutral case, the pressure is constant for the most part of the upstream and downstream distances except across the actuator disk where there is a sudden jump. Under stable free atmosphere conditions, a gradual increase in pressure up to the stagnation point is observed followed by a spike and oscillatory behaviour far downstream. As explained earlier this is supported by the excitation of AGWs due to thermal stratification. This behaviour is also observed in the studies done by Sanchez Gomez et al., 2021. The gradually increasing pressure [adverse pressure gradient] for the stable case also explains the increased velocity deficit observed. Figure 5.5b shows the velocity profile comparison at hub height. As can be seen from the plot, velocity changes vary for the stability conditions. It is clear that throughout the domain at the hub height, a stable free atmosphere case has a stronger influence on the velocity deficit when compared to a truly neutral atmosphere. This behaviour is observed by Allaerts, 2016, Allaerts and Meyers, 2018 and Wu and Porté-Agel, 2017. Stability conditions also lead to enhanced wake deficit due to hindrance of turbulence as observed by Abkar and Porté-Agel, 2015. The wake deficit for the stable case at a downstream distance of $x = 1D$ is found to be $U = 7.64ms^{-1}$ while for the truly neutral case the velocity is $U = 7.82ms^{-1}$. In reality, it would be expected that the velocity in the wake ultimately recovers to the free stream velocity several kilometers downstream [under truly neutral conditions]. This behaviour is not observed in the present study due to the assumption of a `slip` boundary condition thereby eliminating wall-generated turbulence. Along with this, a uniform inflow velocity further simplifies the case due to the lack of wind shear-generated turbulence. The detailed analysis of the wake behaviour under the influence of stability conditions is beyond the scope of this work.

5.2. Hilly Terrain Simulations without Turbine Array

In this section, simulation results of the flow over a hill defined by the mathematical curve 'Witch of Agnesi' is presented. The effects of the flow over the hill with different atmospheric stability conditions are analysed and discussed. The modifications in the flow behaviour due to the hill and the resulting changes in velocity and pressure are discussed in detail. For the baseline case study presented in this section, a hill size of $S_h = 0.1$ with a hill height of $h = 100m$ and a base width of $L = 1000m$ is chosen. As it is apparent that the width is much larger than the height ($L >> h$) makes it a shallow hill.

In order to isolate and understand the effects of blockage caused due to a turbine array placed on top of a hill, simulations are first carried out for an empty hilly terrain. The presence of a hill modifies the

flow over a hill resulting in pressure and velocity variations. This is observed because the profile of the hill creates a constriction in the flow leading to gradual compression of the flow. A direct consequence of the flow compression leads to an acceleration based on Bernoulli's principle. As seen in Figure 5.6, the acceleration of the flow is seen at the summit of the hill. The freestream inlet velocity condition of $U_{ref} = 10ms^{-1}$ is seen to increase nearly by 10%. Consistent with the observations made by Baines, 1979 and Li and Wang, 2016. However, the uniform velocity assumption made in the present study leads to minor discrepancies in the comparison made with other literature. Additionally, inviscid flow assumptions made in this study lead to a potential flow problem. Therefore, the flow directly follows the profile of the hill without necessarily generating turbulence in the flow. The dynamics of the flow observed in this study is similar to the observations made by S Jackson and R Hunt, 1975.

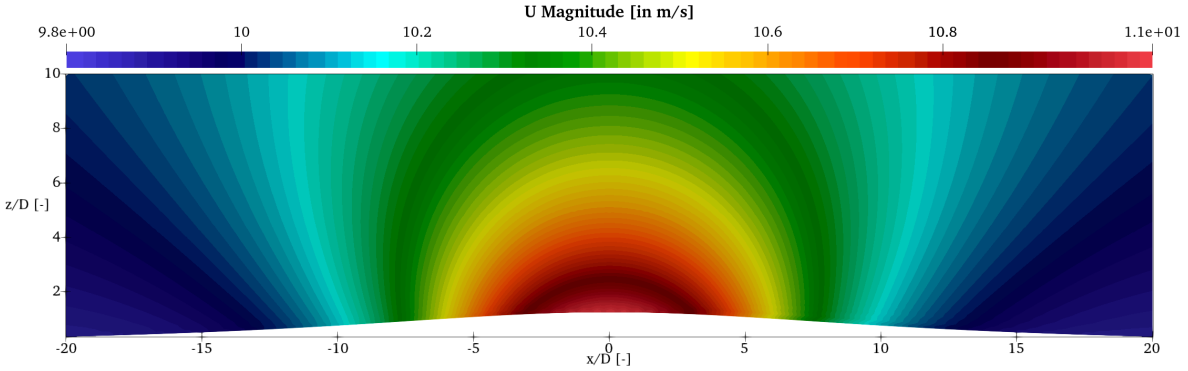

(a) Speedup over hill under truly neutral atmospheric conditions

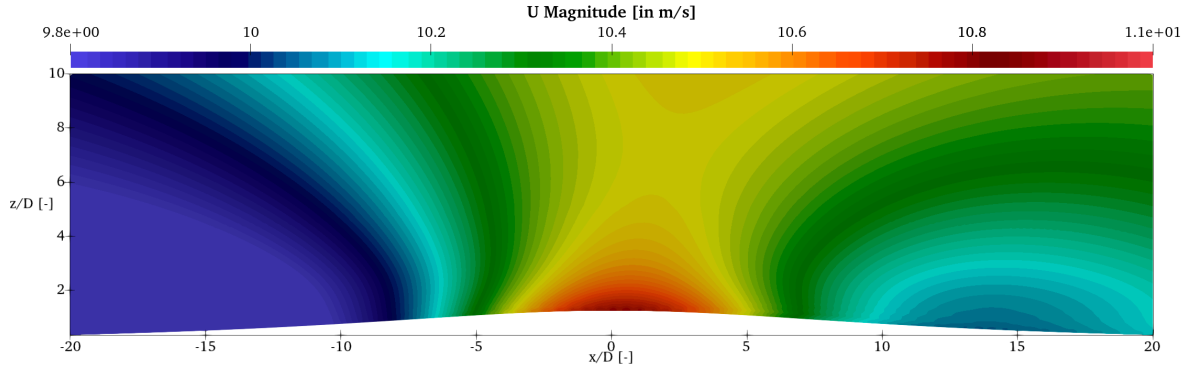

(b) Speedup over hill under stable free atmosphere

Figure 5.6: Velocity contours of hill speed-up along the X-Z plane at the center of the hill

Figure 5.6a shows the flow behaviour in a truly neutral atmosphere where the velocity changes are observed in a radial pattern from the summit of the hill. A maximum speed up of $U = 11.2ms^{-1}$ is evident from the contour plots. The flow across the hill initially experiences a reduction in velocity on the windward side to a magnitude of $U = 9.8ms^{-1}$, eventually leading to a maximum speed up and then reducing on the leeward side. As seen in the figure, the reduction on the windward as well as the leeward side of the hill is of the same magnitude. On the contrary, for stable free atmosphere conditions, the radial pattern is not observed. Additionally, the maximum wind speed is limited to only a few meters above the summit of the hill to a value of $U = 10.6ms^{-1}$. A similar effect is observed by Amahjour and Khamlichi, 2017. The wind speed change is not uniform as in the case of the truly neutral atmosphere possibly explained due to the excitation of AGWs. The range of fluctuations in velocity throughout the profile of the hill shows that the induction caused on the windward side is far more pronounced and is of high magnitude. Additionally, it is important to note that since a shallow hill is considered for this study, flow separation, flow recirculation, and vorticity formation are not observed on the leeward side of the hill.

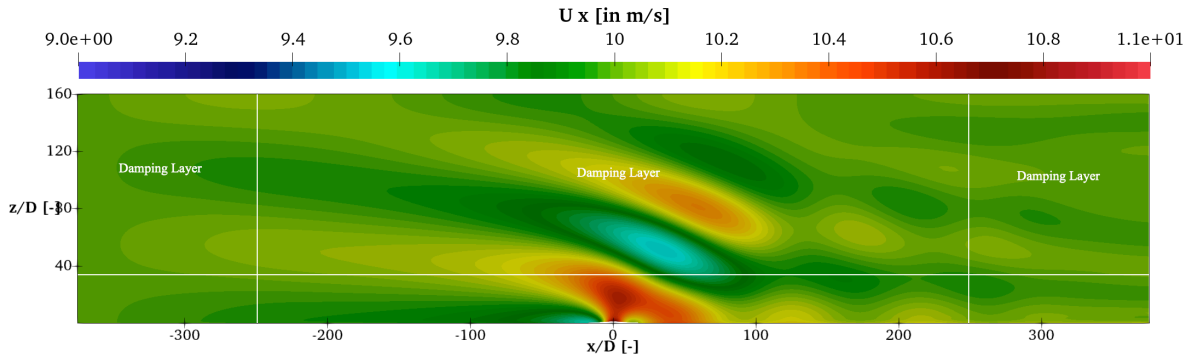

Figure 5.7: Velocity contour displaying excitation of AGWs in a stable free atmosphere due to the presence of the 2-D hill 'Witch of Agnesi' in the terrain

Figure 5.7 shows the excitation of AGWs for the same flow conditions as in the turbine case shown in Figure 5.3. A comparison of the two contour plots shows that for the case with a hill, AGWs are stronger leading to a higher magnitude of fluctuation in velocity. A high-velocity ($U = 10.2ms^{-1}$) wavefront resulting from the hill speed up is followed by a wavefront of low-velocity ($U = 9.6ms^{-1}$) range. Theoretically, the vertical wavelength of the AGWs triggered by the hill is the same as that of the turbine array in flat terrain. This is due to the fact that the vertical wavelength (λ_z) is not a function of the terrain features but of the flow features namely, velocity (U) and Brunt-Väisälä frequency (N). However, it is evident that the horizontal propagation of the AGWs is more outreaching on the windward side of the hill in comparison to the turbine array case. As observed, the effects of AGWs are influential almost $30km$ along the windward direction of the hill. Similar observations were made by Ollier et al., 2018. The inference from this is that the horizontal length of the obstacle ($L = 1000m$) has a higher influence on the AGWs than the vertical length ($h = 100m$) provided that the turbine height considered is also close to the height of the hill. Field observations and theoretical analysis by Reiter and Haurwitz, 1974 also support this postulate.

An adverse pressure gradient is observed on the windward side of the hill for both truly neutral and stable free atmosphere cases. Figure 5.8a and Figure 5.8b show the pressure gradually increasing towards the hill and eventually the resulting flow deceleration as explained earlier. The plots are expressed in terms of the actuator disk diameter for the sake of convenience. In truly neutral atmospheric conditions, since there is no excitation of AGWs both velocity and pressure are recovered to their initial values after a few diameters from the hill. On the contrary, the stable free atmosphere case does not experience full recovery of velocity or pressure due to the horizontally convected AGWs. Additionally, velocity and pressure fluctuations are strongly evident on the leeward side. These effects are also observed by Reiter and Haurwitz, 1974.

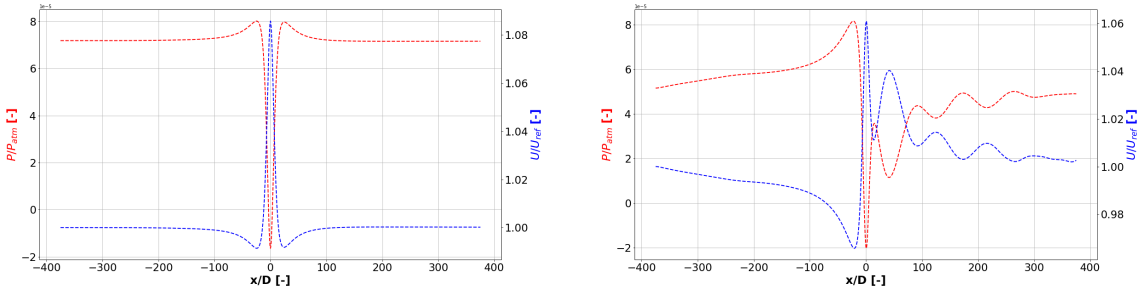

(a) Truly neutral atmospheric conditions

(b) Stable free atmosphere conditions

Figure 5.8: Pressure & velocity profiles at a height of $H = 95m$ in a hilly terrain ($h = 100m$) without a turbine

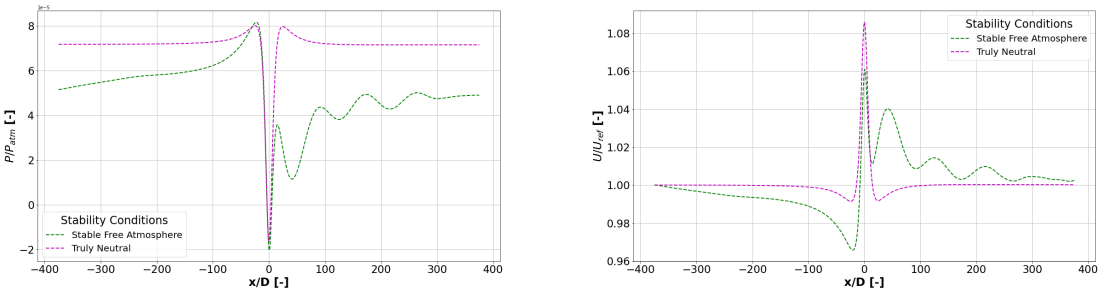

(a) Pressure profile at $H = 95m$ above the hill

(b) Velocity profile at $H = 95m$ above the hill

Figure 5.9: Pressure & velocity profile comparison at a height of $H = 95m$ in a hilly terrain ($h = 100m$) without the turbine array for truly neutral & stable free atmosphere conditions

Figure 5.9a shows the difference in pressure profiles for truly neutral and stable free atmosphere conditions. As explained earlier, induced pressure perturbations are observed throughout the domain when AGWs are excited. Therefore, the pressure on the far windward side of the hill is much lower for the stable case. The smooth adverse pressure gradient results in a substantial deceleration of the flow in the induction region of the hill. After reaching maximum pressure at the stagnation point, there is a sudden reduction in pressure resulting in the acceleration of the flow at the summit. As can be observed from Figure 5.9b, a velocity reduction of nearly 2% to $U = 9.62ms^{-1}$ in reference to the freestream velocity is observed due to the induction of the hill for stable free atmosphere conditions. The hill-induced reduction is seen in the neutral case as well with a reduction to $U = 9.8ms^{-1}$. Nevertheless, there is an acceleration in the flow at the top of the hill eventually leading to higher availability of kinetic energy. An alternating adverse and favourable pressure gradient observed in the flow explains this behaviour. Upon comparison with the velocity profile of the turbine in flat terrain, downstream oscillations are observed to be far more pronounced. That is, the amplitude of the AGWs and the magnitude of fluctuation is much larger for the hilly terrain. This implies that topological features have a larger influence on the flow field compared to a single row of turbines.

5.3. Solution Stability

In this section, the variation of the solution with damping characteristics and the change in time is discussed. The damping characteristics that are implemented in this case and the modifications made to attain a stable solution are discussed. Apart from this, with the use of an unsteady solver, the solution is expected to vary with time. Variation with time and the analysis of the stable solution is discussed therein.

For the same domain specifications as mentioned in Chapter 4, initially, a trial and error method was used to find the optimum damping characteristics. Appropriate damping characteristics are necessary to avoid reflections of the spurious AGWs from the domain walls. The reflection from the domain walls could lead to contamination of the flow field and thus yield an unstable solution. Figure 5.10a, shows the contour plots of the vertical flow velocity component in the presence of a hill. As observed, the AGWs that are excited due to the presence of the hill convects with high intensity towards the top of the domain. Nevertheless, the excited AGWs are haphazard and non-uniform which is far from a plausible physical explanation. Inappropriate damping characteristics lead to reflection from the top domain affecting the flow at the outlet as well as the inlet. Since the AGWs contain wavefronts of high momentum and energy, spurious reflections lead to severe contamination on the windward as well as leeward flow characteristics. Although most dominant effects are observed at the top boundary and leeward side, there are some effects seen on the windward side. Similar observations were made by Haupt et al., 2019 for cases with inappropriate damping characteristics. These reflections can be mitigated by increasing the domain size by large bounds on the inlet, outlet as well as top boundaries. However, this would eventually increase the number of cells and thus the computational costs. In the present study, a $10km$ damping layer is used on all three walls with a damping coefficient of $0.025s^{-1}$. As seen in Figure 5.10b, the vertical velocity contour shows the excitation of gravity waves due to the hill. The vertically standing wavefronts under appropriate damping characteristics show clear oscillation

in the velocity fields. The wavefronts are uniform and are also convected towards the leeward side of the hill. Unlike the previous case, the reflections are minimised to the best possible extent and thus the free stream velocity experienced on the windward side is free of contamination.

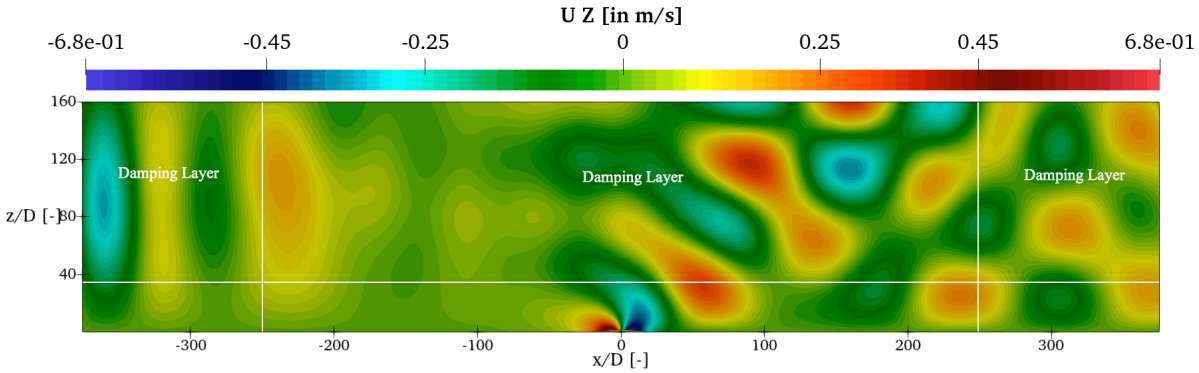

(a) Flow field with incorrect damping characteristics

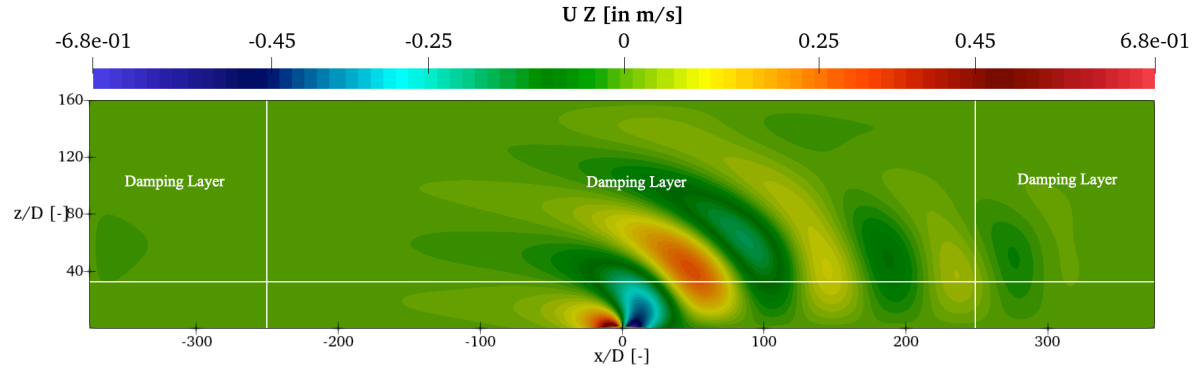

(b) Flow field with the correct damping characteristics

Figure 5.10: Vertical velocity contours in the X-Z plane sliced at the center of the hill

The use of an unsteady solver leads to a time-dependent variation in the velocity profile. This is because the AGWs are a highly unsteady phenomenon. In the present study, the `solverWithoutTurbine` is used as the RANS-based unsteady solver. A step change in time of $\Delta t = 0.05s$ and a CFL number of $CFL = 0.5$ is used. In addition to this, an adjustable time step is allowed after each iteration. Although this slightly increased the computational time of the solver, allowed higher flexibility in arriving at a stable solution. Studies by Sessarego et al., 2018 and Uchida and Li, 2018 showed that typically a $CFL = 0.1$ gives higher accuracy but a delayed stability. The studies compared the results with LES simulations to achieve an equivalent accuracy. However, increasing the CFL number to larger values slightly compromises the accuracy but yields faster stability of the solution. Figure 5.11 shows the variation in velocity profile across the hill at different time iterations. As observed, up to $t = 3000s$ the velocity profile is slightly differing from the ones obtained at higher time iterations. There are minor discrepancies observed on the far windward of the hill and the far leeward side of the hill. However, in the zone of interest where the hill-induced velocity reduction is dominant, the profile is close to achieving time invariance. In comparison, on the leeward side of the hill, the AGWs are dominant. Since AGWs are an unsteady phenomenon, the change in time iteration still leads to instability of the velocity profile specifically on the leeward side. However, at larger time iterations i.e. $t = 9000s, 12000s, 15000s$ velocity profile in the leeward side also is seen to be essentially time-invariant. The faster stability of the solution is partly attributed to the choice of CFL number and time step Δt. While the other reason is that the assumption of a `slip` BC on the lower wall and a uniform inflow velocity simplifies the flow scenario. There is no additional source of turbulence, especially without the turbine array on top of the hill. This in turn leads to further simplification and thus faster stability of the solution.

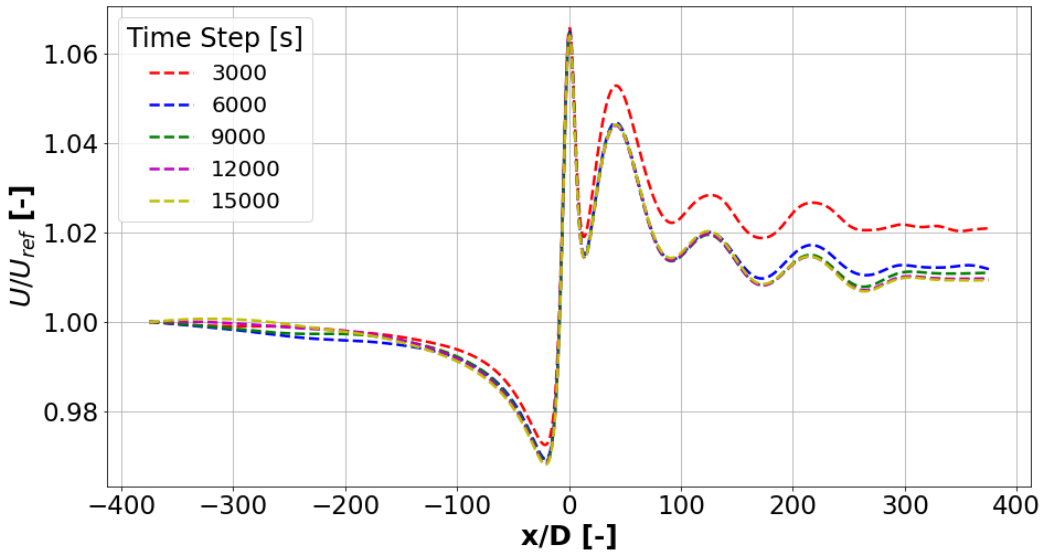

Figure 5.11: Evolution of the velocity profile across the hill at different time steps

Since the velocity profiles are essentially time invariant at higher time iterations, all post-processing of the data is performed for the solution obtained from the last time iteration of $t = 15000s$. The above behaviour is observed in all the cases considered in this study. Therefore, for all the cases presented here, the data files from the last time iteration is used for post-processing

5.4. Hilly Terrain Simulations with Turbine Array

Based on the observations made in the previous section, it is evident that there is a larger availability of kinetic energy at the top of a hill. At this point, it creates a great segue into analysing the flow behaviour with a turbine array on top of the hill. The current section focuses on analysing the flow behaviour on top of the hill and the resulting perturbations due to the turbine array. Detailed analysis of the cumulative induction effects of the turbine along with that of the hill is provided. The same baseline case as the hilly terrain is used with a hill height of $h = 100m$ and a base width of $L = 1000m$ is used. Turbine characteristics of the Vestas V80-2MW are used. The hub height considered is at $H = 95m$ and a rotor diameter of $D = 80m$. As mentioned earlier, the effects of the tower are neglected in the present study.

Figure 5.12 shows the velocity contours of the flow across the turbine array placed on top of the hill. As observed in both truly neutral and stable free atmosphere conditions, flow acceleration is observed at the summit of the hill. This is a direct consequence of the altering pressure field across the hill. On the windward side of the hill, a velocity drop is observed which is a consequence of the hill-induced effects. As the flow approaches the summit, an acceleration is observed to the same order of magnitude as in the case of a hilly terrain without the turbine array. Therefore, it results in higher kinetic energy availability for the turbines to extract from the wind. Same observations were made by Liu and Stevens, 2021 and Zhang et al., 2022.

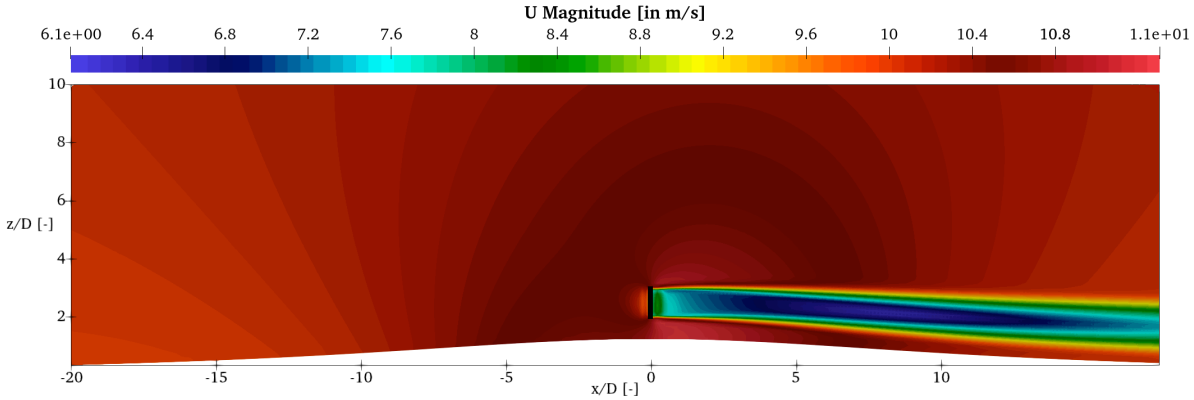

(a) Truly neutral atmosphere conditions

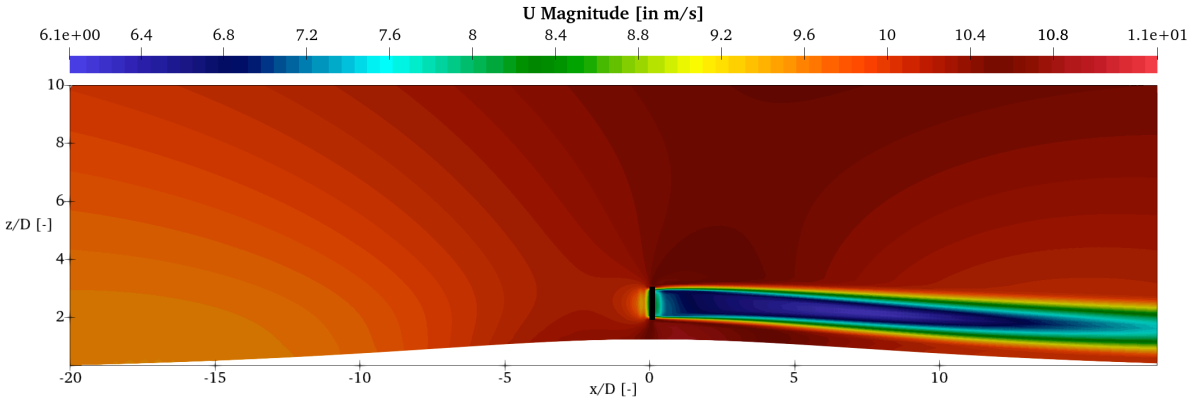

(b) Stable free atmosphere conditions

Figure 5.12: Velocity contour in the X-Z plane along the turbine array in a hilly terrain

Similar to the effects seen for a turbine array in flat terrain, truly neutral atmosphere conditions result in a radially uniform flow field around the hill [see Figure 5.12a]. A cumulative effect of the flow acceleration caused by the hill and also by the flow passing above the turbine array is evident from the contour plots. For neutral conditions, there are no additional pressure perturbations caused apart from the hill-induced pressure variations. Therefore, a radially uniform flow field is observed around the turbine array as well as the hill. Figure 5.12b shows velocity contours for a turbine array situated on top of the hill under stable free atmosphere conditions. As it can be seen the flow speed-up due to the hill inhibited as a consequence of the triggering of AGWs. This in turn leads to larger perturbations in the flow in terms of both velocity as well as pressure gradient. It is interesting to note that the contours of the induction region caused by the turbine are deflected vertically due to the presence of the hill. Subsequently, the center of the wake is also displaced by virtue of the hill. These effects were observed by Shamsoddin and Porté-Agel, 2018 and Yang et al., 2015. Again, as in the case of a turbine array on flat terrain, induction effects of both the hill and the turbine are radially uniform in a truly neutral atmosphere. On the other hand, deformed induction effects are observed in stable atmospheric conditions.

However, it is interesting to see that the wake of the turbine follows the profile of the hill on the leeward side. As it would have been for flat terrain. These observations were also made by Yang et al., 2015, Shamsoddin and Porté-Agel, 2018, Hyvarinen and Segalini, 2017 and Liu and Stevens, 2021. The placing of the turbine array on a hill seems to influence the velocity field. However, it is interesting to note that the induction effects of the hill, speed up at the summit of the hill and eventual deceleration on the leeward side of the hill are still observed despite the presence of the turbine array.

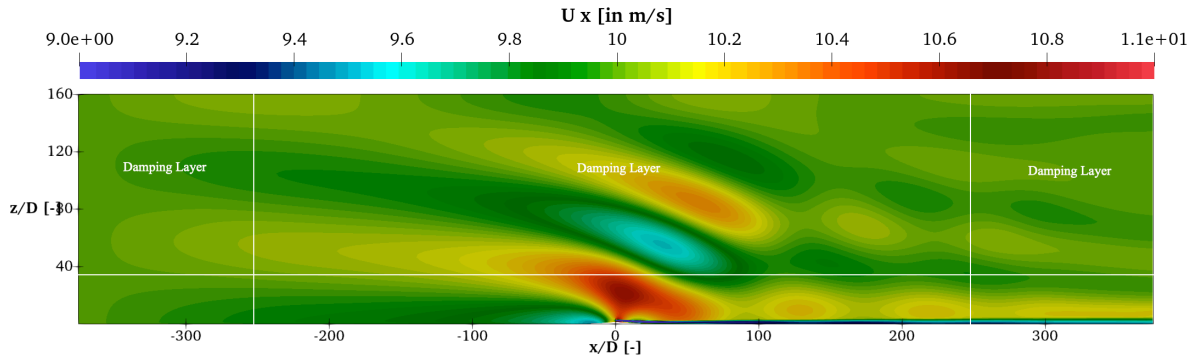

Figure 5.13: Velocity contour displaying excitation of AGWs in a stable free atmosphere due to the presence of the spanwise-infinite turbine array on a 2-D hill 'Witch of Agnesi'

As observed in both the turbine array on flat terrain and a hilly terrain without the turbine array, an upward displacement of the flow is observed. Thus leading to the excitation of AGWs in stably stratified atmosphere conditions. Figure 5.13 shows the excitation of AGWs due to the presence of the hill as well as the turbine array atop. The vertical displacement of the air parcel due to the topological feature of the hill is further excited by the turbine. Therefore, the fluctuation in the magnitude of velocities is much stronger while retaining the same vertical wavelength. The horizontal convection of the AGWs is also more pronounced and travels farther upstream and downstream. When observed closely, it is evident that the AGWs are far more outreaching almost up to $x = 200D$ upstream. A high-velocity patch of $U = 10.4ms^{-1}$ is observed above the hub height followed by a patch of low velocity at $U = 9.6ms^{-1}$. In the induction region of the hill, the velocity is seen to reduce to below $10ms^{-1}$. This is explained by the adverse pressure gradient and the cumulative induction effects of both the turbine array and the hill. Liu and Stevens, 2020 and Tsuda, 2014 attributed these effects to largely influence the flow field throughout the domain. Thus resulting in wind farm-induced blockage.

Figure 5.14a shows the pressure and velocity fluctuations across the turbine array on top of the hill. In the case of truly neutral atmospheric conditions, an adverse pressure gradient is seen just ahead of the hill resulting in a reduction in velocity [hill-induced effects]. This is followed by a favourable pressure gradient resulting in flow acceleration. From the figure, it can be seen that there is a drastic change in pressure resulting in a subsequent velocity reduction [turbine-induced effects]. Eventually, on the leeward side, again an adverse pressure gradient is experienced. This causes delayed wake recovery for a turbine on top of the hill in comparison to the flat terrain case. Studies by Shamsoddin and Porté-Agel, 2018 and Hyvarinen and Segalini, 2017 supports this postulate. On the other hand, for a stable case, the induction region effects of both the hill and the turbine are much stronger. This is evident from Figure 5.14b. Eventually, on the leeward side, oscillatory behaviour in pressure and velocity fields is observed due to the excitation of AGWs. The velocity profile obtained in this follows the same trends predicted by Hyvarinen and Segalini, 2017.

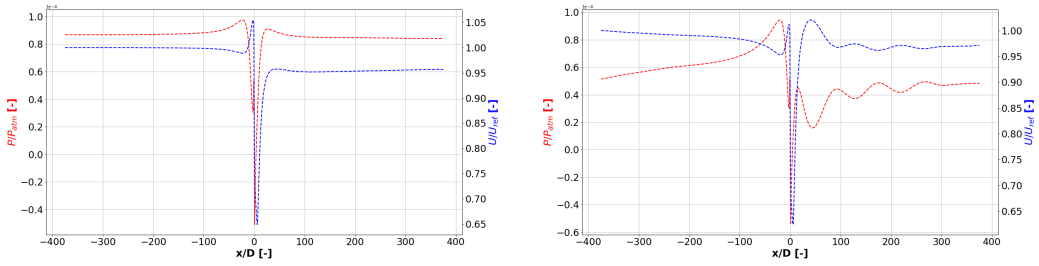

(a) Truly neutral atmospheric conditions (b) Stable free atmosphere conditions

Figure 5.14: Pressure & velocity profiles at hub height $H = 95m$ on top of the hill with a height of $h = 100m$

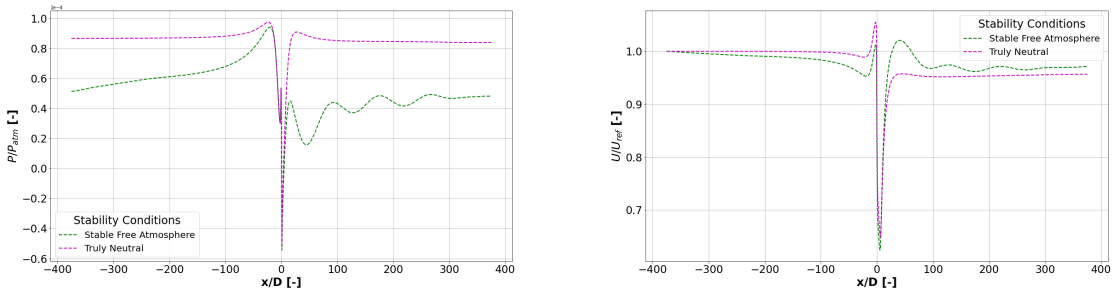

(a) Pressure profile at $H = 95m$

(b) Velocity profile at $H = 95m$

Figure 5.15: Pressure & velocity profile comparison at a hub height of $H = 95m$ in a hilly terrain with a turbine array for truly neutral & stable free atmosphere conditions

Furthermore, a comparison of pressure profiles for neutral and stable cases is shown in Figure 5.15a. The pressure gradient follows the same trend for both stability conditions whereas, the degree of variation is quite different. This is again explained by the flow perturbations observed throughout the domain in stable conditions. The velocity profile shown in Figure 5.15b shows the extent to which the flow field is affected. Both stability conditions experience deceleration on the windward side followed by acceleration at the summit. However, under stable conditions, the hill-induced effects result in a stronger deceleration to a maximum value of around $U = 9.4ms^{-1}$. On the contrary, neutral conditions see a deceleration of about $U = 9.8ms^{-1}$. The cumulative induction effects of the hill and the turbine array, are observed all the way up to the domain inlet. While for the truly neutral atmosphere case, the induction effects are restricted only to certain diameters upstream at $x = 80D$. This large difference in the induction effects predicted for stable conditions is by virtue of the pressure fluctuations and AGWs triggered. Consequently, resulting from the pressure fluctuations, the turbine array on a hill inhibits the flow speed-up at the top. A neutral atmosphere only sees an acceleration of about $U = 10.5ms^{-1}$ while it is even lower for the stable case at $U = 10.2ms^{-1}$.

5.5. Sensitivity Studies

In this section, changes in the flow behaviour by varying certain domain parameters based on the considerations made in Chapter 4. At first, the flow analysis is made for a turbine array on top of the hill by changing the lateral spacing. Later, the analysis is extended for variation in hill size and the resulting flow induction.

5.5.1. Inter-array Spacing

In this section, the effect of change in the spacing of the laterally infinite turbine array is presented and discussed. Figure 5.16 show the contour plots of the flow across the turbine array on top of the hill. A slice is made at a hub height of $H = 95m$ above the $h = 100m$ hill along the X-Y plane. From the figure, the induction effects caused by the turbine are evidently visible. The turbine array is placed at $x/D = 0$ which coincides with the summit of the hill. Therefore at this location on the contour plots, a flow speed-up of $U = 10.4ms^{-1}$ is observed in each of these cases while the turbine spacing is found to have little to no influence. On the other hand, the hill height and base width remain the same as in the baseline studies, hill induced effects also remain unchanged. Upon closer examination of the contour plots from Figure 5.16a, it can be perceived that a dense spacing of $\Delta_y = 1.5D$ shows that the turbine scale induction effects have a larger influence on the flow. The induction effects are also seen to be advecting in the lateral directions and eventually interacting with adjacent turbines. As the spacing increases as in Figure 5.16b, the induction effects seem to be less laterally advecting. As the spacing increases the induction effects become more constrained.

At an upstream location of $x/D = 5$, the lowest velocity reduction is observed for spacing of $\Delta_y = 3D$ [see Figure 5.16d]. As the lateral spacing reduces, the velocity reduction seems to be increasing especially for near upstream locations. Meyer Forsting et al., 2017 predicted a similar behaviour of increased performance for tight spacing. However, Strickland and Stevens, 2020 observed a contrasting behaviour with increased power production for tight spacing of the turbines. The authors attributed this

behaviour to the Venturi effect leading to a speed-up of velocity giving an advantage with the production of power. This effect is also observed in the present study depicted by the acceleration of the flow between the turbine and the domain walls. Figure 5.16c and Figure 5.16d with a lateral spacing of $\Delta_y = 2.5D$ and $\Delta_y = 3D$ display more acceleration. This is a consequence of the expansion of the flow around the turbines leading to a reduction in pressure. But the Venturi effect seems to be playing a negligible role in enhancing the kinetic energy availability ahead of the turbine array in the present case. A possible explanation for this is due to the dominating hill induction effects which reduce the availability of energy to be harvested by the turbines.

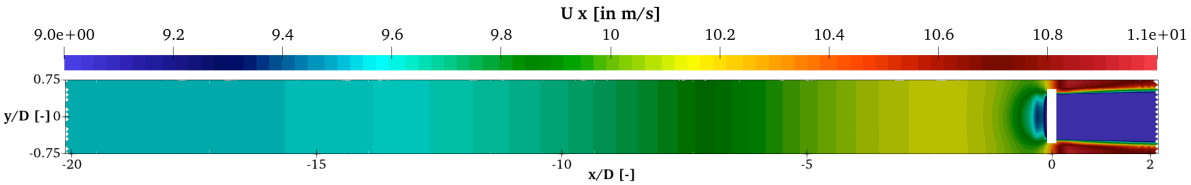

(a) $\Delta_y = 1.5D$

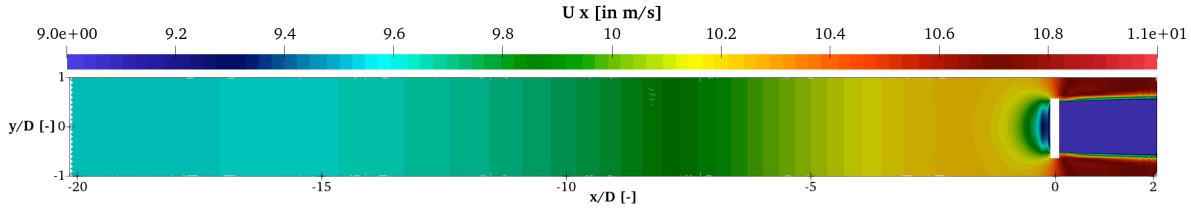

(b) $\Delta_y = 2D$

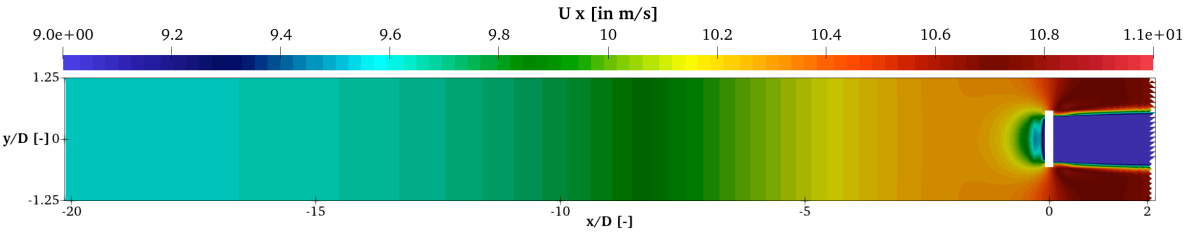

(c) $\Delta_y = 2.5D$

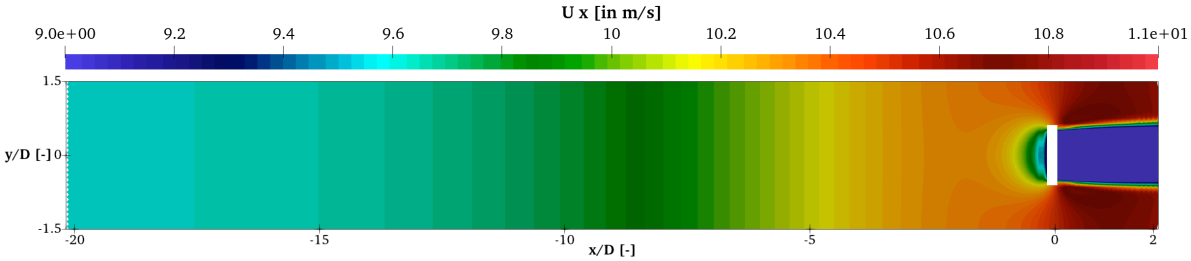

(d) $\Delta_y = 3D$

Figure 5.16: Velocity contour of the turbine on a hill with varying lateral spacing Δ_y along the X-Y plane of the computational domain

Figure 5.17, provides a comparison of the pressure and velocity profiles at hub height ($H = 95m$) above the hill for the varying lateral spacing. From the pressure profile shown in Figure 5.17a, there seems to be little to no difference for the varying spacing (Δ_y). An exception is a tightly spaced domain $1.5D$, where a marginal increase in pressure is observed on the near windward side of the hill. The marginal variation eventually leads to a reduction in velocity as a result of the cumulative induction effects of the turbine array and the hill. Figure 5.17b, shows that the variation in velocity on the windward side is marginally changing for the different lateral spacing. On the other hand, velocity fluctuations on the leeward side of the hill seem to display larger variation. The magnitude of the AGWs triggered varies due to the spacing of the turbines. The mean flow to which the AGWs damp out changes due to the spacing of the turbines. The lateral spacing marginally changes the flow characteristics that govern

the triggering of AGWs. Therefore, the mean velocity changes are observed on the leeward side of the hill.

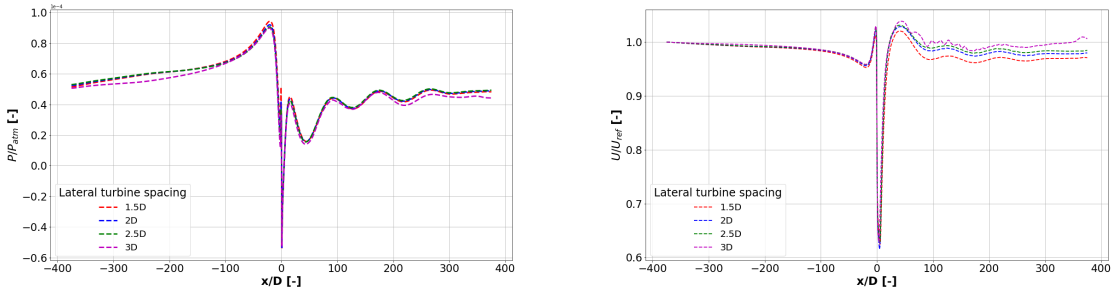

(a) Pressure profiles at hub height

(b) Velocity profiles at hub height

Figure 5.17: Pressure & velocity profiles at hub height $H = 95m$ for varying lateral turbine spacing of $\Delta_y = 1.5D, 2D, 2.5D, 3D$

5.5.2. Hill Size Variations

As seen in previous sections, AGWs play an important role in the upstream velocity reduction. Therefore, an analysis of hill size (S_h) effects on the AGWs and the resulting blockage is carried out in this section. The three S_h cases apart from the baseline considered here are $S_h = (0.08, 0.125, 0.17)$ corresponding to the varying base widths of the hill. The baseline case for hill height $h = 100m$ and base width of $L = 1000m$, the hill size corresponds to $S_h = 0.1$. A comparison of the cases is made with reference to the baseline case. The variation in base width of the hill results in variation in the flow cases. Particularly variation in Froude number Fr of the flow is caused as explained in Chapter 4. This analysis is not considered in the present study and thus becomes a good starting point for future research.

Figure 5.18 shows the comparison of pressure and velocity profiles for the various hill sizes mentioned above. Increasing hill size indicates a higher slope and this implies a steeper profile of the hill. This determines the variation in pressure profile across the hill. Figure 5.18a indicates that as the hill gets steeper with $S_h = 0.17$, the flow becomes more constrained leading to elevated pressure. However, an adverse pressure gradient is created leading to a higher reduction in velocity as indicated in Figure 5.18b. Induction effects caused by the hill is higher for steeper hills indicated by the reduction to a velocity of $U = 9.6ms^{-1}$ and eventually, the degree of reduction is lower as the steepness of the hill reduces. For $S_h = 0.125$, the velocity is reduced to $U = 9.7ms^{-1}$ due to the induction effects of the hill. On the other hand, for the least steep case, the induction effects of the hill are far more pronounced with a reduction of up to $9.6ms^{-1}$. Followed by this, the speed-up observed at the summit is much higher for a steep hill at $U = 10.9ms^{-1}$ as the slope of the hill reduces the speed-up also reduces. Similar trends are observed by Liu and Stevens, 2021, Kochanski et al., 2010 and Deaves, 1980. Figure 5.18a also shows that wider the base of the hill stronger the pressure perturbations are. The basic inference that can be drawn is that with increasing hill size, pressure perturbations are subsequently displaced. The adverse pressure gradient also increases with the steepness leading to stronger induction regions on the windward side. The excitation of AGWs leads to fluctuations on the leeward side as seen in Figure 5.18b. It is interesting to note that the mean velocity to which the AGWs damp out is displaced downwards with the increasing steepness of the hill.

Figure 5.19 shows the contour plots of the varying S_h with the turbine array placed on top of the hill. All three cases show the excitation of AGWs resulting from thermal stratification in the domain. However, from the contour plots, qualitatively it can be visualized that the pattern and magnitude of the vertical wavefronts show large variations. For a hill size of $S_h = 0.08$, as shown in Figure 5.19a, the wavefronts due to the excited AGWs are strongest and the upstream convection is also far-reaching. The magnitude of the wavefronts ranges from a maximum velocity of $U_{max} = 10.5ms^{-1}$ to a minimum of $U_{min} = 9.4ms^{-1}$. The induction effects of the hill are also reaching far upstream. As the base width reduces, the variation in magnitude also becomes smaller. For a hill size of $S_h = 0.125$, the magnitude varies from $10.3ms^{-1}$ to $9.6ms^{-1}$ and for a hill size of $S_h = 0.17$, the magnitude further goes

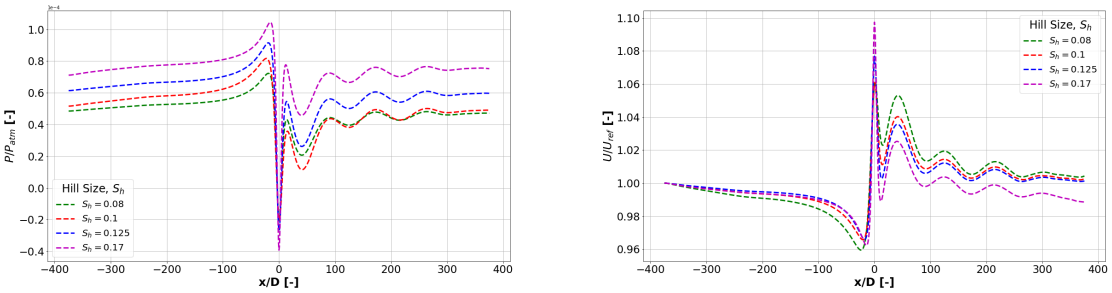

(a) Pressure profiles at hub height

(b) Velocity profiles at hub height

Figure 5.18: Pressure & velocity profiles at hub height $H = 95m$ for different hill sizes corresponding in the absence of the turbine array

down. However, the induction effects on the windward side are stronger which would lead to a higher magnitude of velocity reduction.

As a consequence of the adverse pressure gradient seen in Figure 5.20a, induction effects are dominant. The pressure gradient is steep in coherence with the steepness of the hill. Therefore, the velocity reduction is also amplified. However, the speed-up over the hill is inhibited due to the existence of the turbine array similar to the observation made in previous case studies. It is interesting to note that unlike the case without the turbine array, the acceleration of the flow is at the same value of $U = 10.8ms^{-1}$ for all the variations in hill sizes [see Figure 5.20b]. This is an indication that the inhibition caused by the turbine scale inductions effects are far more consistent than the induction effects caused by the hill. In contrast to the observations made with the case without the turbine array, the mean velocity to which the AGWs get damped is also consistent with an exception of the hill size case of $S_h = 0.17$.

5.6. Blockage Effects

In this section, the change in velocity fields that eventually cause farm-induced blockage are quantified and discussed. First, the blockage effects are quantified for the baseline cases. Second, the sensitivity of the blockage magnitude to array spacing and hill sizes is discussed.

5.6.1. Baseline Cases

The velocity fields obtained from the case studies of flat terrain with and without a turbine array are compared. This is followed by a comparison of the velocity fields of hilly terrain with and without the turbine array. One after the other, the particular effects of the wind farm-induced blockage and hill-induced blockage are isolated and compared for the stability conditions. All velocity comparison is made at the hub height of $H = 95m$ in both flat and hilly terrain. To understand the upstream effects, the velocity reduction is computed at upstream locations of $x = 3D, 5D, 7D, 10D, 15D$.

For a domain without any topological features or obstacles, the velocity remains the same throughout as that of the reference wind speed ($U_{ref} = 10ms^{-1}$). Figure 5.21a and Figure 5.21b show the velocity profile comparison for a flat terrain in the presence and absence of the turbine array. It can be observed that the velocity profile begins to deviate from the reference wind speed which is explained by the presence of the turbine array. Under truly neutral atmosphere conditions, the deviation occurs much closer to the turbine array upstream at around $x = 16D$. On the other hand, for stable free atmosphere conditions, an adverse pressure gradient results in the deceleration of the flow much farther upstream. As observed, turbine array-induced effects are caused much farther upstream and the velocity seems to asymptotically reach the reference velocity. However, in both conditions, induction effects are much more dominant in near-upstream regions and gradually reduce albeit non-negligible farther from the turbine array up to almost $x = 15D$. Similar observations were made by Sanchez Gomez et al., 2021. Stable atmosphere conditions cause a reduction up to $U = 9.6ms^{-1}$ at $x = 3D$ and the truly neutral counterpart sees a reduction up to $U = 9.8ms^{-1}$. Bleeg and Montavon, 2022 and Medici et al., 2011 predicted similar trends in the wind speed reduction. This is followed by a comparison of the velocity

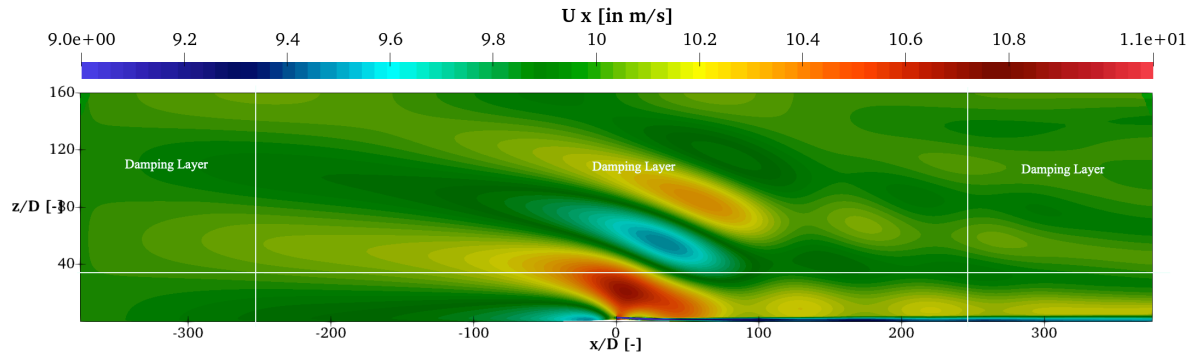

(a) $h = 100m$ & $L = 1200m$ with a hill size of $S_h = 0.08$

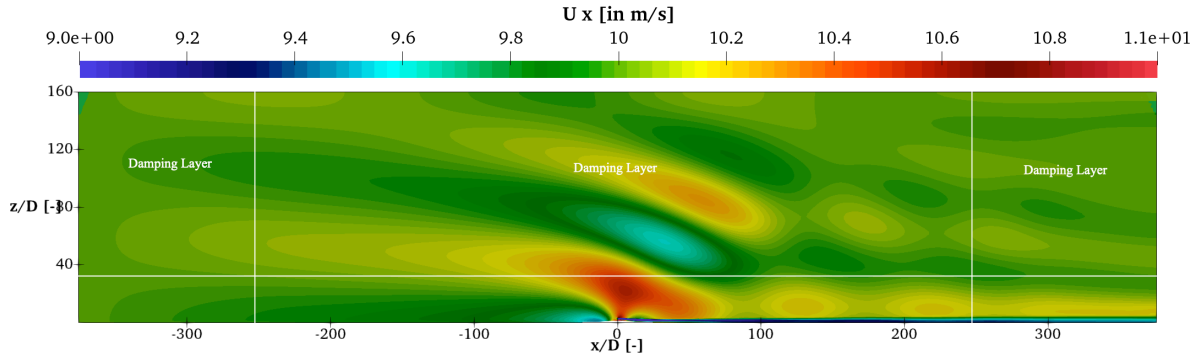

(b) $h = 100m$ & $L = 800m$ with a hill size of $S_h = 0.125$

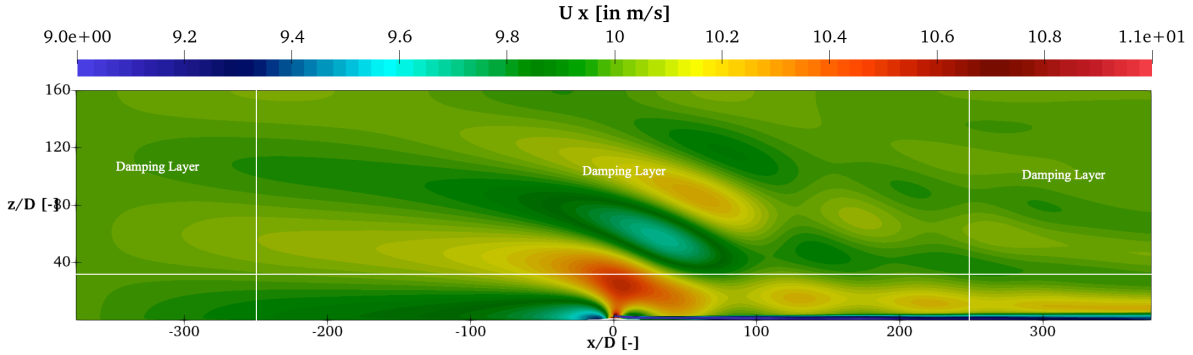

(c) $h = 100m$ & $L = 600m$ with a hill size of $S_h = 0.17$

Figure 5.19: Velocity contour of the turbine array on a hill with varying hill sizes S_h along the X-Y plane of the computational domain

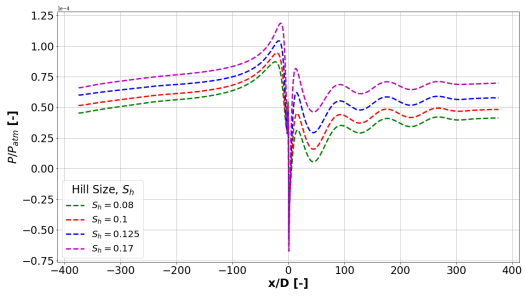

(a) Pressure profiles at hub height

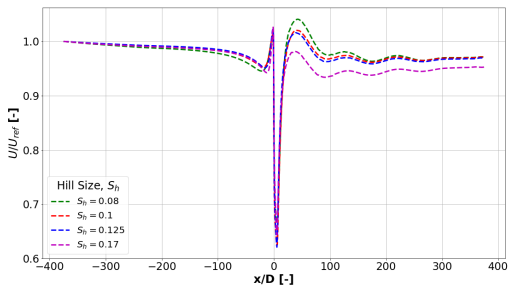

(b) Velocity profiles at hub height

Figure 5.20: Pressure & velocity profiles at hub height $H = 95m$ for different hill sizes corresponding to different Froude numbers

profiles for a hilly terrain which reveals that the variation in velocity is more pronounced. As explained earlier an adverse pressure gradient is induced in both atmospheric conditions resulting in a reduction of velocity. Figure 5.21c shows the cumulative induction effects of both the hill and the turbine array. As opposed to the flat terrain velocity profiles, the velocity reduction is marginally higher and extends farther upstream of the hill. On the other hand, from Figure 5.21d a stable free atmosphere imposes an adverse pressure gradient coupled with the excitation of AGWs leading to a larger deviation.

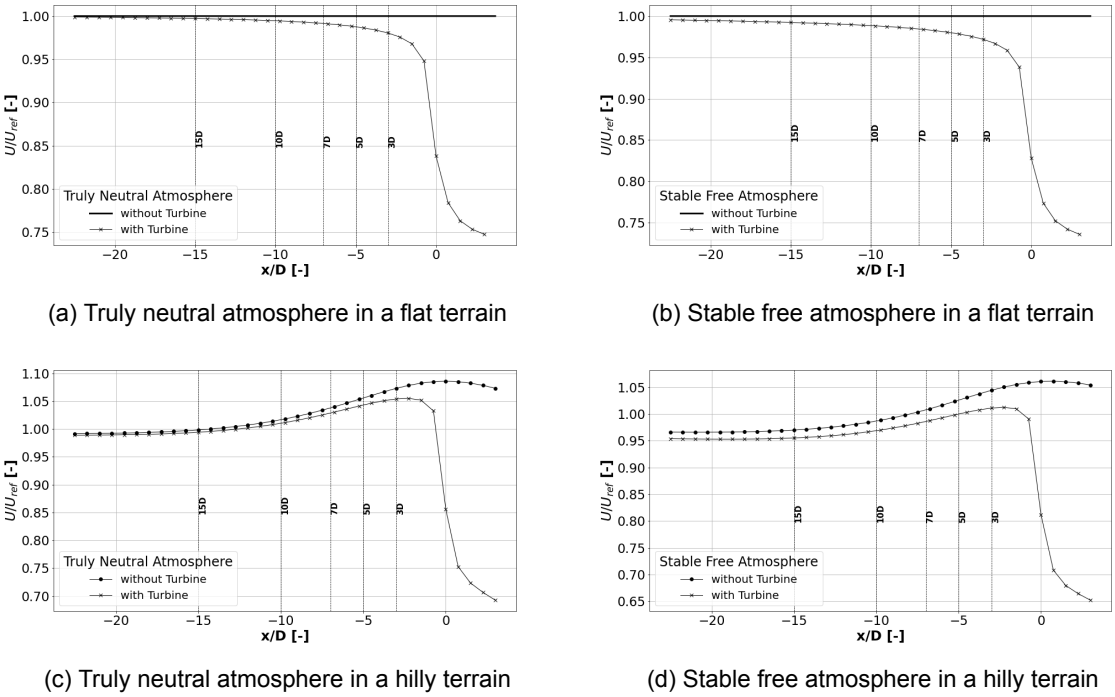

(a) Truly neutral atmosphere in a flat terrain

(b) Stable free atmosphere in a flat terrain

(c) Truly neutral atmosphere in a hilly terrain

(d) Stable free atmosphere in a hilly terrain

Figure 5.21: Velocity profile comparison at hub height $H = 95m$ for cases with & without turbine array

The turbine array-induced velocity reduction is obtained by taking a difference between the velocity profile from simulations with and without the turbine array. In order to get a relative reduction with the free stream wind speed, the difference is normalised with $U_{ref} = 10ms^{-1}$. The comparison is made from $x = 3D$ where the array-induced effects are expected to be dominant. Meyer Forsting et al., 2017, Strickland and Stevens, 2020 and Popescu and Flåtten, 2021 found that the turbine scale induction effects are found to be dominant up to to $2 - 2.5D$ upstream. Although a number of other factors such as the thrust coefficient, wind speed, and rotor diameter influence these hypotheses. As observed in Figure 5.22, the reduced velocity effects are compared for a stable free atmosphere and a truly neutral condition in flat and hilly terrain. The array-induced blockage effects are dominant in all the cases however, the presence of a turbine array and a hill seems to augment the blockage effects. The velocity reduction of nearly 3.3% at $x = 3D$ is induced and gradually goes down albeit non-negligible farther upstream close to 1.4% at $x = 15D$. Figure 5.22b and Table 5.1 gives a detailed quantitative effects of this phenomenon. The reduction, however, is much smaller for the neutral case with 1.9% and 1.95% at $x = 3D$ and gradually reducing to 0.4% and 0.28% at $x = 15D$ for hilly and flat terrain respectively. The key inference that can be drawn from the effects observed here is that the excitation of AGWs and the resulting adverse pressure gradient in the upstream heavily influences the velocity reduction. More so in the case of the turbine array placed on top of the hill. Complimentary to the predictions made by Allaerts and Meyers, 2018, Smith, 2010 and Sivanandan, 2021.

The Table 5.1 further highlights the effects of blockage caused due to the individual case considered in this study.

In this part of the section, the effects of blockage caused due to the presence of the hill are isolated and compared for the truly neutral and stable free atmosphere conditions. These effects are isolated by simply taking a difference in the velocity reduction caused on hilly terrain and on flat terrain. Figure 5.23,

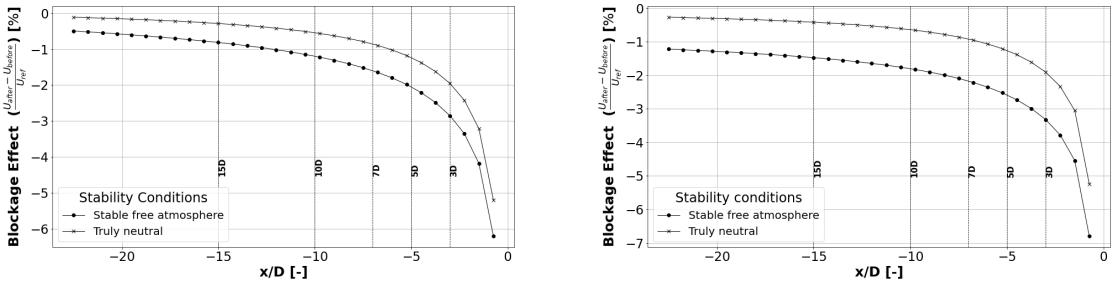

(a) Blockage in a flat terrain

(b) Blockage in a hilly terrain

Figure 5.22: Blockage effects at different upstream distances ahead of the turbine at $x/D = 3D, 5D, 7D, 10D$ along the hub height $H = 95m$

Stability Conditions	Terrain	Blockage Effects [in %]				
		3D	5D	7D	10D	15D
Stable free atmosphere	Hilly	-3.32	-2.52	-2.21	-1.86	-1.47
	Flat	-2.85	-1.98	-1.64	-1.22	-0.81
Truly neutral	Hilly	-1.91	-1.2	-0.95	-0.66	-0.42
	Flat	-1.95	-1.17	-0.89	-0.56	-0.28

Table 5.1: Velocity reduction at upstream distances from the turbine due to blockage effects for the baseline cases

shows that the change in velocity reduction is higher at the farther upstream distances of $x = 10-15D$. The reduction is smaller in the near upstream regions where the array-induced effects are dominant in comparison to the hill-induced effects. The higher reduction in the farther upstream regions is supported by the excitation of AGWs and the resulting adverse pressure gradient. On the other hand, for truly neutral atmosphere conditions, the change in velocity reduction is nearly 10 times lower than the stable free atmosphere counterpart. The hill effective blockage is quantified in Table 5.2

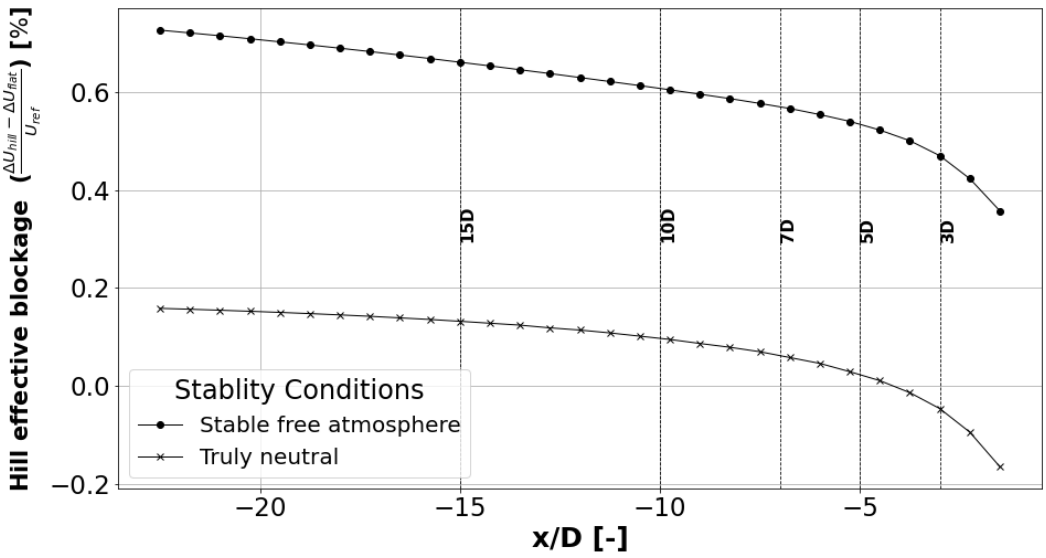

Figure 5.23: Effective blockage caused due to the hill under different atmospheric stability conditions

Stability Conditions	Hill Effective Blockage [in %]				
	3D	5D	7D	10D	15D
Stable free atmosphere	0.47	0.54	0.57	0.60	0.66
Truly neutral	-0.05	0.03	0.06	0.09	0.13

Table 5.2: Velocity reductions caused due to blockage by isolating the effects of the hill for stable & neutral conditions

Lateral Spacing (Δ_y)	Blockage Effects [in %]				
	3D	5D	7D	10D	15D
1.5D	-3.32	-2.52	-2.21	-1.86	-1.47
2D	-2.86	-2.05	-1.89	-1.37	-1.01
2.5D	-2.29	-1.64	-1.51	-1.09	-0.88
3D	-2	-1.43	-1.32	-0.97	-0.8

Table 5.3: Velocity reduction at upstream positions of the turbine leading to blockage effects for varying lateral turbine spacing Δ_y

5.6.2. Blockage Sensitivity to Array-spacing Variations

In this section, a comparative study of the velocity profile for changing lateral spacing is conducted. The resulting turbine induction effects are quantified and discussed. Figure 5.24, shows a quantitative comparison of the velocity profiles across the turbine placed on top of the hill. For each of these cases with a varying lateral spacing of $\Delta_y = 1.5D, 2D, 2.5D, 3D$ a comparison is made with the baseline hilly terrain velocity profile without the turbine array. The turbine array is placed at $x/D = 0$ coinciding with the summit of the hill where a speed-up is also observed. A flow acceleration is observed at the top of the hill to a velocity of $U = 10.5ms^{-1}$ in comparison with the reference velocity of $U_{ref} = 10ms^{-1}$. In each of these plots, it is evident that the turbine array hinders the flow acceleration at the top. The induction effects of the hill begin to appear on the windward side of the hill at the upstream location of $x = 8D$ eventually leading to a maximum reduction to $U = 9.8ms^{-1}$. From Figure 5.24a, for a lateral spacing of $\Delta_y = 1.5D$, the speed-up is reduced to nearly $U = 10.1ms^{-1}$. This effect is attributed to the adverse pressure gradient resulting due to the excitation of AGWs by the cumulative effect of the hill as well as the turbine array. The velocity profile of the turbine case is marginally displaced changing the flow field on the windward side of the hill and also a higher magnitude of cumulative induction effects at $U = 9.6ms^{-1}$. As explained earlier, the strong hill induction effects overplay the role of the Venturi effect thus leading to a marginal acceleration in the flow with increasing lateral spacing. With increasing lateral spacing, the flow speed-up is also slightly increased. For instance, the Figure 5.24b shows $U = 10.2ms^{-1}$ for a spacing of $\Delta_y = 2D$ and Figure 5.24d shows the maximum velocity at approximately $U = 10.4ms^{-1}$ for a spacing of $\Delta_y = 3D$. The cumulative induction of the hill and turbine array also seems to be slightly displaced from close to $x = 5D$ for the densely spaced array to gradually increase to $x = 6D$, $6.2D$, and $6.5D$ with increasing spacing. The resulting flow blockage effects are expected to be influenced due to these observed phenomena.

As explained in the velocity profile comparison, the relative velocity reduction for the smallest lateral spacing seems to be the highest in the near upstream region of $x = 3D$ to a maximum of 3.3%. Eventually, in the far upstream flow converges to a lower reduction of velocity. Figure 5.25 shows that the trend followed by the variation in lateral spacing is similar for all the cases. Nevertheless, the change in velocity reduction is non-negligible. The percentage blockage reduction due to varying array spacing at different upstream positions is shown in Table 5.3. The maximum reduction is observed in the region close to the turbine [$x = 3D$] due to enhanced induction effects at the turbine scale. Eventually, the blockage reduces and attains a more uniform profile at upstream positions of $x = 20D$. Similar trends are observed by Sanchez Gomez et al., 2021, Segalini and Dahlberg, 2019 and Meyer Forsting et al., 2017. The apparent advantage experienced with increased spacing is attributed to the flow expansion around the turbines [reduction in pressure leading to a subsequent increase in velocity].

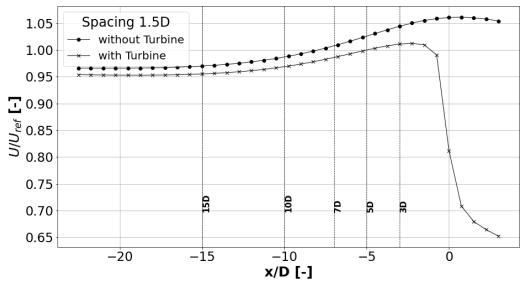

(a) Lateral spacing $\Delta_y = 1.5D$

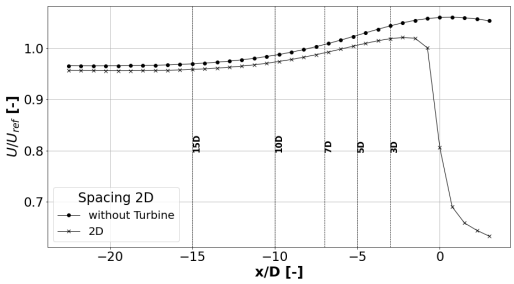

(b) Lateral spacing $\Delta_y = 2D$

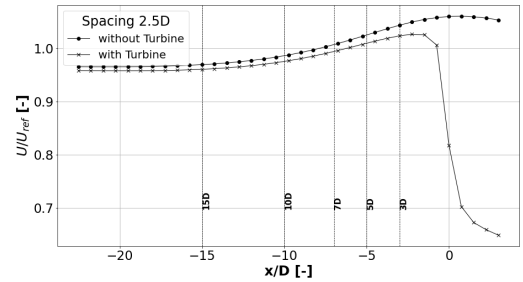

(c) Lateral spacing $\Delta_y = 2.5D$

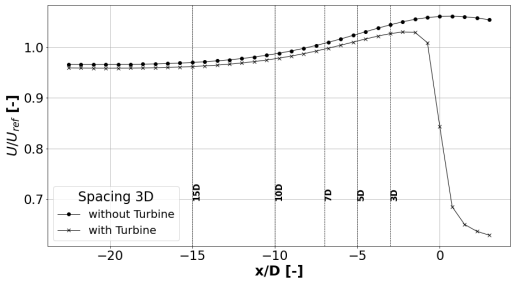

(d) Lateral spacing $\Delta_y = 3D$

Figure 5.24: Velocity profile comparison for on a hilly terrain with and without the turbine array at hub height $H = 95m$ above the hill

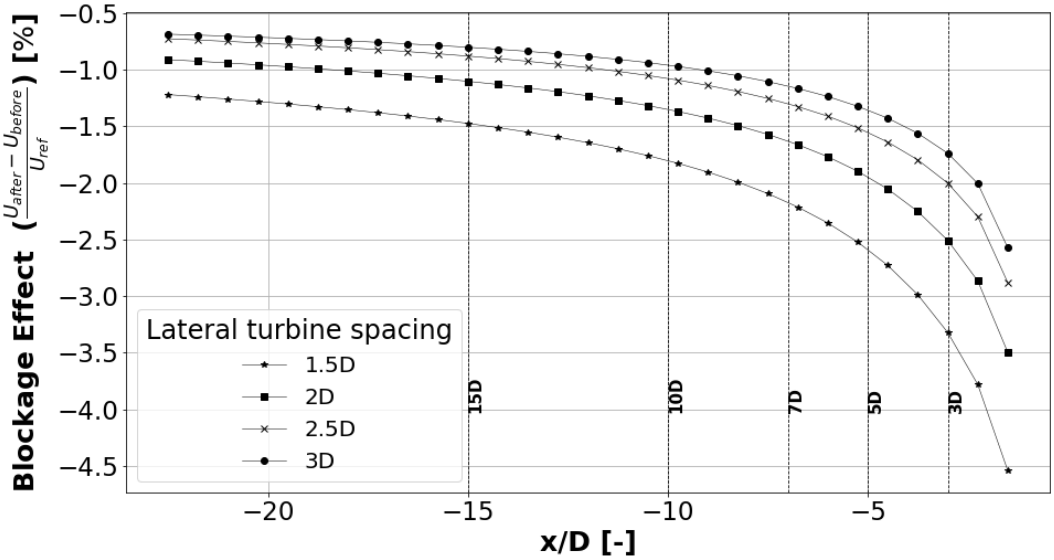

Figure 5.25: Blockage effects at different upstream distances of the turbine array at $x/D = 3, 5, 7, 10$ for a lateral spacing of $\Delta_y = 1.5D, 2D, 2.5D, 3D$

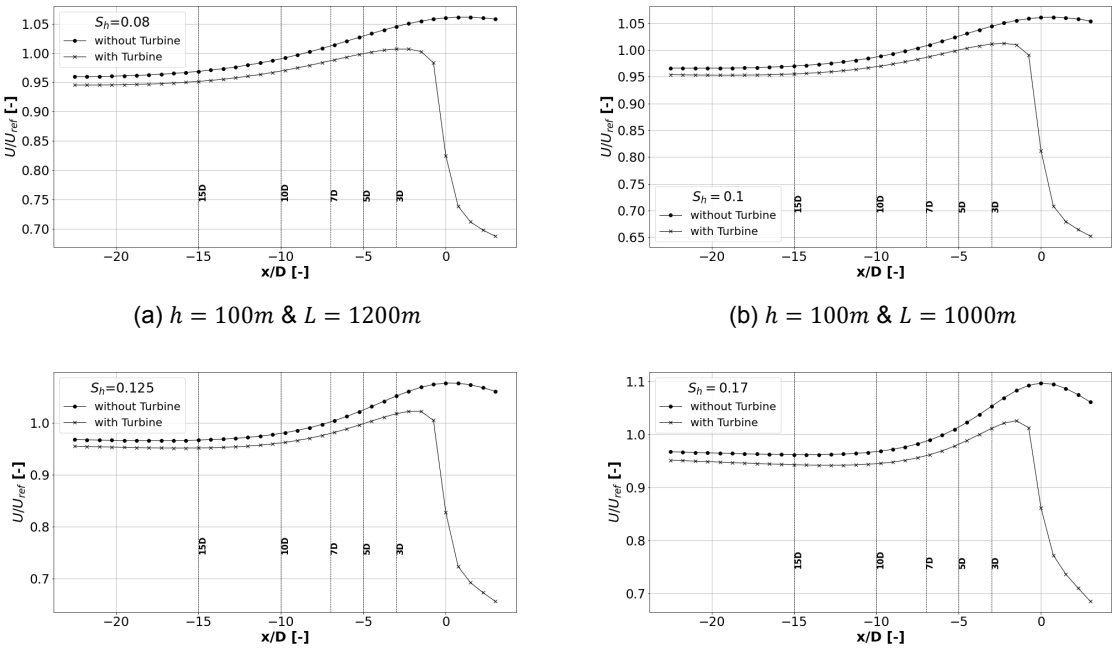

(a) $h = 100m$ & $L = 1200m$

(b) $h = 100m$ & $L = 1000m$

(c) $h = 100m$ & $L = 800m$

(d) $h = 100m$ & $L = 600m$

Figure 5.26: Velocity profile comparison on hilly terrain with and without the turbine array at hub height $H = 95m$ above the hill for varying hill sizes

5.6.3. Blockage Sensitivity to Hill-size Variations

In this section, a comparative study of the velocity profiles for varying hill sizes (S_h) is carried out. First, the velocity profile for varying hill widths in the absence of the turbine array is compared with the one with a turbine array atop. This is followed by the comparison of blockage magnitude for the various cases. Figure 5.26 is a comparison of the velocity profile for the baseline case of $S_h = 0.1$ and subsequently followed by the other cases of hill sizes. As explained in the previous sections, hill size has a major impact on the induction effects on the windward side of the hill and also the subsequent speed-up at the summit. This behaviour is attributed to the alternating adverse and favourable pressure gradient across the hill in turn leading to alternating velocity decrease and increase. The behaviour for the baseline case of $S_h = 0.1$ is already discussed in the previous section. The same argument is applicable for the case with a hill size of $S_h = 0.08$, where the hill is made shallower than the previous case with a base width of $L = 1200m$. The trend and behaviour of the flow velocity without the turbine array seem to match well with the baseline case. However, the turbine array-induced effects are observed to influence the velocity profile of the case with $S_h = 0.08$. All the cases with turbines show inhibition in the speed-up over the hill, but Figure 5.26a shows more reduction at the hill summit. Subsequently, for the steeper case of $S_h = 0.125$ and $S_h = 0.17$, the speed-up is higher at $U = 10.8ms^{-1}$ and $U = 11ms^{-1}$ respectively. But the turbine cases again inhibit the speed-up to nearly $U = 10.2ms^{-1}$ in both cases. This is an indication that the induction effects especially at the turbine scale are solely driven by the thrust coefficient (C_T). An argument supported by Forsting et al., 2016 and Nygaard et al., 2020. It is interesting to note that induction effects on the windward side of the hill are higher for steeper hills as the gradient of pressure is sharper. [See Figure 5.26c and Figure 5.26d]. The same behaviour is observed for the case with the turbine array atop these hill cases, the induction effects are much stronger and convecting farther upstream. Whereas, in the shallow hill cases of $S_h = 0.08$ and 0.1, the induction effects are albeit dominant but form a plateau [see Figure 5.26a and Figure 5.26a]. This is again a result of the gradient of pressure on the windward side of the hill. A smooth gradient of pressure results in a narrower reduction of velocity in the induction region. This behaviour was observed in the studies done by Zhang et al., 2022 and Yang et al., 2015.

A relative reduction in the velocity fields of the cases with and without the turbines yields the effects of blockage. A comparison of the effects of blockage caused due to the turbine array is shown in

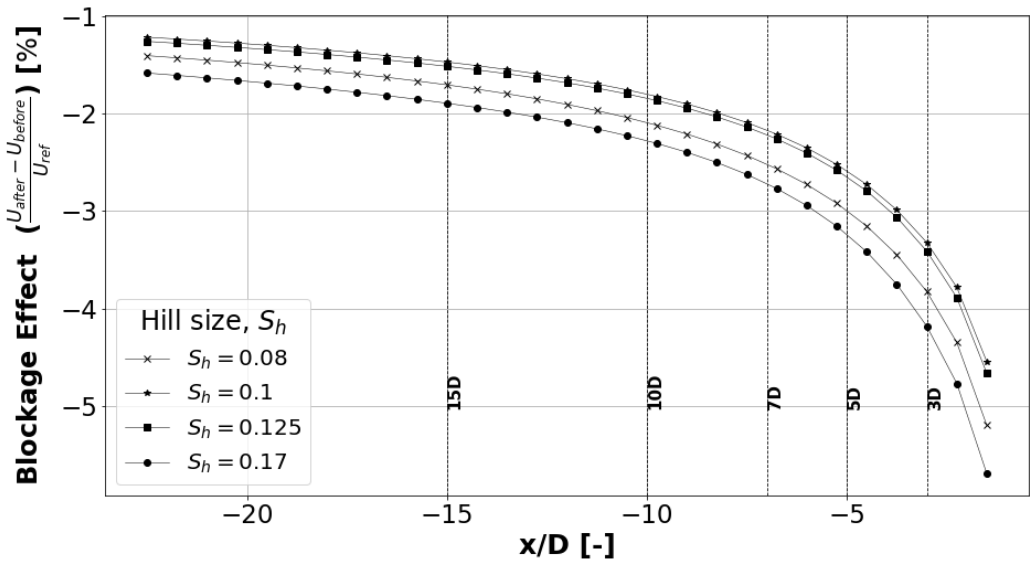

Figure 5.27: Blockage effects at different upstream distances ahead of the turbine array for different hill sizes corresponding to certain Froude numbers

Hill Size (S_h)	Blockage Effects [in %]				
	3D	5D	7D	10D	15D
0.08	-3.83	-2.92	-2.57	-2.12	-1.71
0.1	-3.32	-2.52	-2.21	-1.86	-1.47
0.125	-3.41	-2.58	-2.26	-1.87	-1.52
0.17	-4.18	-3.16	-2.77	-2.31	-1.89

Table 5.4: Velocity reduction at upstream positions of the turbine leading to blockage effects for varying hill sizes S_h

Figure 5.27. As seen in the figure and explained earlier in this section, the effects of blockage are higher in the near upstream regions at $x = 3D$. All the cases follow a similar trend where the blockage effects are the highest in the near upstream region of the turbine array at $x = 3D, 5D$ eventually the effects reduce in the far upstream. The blockage effects are seen to be highest when the hill steepness is at its maximum. Table 5.4 shows the percentage reduction in velocity for the varying hill size cases. It is evident that the size of the hill has less impact on the trend in the blockage effects observed. The degree of reduction in velocity for cases with and without the turbine array changes for varying hill sizes. While the maximum reduction is seen for the steepest hill case, the shallowest hills do not necessarily yield the lowest blockage effects. Interestingly, for hill sizes of $S_h = 0.125$ and $S_h = 0.1$ the velocity reduction seems to be very close to one another at different upstream locations. On the other hand for a hill size of $S_h = 0.08$, where the base width is at a maximum value of $L = 1200m$, intermediate effects of velocity reduction are observed. This is again supported by the pressure perturbations that result from the excitation of AGWs, which impact the blockage effects. The steep hill ($S_h = 0.17$) case has higher blockage due to the hill induction effects while in the shallow hill ($S_h = 0.08$) pressure perturbations resulting from stronger AGWs cause a higher magnitude of blockage.

It is also important to know the effective blockage caused by isolating the effects of the hill. Figure 5.28 shows the effective blockage by taking the difference in velocity reduction caused due to the hill and in flat terrain. The effective velocity reduction for the different hill sizes shows rather strange behaviour. For the shallow hill case of $S_h = 0.08$, the change in velocity reduction nearly remains constant at all measured locations on the windward side. Although the differences seen are in the order of magnitude of 10^{-2}. For the baseline case of $S_h = 0.1$, the change in velocity reduction follows a slightly different trend than in the previous case. Similar to this case, the trend observed by the case

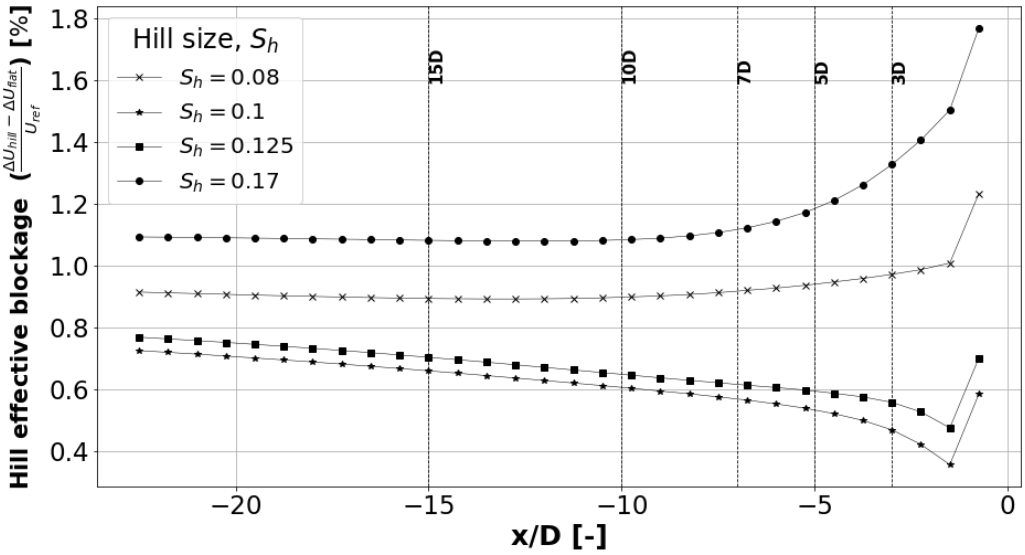

Figure 5.28: Hill effective blockage at different upstream distances ahead of the turbine array for different hill sizes $S_h = 0.08, 0.1, 0.125, 0.17$

Hill Size, S_h	Height, h (in m)	Base width, L (in m)	Hill Effective Blockage [in %]				
			3D	5D	7D	10D	15D
0.08	100	1200	0.97	0.94	0.92	0.89	0.89
0.1		1000	0.47	0.54	0.56	0.60	0.66
0.125		800	0.56	0.59	0.61	0.65	0.70
0.17		600	1.32	1.17	1.12	0.95	0.95

Table 5.5: Velocity reduction caused due to blockage by isolating the effects of the hill for stable conditions

of $S_h = 0.125$ also follows the same pattern. However, the magnitude is slightly shifted by an order of 0.1. However, a heightened difference in velocity reduction is observed for the steep case with a hill size $S_h = 0.17$. This is because of the stronger induction effects caused by the hill in the near upstream regions of the hill. Eventually, the reduction drops in the far upstream as the hill induction effects become negligible. A more convincing understanding of the physics of these different cases is required to understand the behaviour of the effective blockage caused by the hill. Finally, the bottom line inference from this analysis is that the hill-induced effects are more significant than the turbine-induced reduction. This behaviour is again explained due to the pressure gradients observed in the flow and the resulting velocity changes. The quantified hill effective blockage at each upstream probe location for the various hill sizes is shown in Table 5.5.

5.7. Summary

This section sheds light on the main conclusions drawn from the results obtained in this study. Velocity reduction effects under different stability conditions and terrain conditions are examined and presented herewith. The primary conclusions are as follows -

- Momentum deficit and an equivalent velocity reduction are evident upstream of a wind turbine array. The highest reduction is observed in the near upstream of an array and gradually reaches freestream velocity several diameters downstream.
- In coherence with the observations made by other similar studies, velocity deficit is influenced by changing atmospheric stability conditions. The observed wake deficit is substantially higher

for stable atmospheric conditions in comparison with a truly neutral atmosphere. On the other hand, the upstream deficit is also higher for stable atmospheric conditions. This is attributed to the pressure perturbations resulting from the excitation of AGWs.

- Induction effects caused in a truly neutral atmosphere are found to be radially uniform. On the other hand, the effects are not radially uniform but convect farther upstream in a stable free atmosphere condition.
- Flow in a domain across a 2-D hill leads to a speed-up at the summit and further leads to higher availability of kinetic energy. The speed-up is observed to be higher in a neutral atmosphere than in stable conditions. This hindrance is again attributed to the AGWs excited topological changes due to the hill. On the windward side, an adverse pressure gradient is created subsequently resulting in a reduction in velocity. This forms the induction region of the hill. Stable atmospheric conditions have a higher velocity reduction compared to the neutral case owing to the steeper adverse pressure gradient.
- In the case of a turbine array atop a hill, speed-up effects is hindered. This is attributed to the turbine scale induction effects based on a chosen thrust coefficient (C_T). Both stability conditions observed these effects but with a slightly higher reduction under stable free atmosphere conditions. The hill induction region is amplified due to the added induction effects of the turbine array. A stable free atmosphere is observed to give rise to more dominant induction effects caused by the pressure perturbations resulting from AGWs.
- Blockage effects were computed for all the cases studied in the present research. The blockage effects were seen to be dominant under stable conditions in comparison with the truly neutral conditions. These effects were attributed to the excited AGWs and the subsequent adverse pressure gradient upstream. Neutral conditions also pose non-negligible blockage effects but the magnitude is considerably lower than the stable conditions. As an extension of these effects, hill effective blockage was also found to be higher for stable conditions.
- Sensitivity of the blockage effects was carried out for varying lateral spacing and hill sizes. Larger spacing between the turbines within the array provided a flow acceleration. Thus reducing the blockage magnitude as the spacing increases from $\Delta_y = 1.5D, 2D, 2.5D, 3D$. Although the magnitude of fluctuations of the AGWs almost remains the same for these cases, the predicted flow acceleration is observed due to the expansion between the turbines.
- With the varying hill sizes, the velocity fluctuations and pressure perturbations due to AGWs are considerably altered. Therefore, the hill induction region is affected due to the adverse pressure gradients observed in these cases. The steepest hill provided the highest blockage as the hill-induced velocity reduction was highest. However, a major inference is that the steepness alone does not drive the magnitude of blockage. As the base width of the hill increases, the hill induction effects are observed farther downstream. Therefore, the magnitude of blockage is still higher for the hill size with a wider base. This was attributed to the variation in the pressure fields for each of these hill cases.
- The overall energy production estimated using the 'wakes-only' approach creates a non-negligible bias. This needs to be accounted for by calculating the power production bias resulting from the blockage effects. The current research comprehensively proves that the bias caused due to blockage is more amplified in complex terrain. Wind farm planning and estimations need careful consideration of these effects and met-mast measurements need to be carefully calibrated for such scenarios.

6

Conclusions & Recommendations

The main conclusions of the results obtained in the present study are enlisted in the previous chapter. However, there are several other observations that are made throughout the research which are briefly summarised in this chapter. Along with this, there are a few shortcomings of the present steady which are mentioned. A leeway is also provided into ways in which this study can be further extended by wind energy enthusiasts.

6.1. Main Conclusions

In this section, the main conclusions made in this study are listed. These are -

- The atmospheric stability conditions have a major impact on the velocity and pressure fields. This was found to be of particular interest when topological abnormalities or obstacles were found in the domain.
- In all of the cases under stable free atmosphere conditions, vertically standing atmospheric gravity waves (AGWs) were generated, leading to velocity and pressure fluctuations. In particular, AGWs created an adverse pressure gradient in the windward direction leading to a substantial reduction in the velocity of the flow.
- A good balance between the domain size and the damping characteristics is necessary in order to minimise the spurious AGW reflection from the domain walls. In this study, an optimum damping coefficient of $0.025s^{-1}$ and damping layer thickness of $10km$ are found to minimise the reflections to the best possible extent.
- The wavelength of AGWs seems to be solely driven by the background flow parameters such as the Brunt-Väisälä frequency (N) and freestream velocity (U_{ref}). But the amplitude of the AGWs and the fluctuation in velocity are found to be dependent on the dimensions of the obstacle. In this case, the base width of the hill seemed to have more impact than the hill height or the height of the turbines within the array.
- AGWs play a major role in accounting for the blockage effects that are caused even in flat terrain and more pronounced in hilly terrain. This implies that the blockage effects are amplified due to the stability conditions of the atmosphere. However, albeit of lower magnitudes, considerable losses in kinetic energy (Velocity) were also observed under truly neutral atmospheric conditions.
- Although the AGWs seemed to be less sensitive to changing turbine spacing parameters, blockage effects seemed to be more susceptible. This was found to be the case, especially for wide lateral spacing due to flow expansion and subsequent acceleration eventually overcoming the AGW-induced velocity reduction.
- AGWs seemed to be more sensitive to changing hill conditions (in terms of base width). As a direct consequence of this, the pressure fields were also perturbed subsequently leading to a higher blockage sensitivity.

6.2. Recommendations

In this section, the limitations of the present study and the ways in which it can be possibly mitigated are discussed. Major limitations throughout the study are classified into the following -

6.2.1. Blockage Magnitude

In the present study, the blockage effects are estimated directly by taking the difference in velocity fields with and without the turbine array. However, the turbine scale and farm scale blockage effects are not clearly distinguished in this methodology. In order to capture the said effects, the velocity fields would have to be observed by isolating a single turbine and comparing them with the ones obtained in an array. By doing so, the consequences of wind farm blockage on met mast measurements, lidar measurements, and inflow velocity for wake deficit measurements are better understood.

Furthermore, studies have shown that wake effects are affected by the location of a turbine array in hilly terrain. For instance, wake deficit varies for a turbine placed on the windward side as opposed to the leeward side or on top of a hill. An extension of this knowledge is necessary on wind farm blockage effects as well. Therefore, research needs to be carried out for flow cases with the turbine array at different locations in hilly terrain. Along with this, further research needs to be conducted with multiple rows of turbines to understand the effects of blockage of the first row and the subsequent rows.

Additionally, the effects of turbulence are minimised in the present case with - `slip` BC and uniform inflow assumption. An extension of the present study needs to be researched by introducing a more realistic `noSlip` BC and a logarithmic velocity profile accounting for the surface roughness as well. However, studies have shown that blockage effects are less affected by turbulence contrary to the wake behaviour.

6.2.2. Future Case Studies

In this study, with the assumption of a `slip` BC, boundary layer formation is not observed. In reality, with the formation of ABL, the AGWs are expected to behave differently. Specifically, in the case of a CNBL, the excited AGWs are trapped in the capping inversion and eventually convect farther upstream distances. Studies have shown that these AGWs cause adverse pressure gradients at hub height and eventually reduce the velocity upstream. The present research needs to be extended with the said considerations to further assess energy production with fewer uncertainties.

Furthermore, the blockage magnitude is expected to be sensitive to the strength and height of the capping inversion. With a lack of boundary layer formations and CNBL formulation, these effects are not explicitly considered in this study. Due to the altering AGW behaviour, the induction region and the subsequent blockage effects are also expected to alter. The inversion strength based on the temperature jump from the bottom to the top of the layer causes sharper density variation. This is expected to influence the amplitude of velocity fluctuations due to the excited AGWs. The resulting pressure perturbations and the adverse pressure gradient upstream also influence the blockage magnitude.

The sensitivity analyses carried out in the study here are restricted only to the base width of the hill. However, in order to assess the influence of flow speed up on the induction region, it is essential to further extend this research with varying heights of the hill. Increasing the height of the hill is expected to increase the ratio of speed-up at the summit and therefore higher energy availability. It would be interesting to understand the behaviour of the blockage effects in such cases.

6.2.3. Simulation Setup

The present study employs the modelling of wind turbines using an actuator disk. This is a major simplification as the effects of the blade mainly the root and tip vortices are not considered. An extended analysis by accounting for these effects is necessary to better understand blockage effects. These effects are expected to specifically influence the turbine scale induction region. This eventually leads to the amplification of the blockage effects.

The directional changes in wind flow are neglected in the present case due to the spanwise infinite considerations. These changes need to be considered to understand the effects of the wind farm and turbine scale induction effects. The induction region might vary in magnitude for varying flow direction changes. In addition, the turbine array is aligned normally to the free stream velocity. Studies have shown that blockage is sensitive to yawed effects of the turbine array. In the present study, this can further be influenced by the induction effects of the hill due to yawing the turbine array.

Appendix - A

Contour Plots - Hill size variations

Vertical Velocity Component

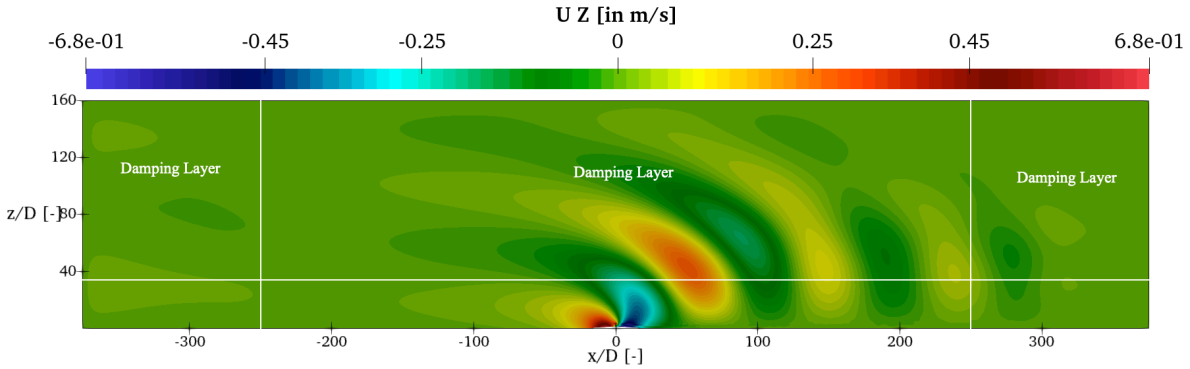

Figure 1: Vertical velocity component for the baseline case with the turbine array in a hilly terrain

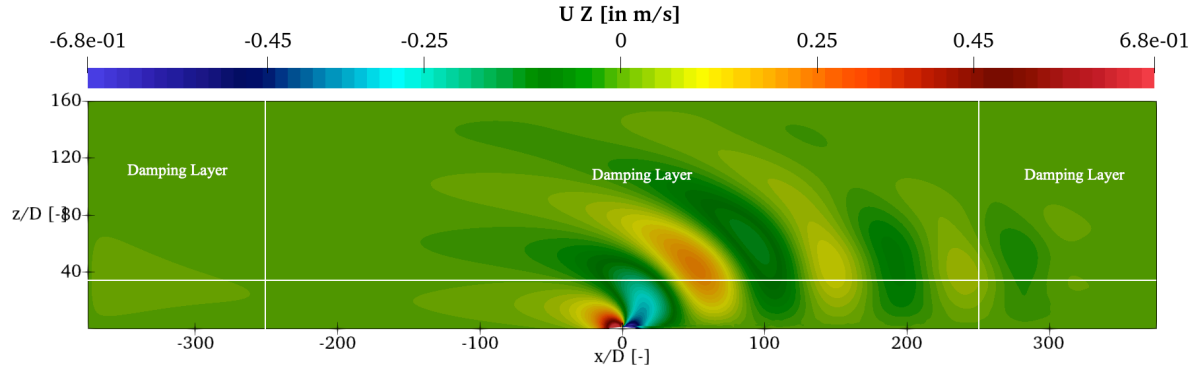

Figure 2: Vertical velocity component for the case of hill size $S_h = 0.17$ with turbine array atop

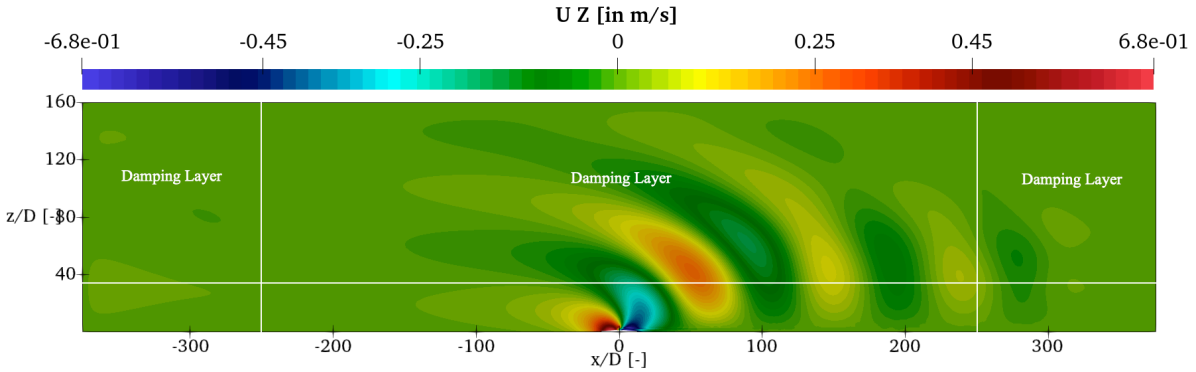

Figure 3: Vertical velocity component for the case of hill size $S_h = 0.125$ with turbine array atop

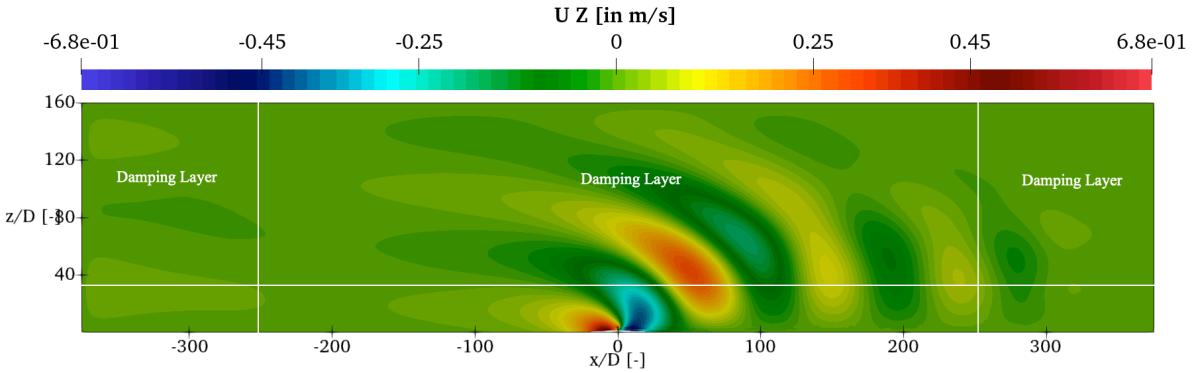

Figure 4: Vertical velocity component for the case of hill size $S_h = 0.08$ with turbine array atop

Horizontal Velocity Component

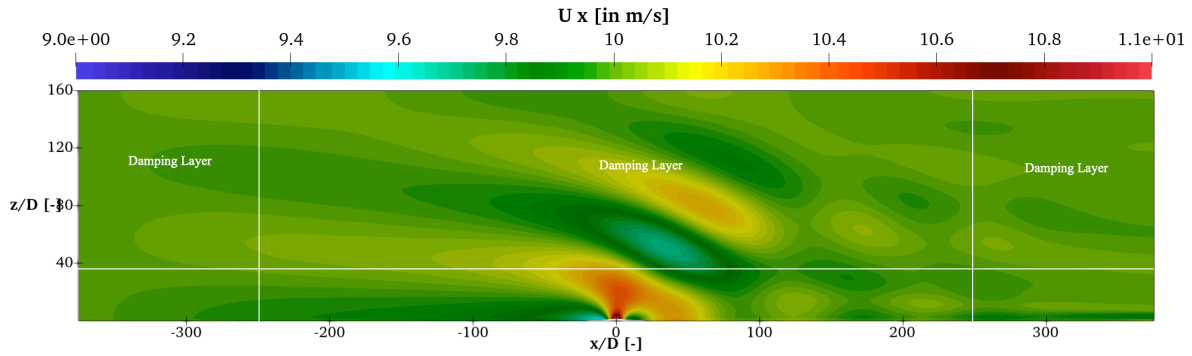

Figure 5: Horizontal velocity component for the case of hill size $S_h = 0.17$ without turbine array

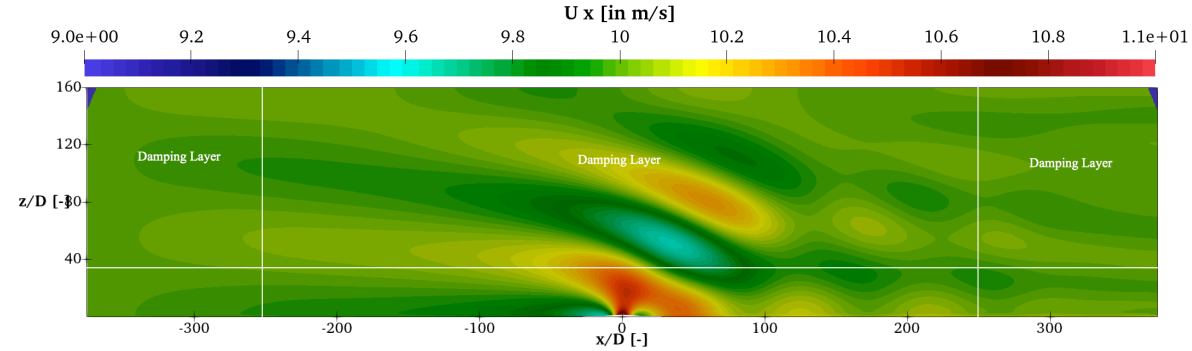

Figure 6: Horizontal velocity component for the case of hill size $S_h = 0.125$ without turbine array

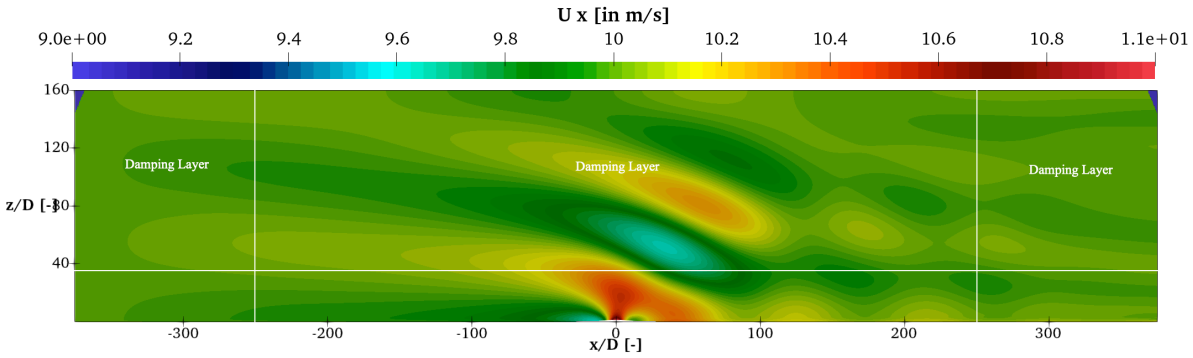

Figure 7: Horizontal velocity component for the case of hill size $S_h = 0.08$ without turbine array

Hill Speed-ups

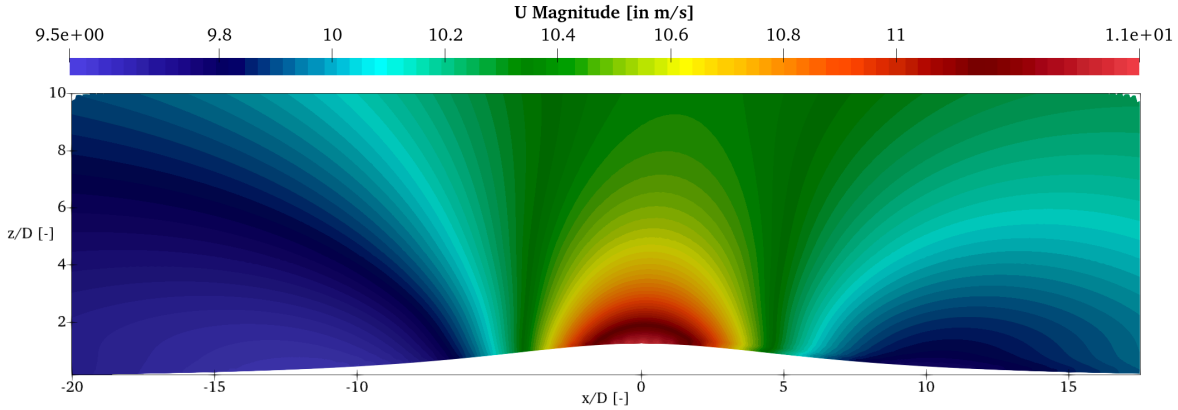

Figure 8: Flow speed-up for the case of hill size $S_h = 0.17$

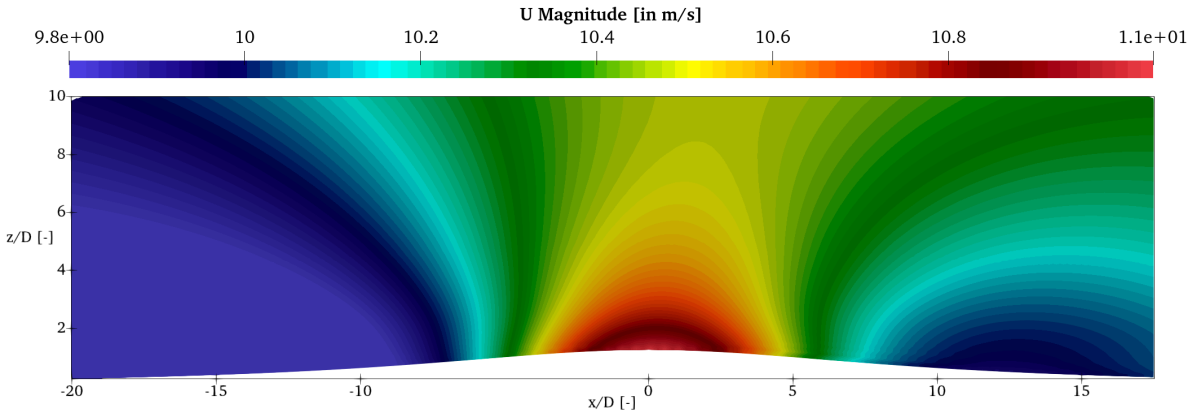

Figure 9: Flow speed-up for the case of hill size $S_h = 0.125$

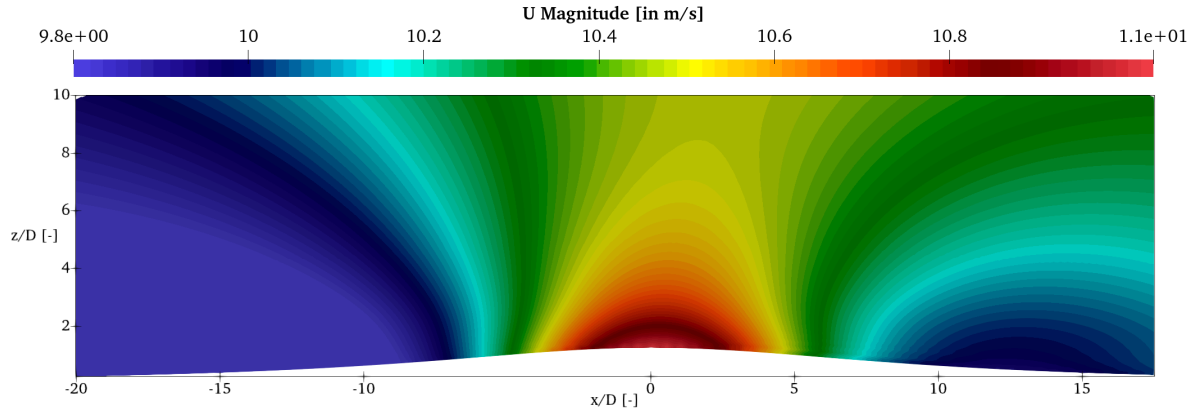

Figure 10: Flow speed-up for the case of hill size $S_h = 0.08$

Bibliography

Abkar, M., & Porté-Agel, F. (2013). The effect of free-atmosphere stratification on boundary-layer flow and power output from very large wind farms. *Energies*, *6*(5), 2338–2361. https://doi.org/10.3390/en6052338

Abkar, M., & Porté-Agel, F. (2015). Influence of atmospheric stability on wind-turbine wakes: A large-eddy simulation study. *Physics of Fluids*, *27*(3). https://doi.org/10.1063/1.4913695

Alfredsson, P. H., & Segalini, A. (2017). Wind farms in complex terrains: An introduction. https://doi.org/10.1098/rsta.2016.0096

Allaerts, D. (2016). *Large-eddy Simulation of Wind Farms in Conventionally Neutral and Stable Atmospheric Boundary Layers* (Doctoral dissertation). KU Leuven. Leuven, Belgium.

Allaerts, D., & Meyers, J. (2014). Wind farm performance in conventionally neutral atmospheric boundary layers with varying inversion strengths. *Journal of Physics: Conference Series*, *524*(1). https://doi.org/10.1088/1742-6596/524/1/012114

Allaerts, D., & Meyers, J. (2017). Boundary-layer development and gravity waves in conventionally neutral wind farms. *Journal of Fluid Mechanics*, *814*, 95–130. https://doi.org/10.1017/jfm.2017.11

Allaerts, D., & Meyers, J. (2018). Gravity Waves and Wind-Farm Efficiency in Neutral and Stable Conditions. *Boundary-Layer Meteorology*, *166*(2), 269–299. https://doi.org/10.1007/s10546-017-0307-5

Amahjour, N., & Khamlichi, A. (2017). Modeling of wind speed in the atmospheric boundary layer in the presence of hill like obstacles. *CFM 2017 - 23ème Congrès Français de Mécanique, Lille, France*.

Avila, M., Folch, A., Houzeaux, G., Eguzkitza, B., Prieto, L., & Cabezón, D. (2013). A parallel CFD model for wind farms. *Procedia Computer Science*, *18*, 2157–2166. https://doi.org/10.1016/j.procs.2013.05.386

Baines, P. G. (1979). Observations of Stratified Flow Past Three-Dimensional Barriers. *Journal of Geophysical Research*, *84*(C12), 7834–7838. https://doi.org/10.1029/JC084iC12p07834

Bastankhah, M., Welch, B. L., Martínez-Tossas, L. A., King, J., & Fleming, P. (2021). Analytical solution for the cumulative wake of wind turbines in wind farms. *Journal of Fluid Mechanics*, *911*. https://doi.org/10.1017/jfm.2020.1037

Bleeg, J., & Montavon, C. (2022). Blockage effects in a single row of wind turbines. *Journal of Physics: Conference Series*, *2265*(2), 022001. https://doi.org/10.1088/1742-6596/2265/2/022001

Bleeg, J., Purcell, M., Ruisi, R., & Traiger, E. (2018). Wind farm blockage and the consequences of neglecting its impact on energy production. *Energies*, *11*(6). https://doi.org/10.3390/en11061609

Branlard, E., & Forsting, A. R. M. (2020). Assessing the blockage effect of wind turbines and wind farms using an analytical vortex model. https://doi.org/10.1002/we

Branlard, E., Quon, E., Meyer Forsting, A. R., King, J., & Moriarty, P. (2020). Wind farm blockage effects: Comparison of different engineering models. *Journal of Physics: Conference Series*, *1618*(6). https://doi.org/10.1088/1742-6596/1618/6/062036

Castellani, F., Astolfi, D., Burlando, M., & Terzi, L. (2015). Numerical modelling for wind farm operational assessment in complex terrain. *Journal of Wind Engineering and Industrial Aerodynamics*, *147*, 320–329. https://doi.org/10.1016/j.jweia.2015.07.016

Clausen, P. D., & Wood, D. H. (1999). Research and Development Issues for Small Wind Turbines. *Renewable Energy 16*, *16*.

Davies, B. (2020). An Article on Climate Change. https://www.antarcticglaciers.org/glaciers-and-climate/climate-change/

Deaves, D. M. (1980). Computations of Wind Flow Over Two-Dimensional Hills and Embankments. *Journal of Wind Engineering and Industrial Aerodynamics*, *6*, 89–111.

Deusebio, E., Brethouwer, G., Schlatter, P., & Lindborg, E. (2014). A numerical study of the unstratified and stratified Ekman layer. *Journal of Fluid Mechanics*, *755*, 672–704. https://doi.org/10.1017/jfm.2014.318

Emeis, S. (2014). Current issues in wind energy meteorology. https://doi.org/10.1002/met.1472

Forsting, A. R., Bechmann, A., & Troldborg, N. (2016). A numerical study on the flow upstream of a wind turbine in complex terrain. *Journal of Physics: Conference Series*, *753*(3). https://doi.org/10.1088/1742-6596/753/3/032041

Forsting, A. R., & Troldborg, N. (2015). The effect of blockage on power production for laterally aligned wind turbines. *Journal of Physics: Conference Series*, *625*(1). https://doi.org/10.1088/1742-6596/625/1/012029

Gadde, S. N., & Stevens, R. J. (2019). Effect of Coriolis force on a wind farm wake. *Journal of Physics: Conference Series*, *1256*(1). https://doi.org/10.1088/1742-6596/1256/1/012026

Garratt, J. (1989). The Internal Boundary Layer - A Review.

Gisinger, S. (2018). Gravity Waves in the Lower Atmosphere in Mountainous Regions and the Role of the Tropopause.

Global Temperatures. (2022). https://www.unep.org/news-and-stories/story/alarming-rise-global-temperatures

Gryning, S. E., Batchvarova, E., Brümmer, B., Jørgensen, H., & Larsen, S. (2007). On the extension of the wind profile over homogeneous terrain beyond the surface boundary layer. *Boundary-Layer Meteorology*, *124*(2), 251–268. https://doi.org/10.1007/s10546-007-9166-9

Hansen, M. O. (2015). *Aerodynamics of Wind Turbines* (Third, Vol. 1). Routledge, Taylor & Francis Group.

Haupt, S., Allaerts, D., Berg, L., Churchfield, M., DeCastro, A., Draxl, C., Gagne, D. J., Hawbecker, P., Jimenez, P., Jonko, A., Juliano, T., Kaul, C., Kosović, B., McCandless, T. C., Mirocha, J., Munoz-Esparza, D., Quon, E., Rai, R., Sauer, J., & Shaw, W. (2019). *FY 2019 Report of the Atmosphere to Electrons Mesoscale-to-Microscale Coupling Project* (tech. rep.). US Department of Energy. Richland, Washington. https://www.ntis.gov/about

Hess, G. D., & Garratt, J. R. (2002). Evaluating Models of The Neutral, Barotropic Planetary Boundary Layer Using Integral Measures: Part II. Modelling Observed Conditions. *Boundary-Layer Meteorology*.

Hills, M. O., & Durran, D. R. (2012). Nonstationary trapped lee waves generated by the passage of an isolated jet. *Journal of the Atmospheric Sciences*, *69*(10), 3040–3059. https://doi.org/10.1175/JAS-D-12-047.1

Hylleberg, J. (2014). Profile of the Danish Wind Industry. www.windpower.org

Hyvarinen, A., & Segalini, A. (2017). Qualitative analysis of wind-turbine wakes over hilly terrain. *Journal of Physics: Conference Series*, *854*(1). https://doi.org/10.1088/1742-6596/854/1/012023

Hyvärinen, A., & Segalini, A. (2017). Effects from Complex Terrain on Wind-Turbine Performance. *Journal of Energy Resources Technology, Transactions of the ASME*, *139*(5). https://doi.org/10.1115/1.4036048

International Renewable Energy Agency, I. (2019). *Future of Wind, IRENA* (tech. rep.). www.irena.org/publications.

Jegede, O. O., & Foken, T. (1999). A study of the internal boundary layer due to a roughness change in neutral conditions observed during the LINEX field campaigns. *Theoretical and Applied Climatology*, *62*(1-2), 31–41. https://doi.org/10.1007/s007040050072

Kim, S.-W., Park, S.-U., & Moeng, C.-H. (2003). Entrainment Processes in The Convective Boundary Layer with Varying Wind Shear. *Boundary Layer Meteorology*.

Klemp, J., & Lilly, D. (1977). Numerical Simulation of Hydrostatic Waves. *Journal Of The Atmospheric Sciences*.

Kochanski, A., Jenkins, M. A., & Krueger, S. (2010). Flow over a simple hill and its impact on wind speed, variability, and turbulence. *Journal of Applied Fluid Mechanics*.

Lavaroni, L., Watson, S. J., Cook, M. J., & Dubal, M. R. (2014). A comparison of actuator disc and BEM models in CFD simulations for the prediction of offshore wake losses. *Journal of Physics: Conference Series*, *524*(1). https://doi.org/10.1088/1742-6596/524/1/012148

Lee, J., & Zhao, F. (2021). *Global Wind Report 2021* (tech. rep.). Global Wind Energy Council. Brussels, Belgium.

Li, C., & Wang, J. (2016). Investigation the speed-up effects of wind flow over typical terrains covered by vegetation. https://doi.org/10.2991/icseee-15.2016.55

Liu, L., & Stevens, R. J. (2020). Effects of Two-Dimensional Steep Hills on the Performance of Wind Turbines and Wind Farms. *Boundary-Layer Meteorology*, *176*(2), 251–269. https://doi.org/10.1007/s10546-020-00522-z

Liu, L., & Stevens, R. J. (2021). Effects of atmospheric stability on the performance of a wind turbine located behind a three-dimensional hill. *Renewable Energy*, *175*, 926–935. https://doi.org/10.1016/j.renene.2021.05.035

Lu, H., & Porté-Agel, F. (2011). Large-eddy simulation of a very large wind farm in a stable atmospheric boundary layer. *Physics of Fluids*, *23*(6). https://doi.org/10.1063/1.3589857

Manwell, J. F., McGowan, J. G., & Rogers, A. L. (2010). *Wind Energy Explained: Theory, Design and Application*. www.ATIBOOK.ir

Martínez, L. A., Leonardi, S., Churchfield, M. J., & Moriarty, P. J. (2012). A comparison of actuator disk and actuator line wind turbine models and best practices for their use. *50th AIAA Aerospace Sciences Meeting Including the New Horizons Forum and Aerospace Exposition*. https://doi.org/10.2514/6.2012-900

McTavish, S., Rodrigue, S., Feszty, D., & Nitzsche, F. (2015). An investigation of in-field blockage effects in closely spaced lateral wind farm configurations. *Wind Energy*, *18*(11), 1989–2011. https://doi.org/10.1002/we.1806

Medici, D., Ivanell, S., Dahlberg, J. Å., & Alfredsson, P. H. (2011). The upstream flow of a wind turbine: Blockage effect. *Wind Energy*, *14*(5), 691–697. https://doi.org/10.1002/we.451

Meyer Forsting, A. R., Troldborg, N., & Gaunaa, M. (2017). The flow upstream of a row of aligned wind turbine rotors and its effect on power production. *Wind Energy*, *20*(1), 63–77. https://doi.org/10.1002/we.1991

Mokhi, C. E., & Addaim, A. (2020). Optimization of wind turbine interconnections in an offshore wind farm using metaheuristic algorithms. *Sustainability (Switzerland)*, *12*(14), 1–24. https://doi.org/10.3390/su12145761

Montavon, C., Jones, I., Staples, C., Stracha, C., & Gutierrez, I. (2009). Practical Issues in the Use of CFD for Modelling Wind Farms. https://www.researchgate.net/publication/287811194

Nishino, T., & Draper, S. (2015). Local blockage effect for wind turbines. *Journal of Physics: Conference Series*, *625*(1). https://doi.org/10.1088/1742-6596/625/1/012010

Nygaard, N. G., Steen, S. T., Poulsen, L., & Pedersen, J. G. (2020). Modelling cluster wakes and wind farm blockage. *Journal of Physics: Conference Series*, *1618*(6). https://doi.org/10.1088/1742-6596/1618/6/062072

Obukhov, A. M. (1971). *Turbulence in an Atmosphere with a Non-uniform Temperature* (tech. rep.). The Institute of Theoretical Geophysics. USSR.

Ollier, S. J., Watson, S. J., & Montavon, C. (2018). Atmospheric gravity wave impacts on an offshore wind farm. *Journal of Physics: Conference Series*, *1037*(7). https://doi.org/10.1088/1742-6596/1037/7/072050

O'sullivan, J., Pecnik, R., & Iaccarino, D. G. (2010). Investigating turbulence in wind flow over complex terrain. *Proceedings of the Summer Program*. http://dutw1479.wbmt.tudelft.nl/~renep/Viewproject

O'Sullivan, R. (2022). *Wind Energy in Europe, 2021 Statistics and the outlook for 2022-2026* (tech. rep.). Wind Europe. Brussels, Belgium.

Pope, S. B. (2000). *Turbulent Flows*.

Popescu, M., & Flåtten, T. (2021). A study of blockage effects at the wind turbine and wind farm scales. *Energies*, *14*(19). https://doi.org/10.3390/en14196124

Porté-Agel, F., Bastankhah, M., & Shamsoddin, S. (2020). Wind-Turbine and Wind-Farm Flows: A Review. *Boundary-Layer Meteorology*, *174*(1), 1–59. https://doi.org/10.1007/s10546-019-00473-0

Prospathopoulos, J. M., Politis, E. S., Rados, K. G., & Chaviaropoulos, P. K. (2011). Evaluation of the effects of turbulence model enhancements on wind turbine wake predictions. *Wind Energy*, *14*(2), 285–300. https://doi.org/10.1002/we.419

Reiter, E. R., & Haurwitz, B. (1974). Internal Gravity Waves in the Atmosphere. *Arch. Met. Geoph. Biokl., Ser. A*, *23*, 101–114.

Revaz, T., & Porté-Agel, F. (2021). Large-eddy simulation of wind turbine flows: A new evaluation of actuator disk models. *Energies*, *14*(13). https://doi.org/10.3390/en14133745

S Jackson, B. P., & R Hunt, J. C. (1975). Turbulent wind flow over a low hill. *Quarterly Journal of the Royal Meteorological Society*, *101*, 929–955.

Sanchez Gomez, M., Lundquist, J., Mirocha, J., Arthur, R., & Muñoz-Esparza, D. (2021). Quantifying wind plant blockage under stable atmospheric conditions. *Wind Energy Science Discussions*, 1–21. https://doi.org/10.5194/wes-2021-57

Sanz Rodrigo, J., Churchfield, M., & Kosovic, B. (2017). A methodology for the design and testing of atmospheric boundary layer models for wind energy applications. *Wind Energy Science*, *2*(1), 35–54. https://doi.org/10.5194/wes-2-35-2017

Segalini, A. (2021). An analytical model of wind-farm blockage. *Journal of Renewable and Sustainable Energy*, *13*(3). https://doi.org/10.1063/5.0046680

Segalini, A., & Dahlberg, J. A. (2019). Global Blockage Effects in Wind Farms. *Journal of Physics: Conference Series*, *1256*(1). https://doi.org/10.1088/1742-6596/1256/1/012021

Segalini, A. (2017). Linearized simulation of flow over wind farms and complex terrains. *Philosophical Transactions of the Royal Society A: Mathematical, Physical and Engineering Sciences*, *375*(2091). https://doi.org/10.1098/rsta.2016.0099

Sessarego, M., Shen, W. Z., van der Laan, M. P., Hansen, K. S., & Zhu, W. J. (2018). CFD simulations of flows in awind farm in complex terrain and comparisons to measurements. *Applied Sciences (Switzerland)*, *8*(5). https://doi.org/10.3390/app8050788

Shamsoddin, S., & Porté-Agel, F. (2018). Wind turbine wakes over hills. *Journal of Fluid Mechanics*, *855*, 671–702. https://doi.org/10.1017/jfm.2018.653

Shingai, K., & Kawamura, H. (2004). A study of turbulence structure and large-scale motion in the Ekman layer through direct numerical simulations. *Journal of Turbulence*, *5*. https://doi.org/10.1088/1468-5248/5/1/013

Shutts, G. J., & Gadian, A. (1999). Numerical simulations of orographic gravity waves in flows which back with height. *Q.J.R. Meteorological Society*, *125*, 2743–2765.

Sivanandan, H. (2021). Numerical Study On The Impact Of Self Induced Gravity Waves On Offshore Wind Farms. http://repository.tudelft.nl/.

Smith, R. B. (2010). Gravity wave effects on wind farm efficiency. *Wind Energy*, *13*(5), 449–458. https://doi.org/10.1002/we.366

Sommer, A. Ø. (2021). *A numerical study of blockage effects in wind farms for different atmospheric conditions* (tech. rep.). www.vindenergi.dtu.dk

Stangroom, P. (2004). CFD Modelling of Wind Flow Over Terrain.

Stergiannis, N., Lacor, C., Beeck, J. V., & Donnelly, R. (2016). CFD modelling approaches against single wind turbine wake measurements using RANS. *Journal of Physics: Conference Series*, *753*(3). https://doi.org/10.1088/1742-6596/753/3/032062

Strickland, J. M., & Stevens, R. J. (2020). Effect of thrust coefficient on the flow blockage effects in closely-spaced spanwise-infinite turbine arrays. *Journal of Physics: Conference Series*, *1618*(6). https://doi.org/10.1088/1742-6596/1618/6/062069

Stull, R. (2017). *Practical Meteorology An Algebra-based Survey of Atmospheric Science*.

Supreeth, R., Arokkiaswamy, A., Hegde, K. M., Srinath, P., Prajwal, H. P., & Sudhanva, M. (2021). Analytical evaluation of performance of a small scale horizontal axis wind turbine rotor blade. *AIP Conference Proceedings*, *2316*. https://doi.org/10.1063/5.0036766

Supreeth, R., Arokkiaswamy, A., Raikar, N. J., & H. P., P. (2019). Experimental Investigation of Performance of a Small Scale Horizontal Axis Wind Turbine Rotor Blade. *International Journal of Renewable Energy Research*, *9*(4).

Supreeth, R., Arokkiaswamy, A., Raikar, N. J., Prajwal, H. P., & Sudhanva, M. (2019). Geometrical design of a rotor blade for a small scale horizontal axis wind turbine. *International Journal of Recent Technology and Engineering*, *8*(3), 3390–3400. https://doi.org/10.35940/ijrte.C5036.098319

Teneler, G. (2011). Wind Flow Analysis on a Complex Terrain: A reliability study of a CFD tool on forested area including effects of forest module.

Thresher, R., Robinson, M., & Veers, P. (2008). *Wind Energy Technology: Current Status and R&D Future* (tech. rep.). http://www.osti.gov/bridge

Tsuda, T. (2014). Characteristics of atmospheric gravity waves observed using the MU (Middle and Upper atmosphere) radar and GPS (Global Positioning System) radio occultation. https://doi.org/10.2183/pjab.90.12

Uchida, T., & Li, G. (2018). Comparison of RANS and LES in the Prediction of Airflow Field over Steep Complex Terrain. *Open Journal of Fluid Dynamics*, *08*(03), 286–307. https://doi.org/10.4236/ojfd.2018.83018

van Til, J. (2021). The impact of atmospheric stability on the global blockage effect of offshore wind farms. http://repository.tudelft.nl/.

Wu, K. L., & Porté-Agel, F. (2017). Flow adjustment inside and around large finite-size wind farms. *Energies*, *10*(12). https://doi.org/10.3390/en10122164

Yang, X., Howard, K. B., Guala, M., & Sotiropoulos, F. (2015). Effects of a three-dimensional hill on the wake characteristics of a model wind turbine. *Physics of Fluids*, *27*(2). https://doi.org/10.1063/1.4907685

Zhang, Z., Huang, P., Bitsuamlak, G., & Cao, S. (2022). Large-eddy simulation of wind-turbine wakes over two-dimensional hills. *Physics of Fluids*, *34*(6). https://doi.org/10.1063/5.0095348